# Metal-Free Photoredox-Mediated Ring-Opening Metathesis Polymerization Methods and Scope

Laura M. M. Pascual

A dissertation

submitted in partial fulfillment of the

requirements for the degree of

Doctor of Philosophy

University of Washington

2018

Reading Committee:

Andrew J. Boydston, Chair

Alshakim Nelson

Gojko Lalic

Program Authorized to Offer Degree:

Department of Chemistry

University of Washington

## Abstract

Photoredox-Mediated Ring-Opening Metathesis Polymerization Methods

Laura M. M. Pascual

Chair of the Supervisory Committee:
Professor Andrew J. Boydston
Department of Chemistry

Metal-free, photoredox-mediated ring-opening metathesis polymerization (MF-ROMP) is a novel approach to the synthesis of ROMP polymers. Whereas traditional, metal-mediated ROMP uses well-defined transition metal-alkylidene initiators in stoichiometric amounts, MF-ROMP uses a photo-oxidant to oxidize an organic vinyl ether initiator. This obviates the need for purification to remove residual metal species for certain applications, such as drug delivery and organic electronics. A variety of pyrylium and thiopyrylium photo-oxidants have been evaluated for efficacy in MF-ROMP. Generally, the more electron-rich (thio)pyrylium salts, which are milder oxidants, achieved higher conversions of norbornene in MF-ROMP, with thiopyrylium salts out-performing corresponding pyrylium salts in both rate and conversion. While 2,4,6-tris(4-methoxyphenyl)pyrylium tetrafluoroborate had been the workhorse for research to date, the corresponding thiopryrylium emerged as a candidate for applications requiring rapidly reaching critical conversion, such as applications requiring gelation or

crosslinking. Inspired by the broad functional group tolerance of metal-mediated ROMP, we sought to expand the scope of MF-ROMP, with particular emphasis on alcohol functionality. We were initially encouraged by the results of additive screenings, which demonstrated that the polymerization was tolerant to sterically hindered alcohols. Comonomers with polar functionality incorporated in copolymerization to varying extents. Remarkably, the TBS-ether functionalized norbornene both homopolymerized and copolymerized with norbornene, with quantitative incorporation in the case of copolymerization. The resulting polymers was deprotected in solution with TBAF. Notably, Boc-carbonate-functionalized norbornene copolymerized with norbornene, and was subsequently deprotected in the solid state to yield an alcohol-functionalized polynorbornene. Interestingly, 2-chloro-2,3-dihydro-*endo*-dicyclopentadiene did not copolymerize. Monitoring the homopolymerization revealed a low rate of conversion and a sigmoidal shape to the conversion vs. time plot, which is consistent with slow initiation kinetics. Each of these polar monomers can facilitate post-polymerization functionalization. An investigation of the stereochemistry of MF-ROMP polymers revealed predominantly trans olefin geometry. Quantitative $^{13}C$ NMR spectroscopy was used to determine that MF-ROMP polymers are atactic. Additionally, block copolymers were synthesized via sequential addition of monomers, consistent with living characteristics. While the unique vinyl ether chain end of MF-ROMP can offer synthetic advantages, minimizing initiator loading improves cost effectiveness. Additionally, low-molecular weight polymers are desirable for certain applications, such as thermosetting. We demonstrated that chain transfer with α-olefins cleaved the vinyl ether chain ends via metathesis and offered molecular weight control.

# TABLE OF CONTENTS

# LIST OF FIGURES

# LIST OF SCHEMES

# LIST OF TABLES

# ACKNOWLEDGEMENTS

First, I would like to thank my advisor, Professor AJ Boydston, for his constant encouragement, patience, and guidance. AJ has stood by me through real highs and lows in the last five years and maintained his patient support of my education. I have learned an immense amount from AJ, from basic science to presentation skills. I have also greatly appreciated the exciting opportunities that AJ has provided for me to present our work at national and international conferences. These will be some of my best memories from these years.

Also, I would like to thank Prof. Scott Grayson from Tulane Universit and his group for a fruitful collaboration that helped us understand chain transfer in PhotoROMP. In particular, I would like to thank Farihah Haque. I addition to elucidating MF-ROMP chain end identities via MALDI-TOF and sharing a multitude of helpful insights, she has genuinely been a pleasure to work with (Chapter 4). I am also indebted to Dr. Dan Knorr (Army Research Labs) and Professor Robert H. Grubbs (California Institute of Technology) for constructive collaborations and guidance.

Additionally, I would like to thank my committee members, Professors Gojko Lalic, Christine Luscombe, Al Nelson, Brandi Cossairt, and Bo Zhang for encouragement and guidance through the years.

I am also incredibly grateful to my undergraduate mentors, especially Prof. Andrea Munro from PLU, Prof. Neal Armstrong from University of Arizona, and Dr. Bret Voss, Dr. Marvi Matos, and Kevin Malone from Boeing. Each of them helped me to understand a multitude of science concepts and professional skills as they guided me in research. I am also grateful to Pacific Lutheran University's chemistry department for preparing me for graduate

school and for building my enthusiasm for chemistry as well as my confidence. The chemistry professors there (Prof. Naasz, Prof. Lytle, Prof. Yakelis, Prof. Saxowsky, and Prof. Fryhle) as well as the physics professors (Prof. Hay, Prof. Underwood, Prof. Greenwood, and Prof. Louie) helped me grow as a scientist and as a person.

I would like to thank each of my co-authors for their contributions to this work. In particular, I would like to thank Dr. Adam Goetz, Dr. Damian Dunford, and Dr. Kelli Ogawa for their contributions to evaluating MF-ROMP photo-oxidants (Chapter 2). I would also like to thank Dr. Damian Dunford, Dr. Adam Goetz, Dr. Kelli Ogawa, and Dr. Dan Knorr for their work on expanding the MF-ROMP scope. For their contributions to understanding the structures of MF-ROMP polymers and co-polymers, I would like to thank Dr. Adam Goetz and Dr. Adrienne Roehrich (Chapter 3). Finally, for contributions to understanding chain transfer in MF-ROMP, I would like to thank Farihah Haque and Jordan Forsythe (Chapter 4).

My lab mates and friends in the department have undoubtedly helped me throught this experience. Dr. Adam Goetz, Dr. Derek Church, Dr. Damian Dunford, Dr. Mike Larsen, Dr. Kelli Ogawa, Dr. Greg Peterson, and Dr. Chang-Uk Lee led by example for me and taught me most of the lab skills that I learned during graduate school. Derek provided endless moral support and encouragement. My fellow graduate students Johanna, Tori, Pengtao, Bo, Dan, Brock, Carl, and Troy have been great friends, have lifted my spirits, and have supported me through ups and downs. My undergrads Johanna, Nasser, Jordan, and Ashlynn have brought meaning and joy to lab. Also, I couldn't have gotten through this experience without my friends from neighboring labs. Spencer, Chloe, my Katies in the Ginger and Anderson labs, Soumya, Sarthak, and Scott have supported me in numerous ways.

I would also like to thank the many experts in the UW Chemistry Department that have kept everything running so beautifully and taught me so much. Dr. Adrienne Roehrich taught me how to do quantitative $^{13}C$ NMR and provided valuable insights for our tacticity paper. Dr. Martin Sadilek helped me in understanding mass spec and collecting meaningful data. Lochlan Hickok has not only helped me track down the resources I needed for lab, but has also been a real friend. Eric Lindahl and Eric Strakbein have both helped me with projects and been a joy to work with.

With all my heart, I would like to thank my family for their enthusiastic support. My husband Justin has provided support in a million ways, from providing rides to lab and packing lunches to attending every one of my conference presentations all over the world. He has been my rock and foundation, and my hope for the future. My nieces and nephew, Kristal, Sophie, and Leo, also have my gratitude for support that they will never know that they gave. They are the light of my life. The laughs and cuddles that they provide lift my spirits every time. I am also deeply grateful to my parents for 27 years of unconditional love and support that have gotten me here. From childhood swim team to college to grad school, they have always supported my dreams. The warm foundation they have provided in my life has helped me feel safe to keep reaching. My little sisters and the loveable brothers-in-law that they brought into my world have also brought me joy that has helped me get through these years. Our wataer park, tulip field, and pumpkin patch trips, the hundreds of snap chats of their darling babies, the home-made ice cream and holidays together have brightened my world. My Aunt Monica and Grandpa Bobby have also always supported me and lifted my spirits. Additionally, I would like to thank my mother-, father-, sister-, and brothers-in-law for embracing me and supporting me in my endeavors.

I would also like to thank several friends, many of whom have been with me since childhood, who have loved and supported me for years and provided joyful breaks from work and studies. I am especially grateful to Dr. Jennifer Reynolds, Victorial Meucci, Emily Gray, Brooks Estes, and Olivia Civile.

Finally, I would like to thank the Army Research Office for funding my education through a National Defense Science and Engineering Graduate Research Fellowship. Additionally, I would like to thank the University of Washington, the Washington Research Foundation, the Army Research Office, and the National Science Foundation for funding my graduate research.

# DEDICATION

To my faithful husband, Justin

# Chapter 1. Introduction to Photoredox-Mediated Metal-Free Ring-Opening Metathesis Polymerization[1,2,3]

## Section 1: Metal-Mediated Ring-Opening Metathesis Polymerization

### *1.1.a Introduction to Ring-Opening Metathesis Polymerization*

Ring-opening metathesis polymerization (ROMP) is one of the most impactful technologies to emerge from transition metal-mediated olefin metathesis, with widespread applications in industry and academia.[1,2] The creative break-throughs in these areas have stemmed from the elucidation of the metal-mediated ROMP mechanism and the design of well-defined transition metal alkylidene initiators.[3] The ROMP mechanism proceeds via a metallacyclobutane intermediate (Scheme 1.1).[3a] Briefly, a trasition metal alkylidene initiator coordinates with a cyclic olefin monomer, which, via a [2+2] cyloaddition, forms a metallacyclobutane intermediate. The metallacyclobutane intermediate undergoes a cycloreversion, giving rise to a new metal-alkylidene with a ring-opened alkene. This metal alkylidene can react with additional monomers, and propagation continues until monomer is consumed, equilibrium is reached, or the reaction is quenched.

---

[1] Adapted with permission from Ogawa, K. A.; Goetz, A. E.; Boydston, A. J. "Metal-free Ring-Opening Metathesisis Polymerizaton." *J. Am. Chem. Soc.* **2015**, *137*, 1400. Copyright 2015 American Chemical Society.

[2] Adapted with permission from Goetz, A. E.; Boydston, A. J. "Metal-free Preparation of Linear and Cross-linked Polydicyclopentadiene." *J. Am. Chem. Soc.* **2015**, *137*, 7572. Copyright 2015 American Chemical Society.

[3] Adapted with permission from Ogawa, K. A.; Goetz, A. E.; Boydston, A. J. "Developments in Externally-Regulated Ring-Opening Metathesis Polymerization." *Synlett.* **2016**, *27*, 203. Copyright 2016 Georg Thieme Verlag KG.

**Scheme 1.1.** Metal-mediated ROMP mechanism.

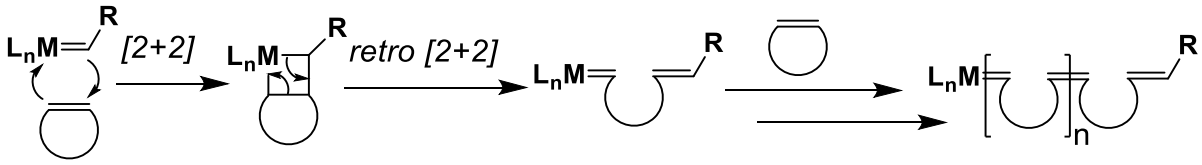


The creative design of a wide variety of metal alkylidene ROMP initiators based on Ru, Mo, and W, examples of which are shown in Figure 1.1, has facilitated numerous applications. Initiator development has enabled a variety of impressive capabilities, including: control over molecular weight and dispersity; stereoselective ROMP; aqueous ROMP; bulk ROMP; outstanding functional group tolerance; ROMP of monomers bearing amino acids, peptides, or nucleobases; surface-initiated ROMP; ROMP of monomers bearing electroluminescent and electroactive moieties; end group functionalization for initiation of orthogonal polymerizations; synthesis of various macromolecular architectures; and more.[1] These break-throughs have enabled applications in fields such as organic electronics, structural and engineering materials, biomedical engineering, and drug delivery.

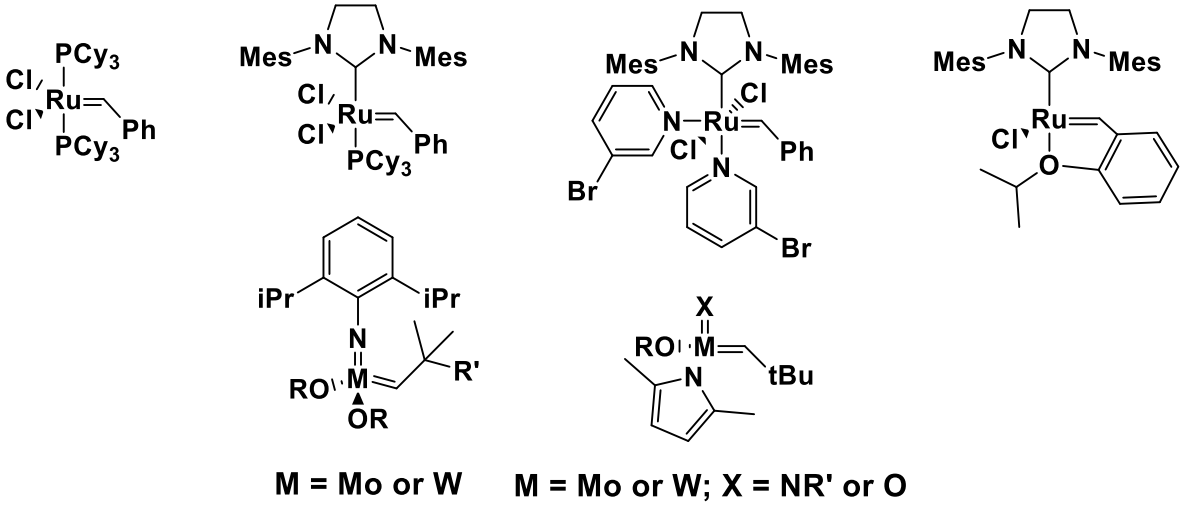


**Figure 1.1**. Representative well-defined ROMP initiators.

*1.1.b Applications*

Polyolefins and hydrogenated polyolefins produced via ROMP have a wide range of industrial applications (Figure 1.2).[2] For example polynorbornene (PNB) is used in oil spill clean-up and sound-proofing, polycylcooctene is a component of rubberized asphalt, and hydrogenated polytetracyclododecene is used in optics applications. Polydicyclopentadiene (PDCPD) has a broad array of structural and engineering applications, as PDCPD is being introduced as a light-weight alternative to metals like steel and aluminum. Examples of these applications include: ballistic impact materials; composite wind blades; thermally insulated pipes; chemically resistant pipes and tanks; and vehicle body panels in commercial trucks, construction equipment, and agricultural equipment.[4] An electric car known as Buddy car is made entirely of PDCPD body panels (Figure 1.3).[4b]

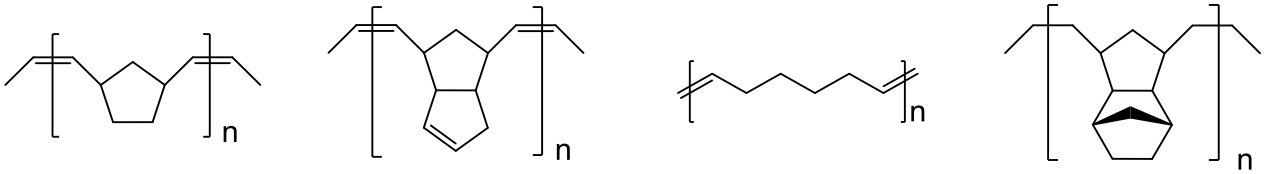


Polynorbornene
**Norsorex®**
(*oil spill cleanup, sound proofing*)

Polydicyclopentadiene
(often cross-linked)
**Prometa,® Metathene,® Telene, ® Metton, ® PENTAM, ® Proxima ®**
(*vehicle hoods & bumpers, sporting goods*)

Polycyclooctene
**Vestenamer®**
(*rubberized asphalt*)

Polytetracyclododecene
**Zeonex®**
(*optics applications*)

**Figure 1.2**. Industrial applications of ROMP polymers and hydrogenated ROMP polymers.

**Ballistic Impact Materials** | **Truck Body Panels** | **Construction Equipment** | **Agricultural Equipment** | **Composite Wind Blades** | **Electric Car Body Panels**

**Figure 1.3**. Examples of industrial applications of ROMP (PDCPD).

*1.1.c Challenges*

While the creative developments in the field of metal-mediated ROMP have enabled a broad range of applications, two general concerns pertaining to the use of transition metal intitiators for ROMP are cost and contamination. Based on list prices, to synthesize 1 ton of 50 kDa PNB, the necessary Grubbs II would cost $2.8 million.[5] The necessary ethyl propenyl ether initiator for the metal-free approach presented herein would cost only $11,000.[6] A metal-free approach to ROMP could present cost benefits.

Additionally, residual metal contaminant from the transition metal initiator could be problematic for certain applications, including optics, electronics, biomedical engineering, and drug delivery. Removing residual metal species to meet purity requirements for these applications poses a challenge. A variety of creative methods have been developed to facilitate catalyst removal, such as employing solid-supported catalysts, water-soluble catalysts, or chelating agents, or using extensive purification procedures.[7] A metal-free approach to ROMP would obviate the need for these intensive purification measures.

For structural and engineering applications of cross-linked PDCPD, the reaction injection molding process produces cross-linked parts with the transition metal trapped in the final part. This creates a recurring expense; the metal ROMP initiator is not truly catalytic as it cannot be recovered and reused. A metal-free approach to ROMP polymers could offer a cost-saving alternative for such applications.

## Section 2: Inspiration for Photoredox-Mediated Metal-Free Ring-Opening Metathesis Polymerization

*1.2.a Electrochemical Olefin Metathesis and Preliminary Electrochemical ROMP Success*

The metal-free approach to ROMP was inspired by Chiba and coworkers' metal-free, electrochemical olefin metathesis. In this ground-breaking work, olefin metathesis was achieved via bulk electrolysis in an electrolyte solution of lithium perchlorate ($LiClO_4$) in nitromethane ($CH_3NO_2$) using carbon fiber electrodes.[8] In this approach, anodic one-electron oxidation of a vinyl ether forms a vinyl ether radical cation, which, in the presence of an α-olefin, forms a cyclobutene radical cation (Scheme 1.2). While reduction of the cyclobutene radical cation intermediate to form the cyclobutane was the major pathway, in select cases the metathesis products were achieved.[8a]

**Scheme 1.2** Electrochemical olefin metathesis.

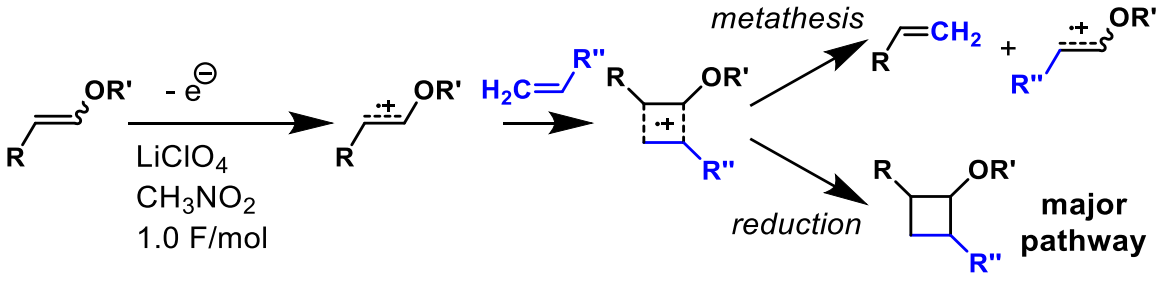


Boydston and coworkers hypothesized that ring strain in a cycloalkane would facilitate metathesis (**C** to **D**) over reduction in electrochemical metathesis (Scheme 1.3).[9] In the proposed mechanism, anodic one-electron oxidation of the vinyl ether (**A**) produces the vinyl ether radical cation (**B**). Coordination of **B** with a cycloalkane would form the [2+2] complex **C**, a cyclobutene radical cation. This fragments to form radical cation **D**, which can react with

additional monomers to form propagating polymer species **E**. This polymer species **E** with active, propagating vinyl ether radical cation chain end was envisioned to exist in equilibrium with its reduced counterpart via reversible redox cycles. A series of reversible deactivation-activation events were envisioned to yield the final polymer species **F**.

**Scheme 1.3.** Envisioned electrochemical ROMP mechanism.

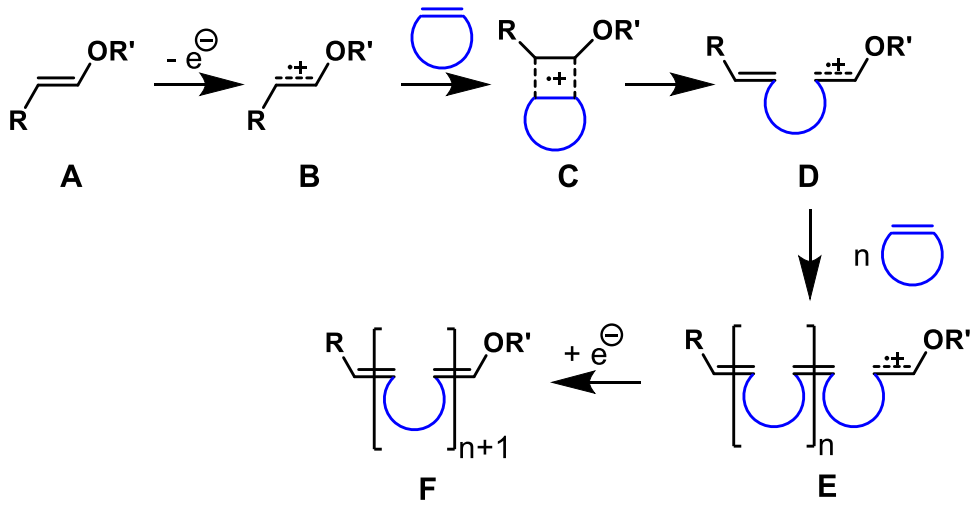


The hypothesis that ROMP could be electrochemically mediated, with ring strain leading metathesis to out-compete reduction, was tested using a bulk electrolysis conditions similar to that of Chiba and coworkers.[9] Carbon fiber working and counter electrodes were employed with $LiClO_4/CH_3NO_2$ electrolyte solution (Figure 1.3). Ethyl propenyl ether (EPE) was evaluated as the initiator and norbornene (NB) as the monomer. While initial results showed no evidence of polymerization in the solution, a white residue was identified on the carbon fiber anode and was identified by $^1H$ NMR spectroscopy as PNB synthesized via ROMP. Gel permeation chromatography (GPC) with refractive index and multi-angle light scattering detection revealed

that the PNB had a number-average molecular weight ($M_n$) of 11.8 kDa and dispersity ($Đ$) of 2.2.[9b] This success constituted the first metal-free ROMP (MF-ROMP) demonstration. Despite this promising lead, initial yields were limited to about 3%. Efforts to improve this by screening various electrolyte solutions revealed that the $LiClO_4/CH_3NO_2$ electrolyte solution was critical, but poor solubility continued to limit conversion. Sonicating by running the electrolysis with the cell in an ultrasonic bath resulted in modest improvements in conversion with various vinyl ether initiators (Table 1.1). Despite these trouble-shooting measures, yields remained limited to 14% conversion. At this point, Boydston and coworkers pondered whether the vinyl ether radical cation active initiator could be accessed via an alternative route.

**Figure 1.4**. ROMP via bulk electrolysis (set-up).

**Table 1.1.** Summary of results from MF-ROMP via bulk electrolysis with vinyl ether initiators and NB monomer.

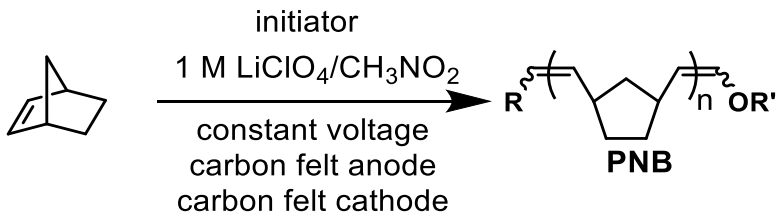


| Initiator | $[M_0]/[I_0]$[a] | $M_n$ (kDa)[b] | $Đ$[c] | Yield (%)[d] |
|---|---|---|---|---|
| 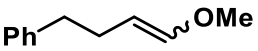 | 28/1 | 6.7 | 1.5 | 13 |
| 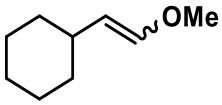 | 28/1 | 4.8 | 1.5 | 14 |
|  | 28/1 | 6.2 | 1.4 | 12 |

[a] Ratio of initial monomer (NB) and initiator (vinyl ether) concentrations. [b] Number-average molecular weight calculated from weight-average molecular weight determined by GPC with refractive index and multi-angle laser light scattering detectors. [c] Dispersities determined by GPC analysis. [d] Isolated yield after precipitation.

*1.2.b Photoredox-Mediated Cycloadditions*

Seeking alternative methods to externally regulate MF-ROMP via exogenous stimuli, Boydston and coworkers were inspired by recent reports of photocatalyzed polymerizations with spatiotemporal control, including examples with metal-free photocatalyst systems.[10] In the pursuit of alternative approaches towards exogenous activation of MF-ROMP via one-electron oxidation of the vinyl ether initator, Boydston and coworkers were inspired by demonstrations of photoredox-mediated [2+2] cycloadditions.[11] Examples include the [2+2] cycloadditions of styrenes catalyzed by a tris(bipyrimidine)ruthenium(II) photo-oxidant (Scheme 1.5)[11b] and lignan synthesis catalyzed by pyrylium photo-oxidant (Scheme 1.6).[11a] The latter photocatalyst was

particularly attractive for our application as it offered a metal-free approach to oxidizing the vinyl ether initiator.

**Scheme 1.4.** Photoredox-mediated [2+2] cycloaddition with pyrylium photo-oxidant.

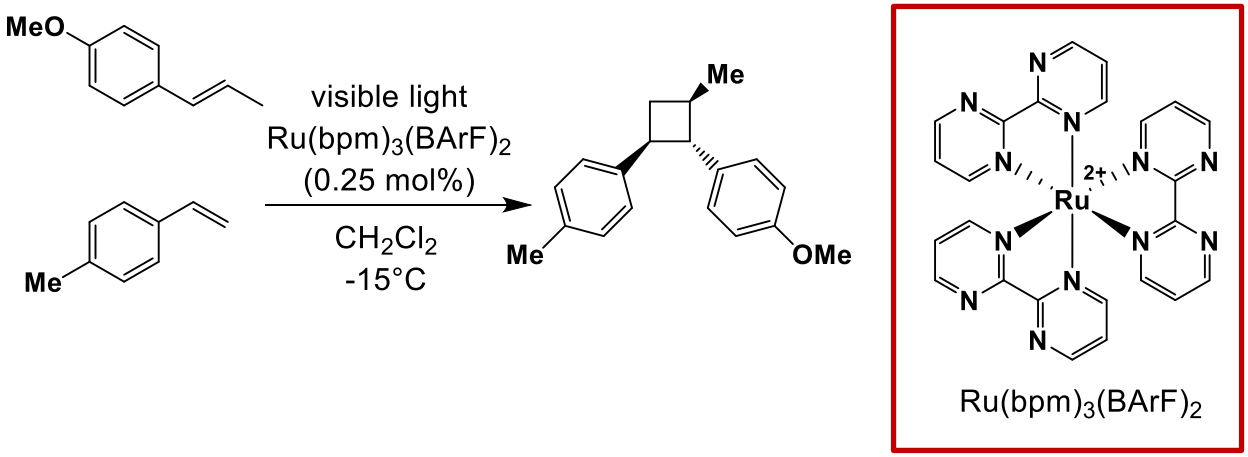


**Scheme 1.5.** Photoredox-mediated [2+2] cycloaddition with tris(bipyrimidine)ruthenium(II) photo-oxidant.

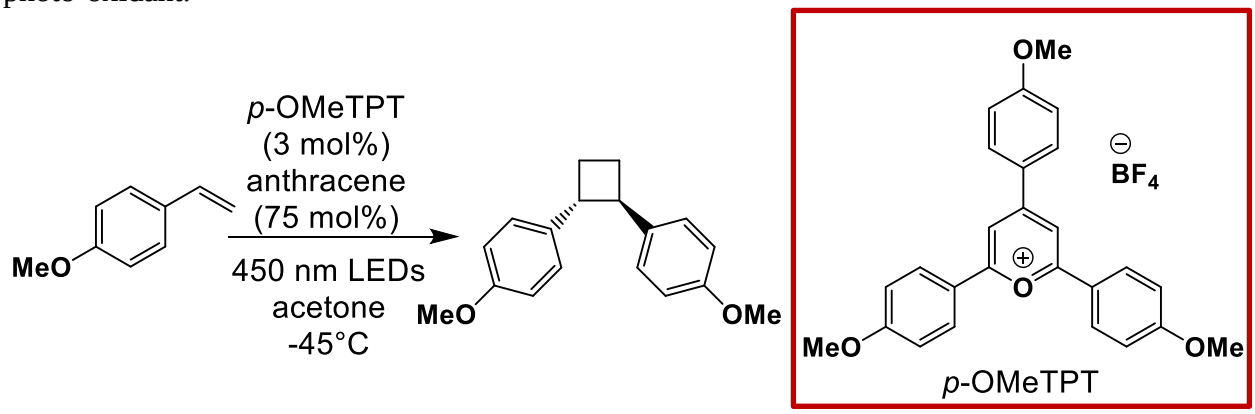

**Section 3: Metal-Free Photoredox-Mediated Ring-Opening Metathesis Polymerization**

*1.3.a Proof of Concept*

A variety of conditions using metal-free photoredox-mediators were evaluated for MF-ROMP.[9] Successful conditions using vinyl ether initiators, 2,4,6-tris(4-methoxyphenyl)pyrylium tetrafluoroborate as the photo-oxidant, NB as the monomer, and dichloromethane ($CH_2Cl_2$) as the solvent. Polymerizations were carried out under nitrogen with stirring in a 2 dram vial with Teflon cap, stirring and irradiating with a 2 W, 450 nm blue LED bulb (Figure 1.2, Scheme 1.6). Several vinyl ether initiators were evaluated (Table 1.2). The vinyl ether initiators resulted in comparable conversions of NB and initiation efficiencies. Ethyl propenyl ether (**1c**) became the workhorse for MF-ROMP initiation due to commercial availability.

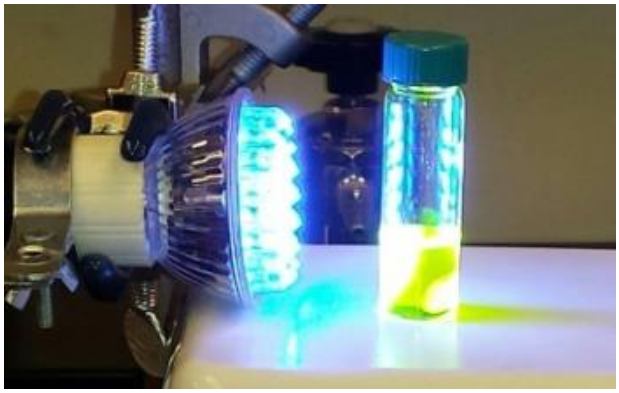

**Figure 1.5**. Photoredox-mediated MF-ROMP set-up with blue LED, screw cap vial, and stir plate.

**Scheme 1.6.** Photoredox-mediated ROMP method.

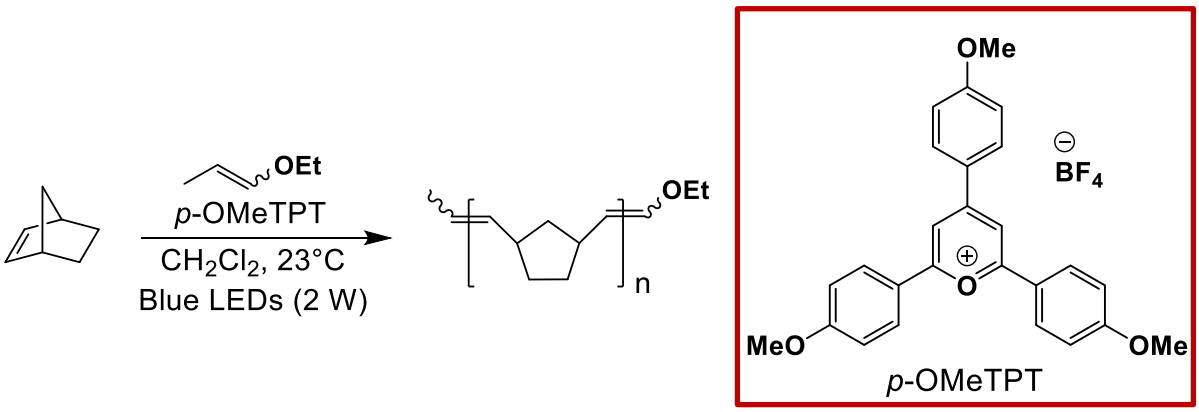


**Table 1.2.** Photoredox-mediated MF-ROMP with various vinyl ether initiators.

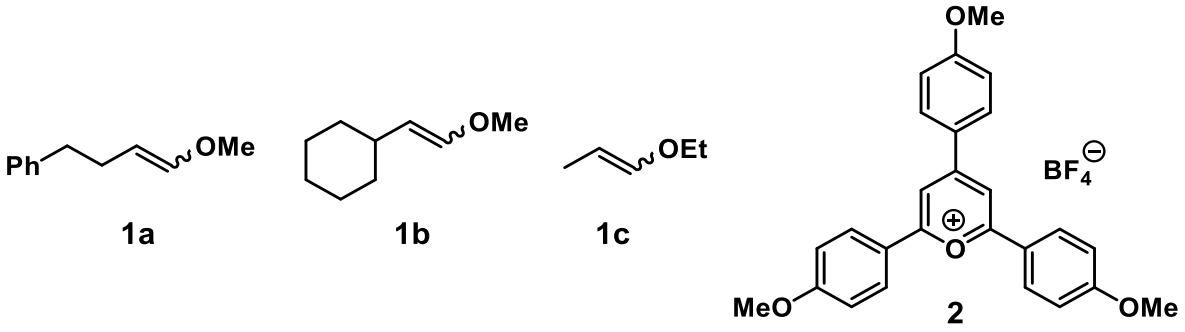


| Initiator | NB : 1 : 2[a] | $[NB]_0$ (M)[b] | conversion (%)[c] | $M_{n,\ theo}$ [kDa][d] | $M_{n,\ exp}$ [kDa][e] | $Đ$[f] |
|---|---|---|---|---|---|---|
| **1a** | 97 : 1 : 0.03 | 1.9 | 88 (73) | 8.0 | 15.1 | 1.7 |
| **1b** | 97 : 1 : 0.03 | 1.9 | 92 (80) | 8.4 | 14.9 | 1.6 |
| **1c** | 106 : 1 : 0.03 | 2.0 | 87 (67) | 9.0 | 15.8 | 1.6 |

[a] Initial molar ratio of **NB**, **1**, and **2**. [b] Initial concentration of **NB** (M). [c] Conversion of **NB**, as determined by $^1$H NMR analysis; isolated yields after precipitation given in parentheses. [d] $M_{n,\ theo}$ is theoretical number-average molecular weight calculated from initial **NB**:**1** ratio and % conversion of **NB**. [e] $M_{n,\ exp}$ is experimental number-average molecular weight, calculated from a weight-average molecular weight determined by GPC using multiangle laser light scattering (MALLS). [f] Dispersities (Đ) determined by GPC analysis.

Having identified EPE as the workhorse initiator for photoredox-mediated MF-ROMP, a variety of reaction conditions were then considered (Table 1.3). Most notably, varying the monomer to initiator ratio afforded some control over molecular weight, with molecular weights ($M_n$) ranging from 4.3 to 57.4 kDa (corresponding to initial NB:EPE molar ratios of 48:1 and 1000:1, respectively). The initiator, photoredox mediator, and LED bulb were all critical to the polymerization- no polymerization was observed in the absence of either of these reagents or in the dark. The discrepancy between $M_{n,\ theor}$ and $M_{n,\ exp}$ indicates low initiation efficiency ($M_{n,\ theor}/M_{n,\ exp}$). The lowest initiation efficiency observed was 53% (Table 1.3, row 1). In general, initiation efficiency increased with increasing initial ratio of moles of monomer to initiator.

**Table 1.3.** Photoredox-mediated MF-ROMP under various reaction conditions.

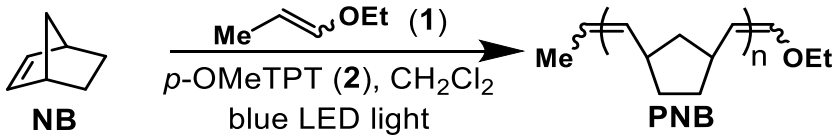


| NB : 1c : 2[a] | $[M]_0$ (M)[b] | conversion (%)[c] | time (min) | $M_{n,\ theo}$ [kDa][d] | $M_{n,\ exp}$ [kDa][e] | $Đ$[f] |
|---|---|---|---|---|---|---|
| 48 : 1 : 0.03 | 1.8 | 95 (78) | 60 | 4.3 | 8.1 | 1.4 |
| 57 : 1 : 0.03 | 1.2 | 93 (58) | 120 | 5.0 | 11.5 | 1.4 |
| 491 : 1 : 0.03 | 5.3 | 51 (25) | 120 | 23.6 | 22.2 | 1.5 |
| 494 : 1 : 0.03 | 1.8 | 72 (50) | 60 | 33.4 | 43.9 | 1.5 |
| 1000 : 1 : 0.03 | 1.9 | 61 (47) | 120 | 57.4 | 60.2 | 1.6 |

[a] Initial molar ratio of **NB**, **1**, and **2**. [b] Initial concentration of **NB** (M). [c] Conversion of **NB**, as determined by $^1$H NMR analysis; isolated yields after precipitation given in parentheses. [d] $M_{n,\ theo}$ is theoretical number-average molecular weight calculated from initial **NB**:**1** ratio and % conversion of **NB**. [e] $M_{n,\ exp}$ is experimental number-average molecular weight, calculated from a weight-average molecular weight determined by GPC using multiangle laser light scattering (MALLS). [f] Dispersities (Đ) determined by GPC analysis.

*1.3.b Mechanistic Considerations*

Boydston and coworkers proposed a mechanism for photoredox-mediated MF-ROMP (Figure 1.3). In this mechanism, upon exposure to blue light, excited-state pyrylium (*p*-OMeTPT$^{*+}$) oxidizes the vinyl ether initiator (**A**) to form a vinyl ether radical cation (**B**). The vinyl ether radical cation (**B**) forms a [2+2] cycloaddition complex (**C**) with a cycloalkene monomer, such as norbornene. Ring strain then leads metathesis to out-compete reduction, forming the ring-opened vinyl ether radical cation (**D**), which is proposed to exist in equilibrium with its reduced form (**E**). Since radical cation intermediates like the vinyl ether are susceptible to deleterious side-reactions, such as nucleophilic attack by alcohols, reversible deactivation as depicted in Fig. 1.3 would be advantageous in preventing death of the chain end.[12] The ring-opened vinyl ether radical cation then reacts with additional monomers to form the propagating polymer species (**F**), which also exists in equilibrium with its reduced counterpart (**G**). Reduction gives neutral polymer (**H)**. At any point, pyranyl (*p*-OMeTPT$^{\bullet}$) can reduce the vinyl ether radical cation to the vinyl ether (eg. **F** to **G**), and pyrylium can reactivate the polymerization by oxidizing the vinyl ether back to the vinyl ether radical cation (eg. **G** to **F**).

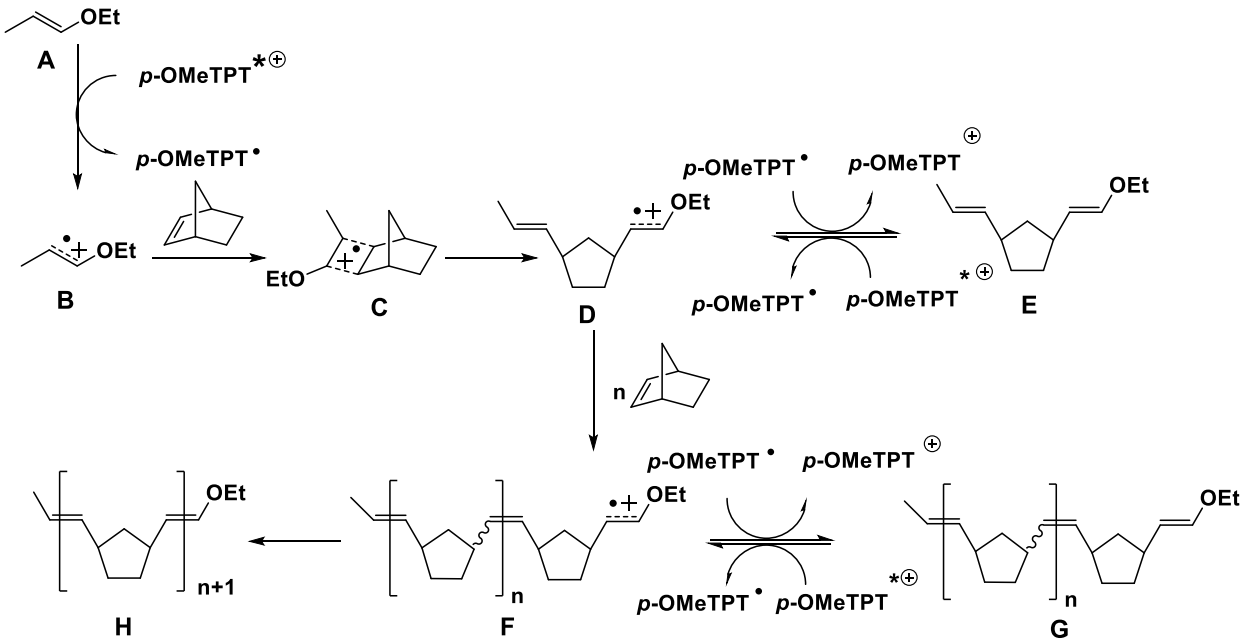


**Figure 1.6**. Proposed mechanism for photoredox-mediated MF-ROMP.

To explore the mechanism of MF-ROMP, $M_n$ and $Đ$ were monitored over the course of the polymerization (Figure 1.4). The gradual, approximately linear increase in $M_n$ with increasing conversion is consistent with a chain-growth mechanism. However, the linear correlation of $M_n$ vs conversion for ROMP via this alternative mechanism is weaker positive correlation than in metal-mediated ROMP.[13]

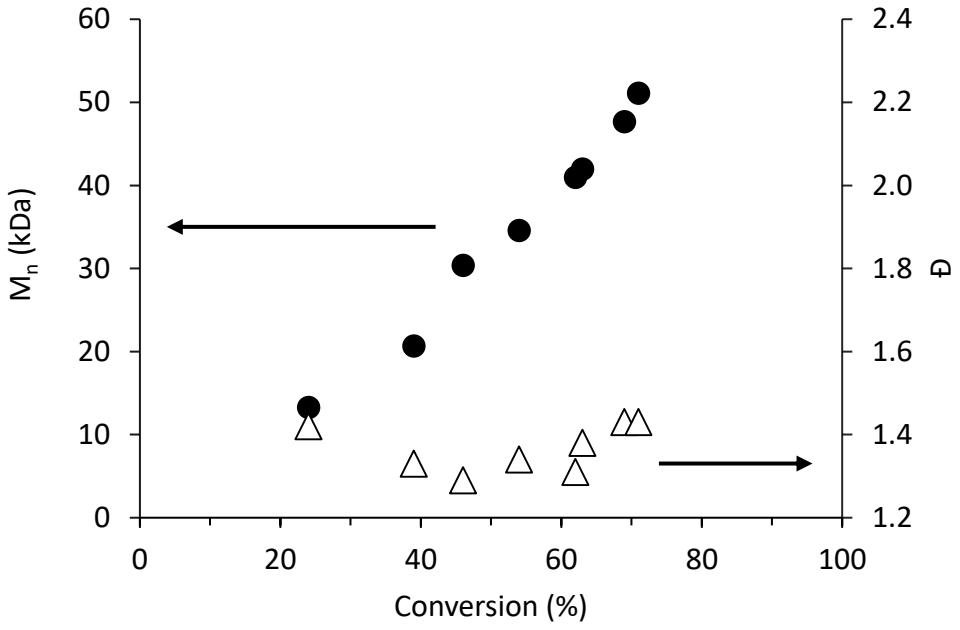


**Figure 1.7.** Plot of $M_n$ (●) and $Đ$ (△) vs % conversion of monomer using initial **NB**:**1c** of 500:1.

To probe the dynamic nature of the chain end redox couple, conversion of photoredox-mediated MF-ROMP was monitored in a light cycling experiment (Figure 1.5). Conversion increased during periods of light exposure and halted during periods of dark exposure. The observed reversible activation and deactivation is consistent with the proposed vinyl ether chain end redox couple. Furthermore, while creative approaches for have been employed for activation of MF-ROMP using exogenous stimuli via application of redox-, photochemically-, mechanically-, thermally-, and acid-activated ROMP transition metal initiators, MF-ROMP was a unique demonstration in the ability to reversibly *deactivate* ROMP.[9b] Furthermore, the GPC traces of reaction aliquots at each time point in light cycling (Figure 1.5 bottom) indicate that polymer chain growth halts upon dark exposure, and resumes upon light exposure, as opposed to initiation of new chains.

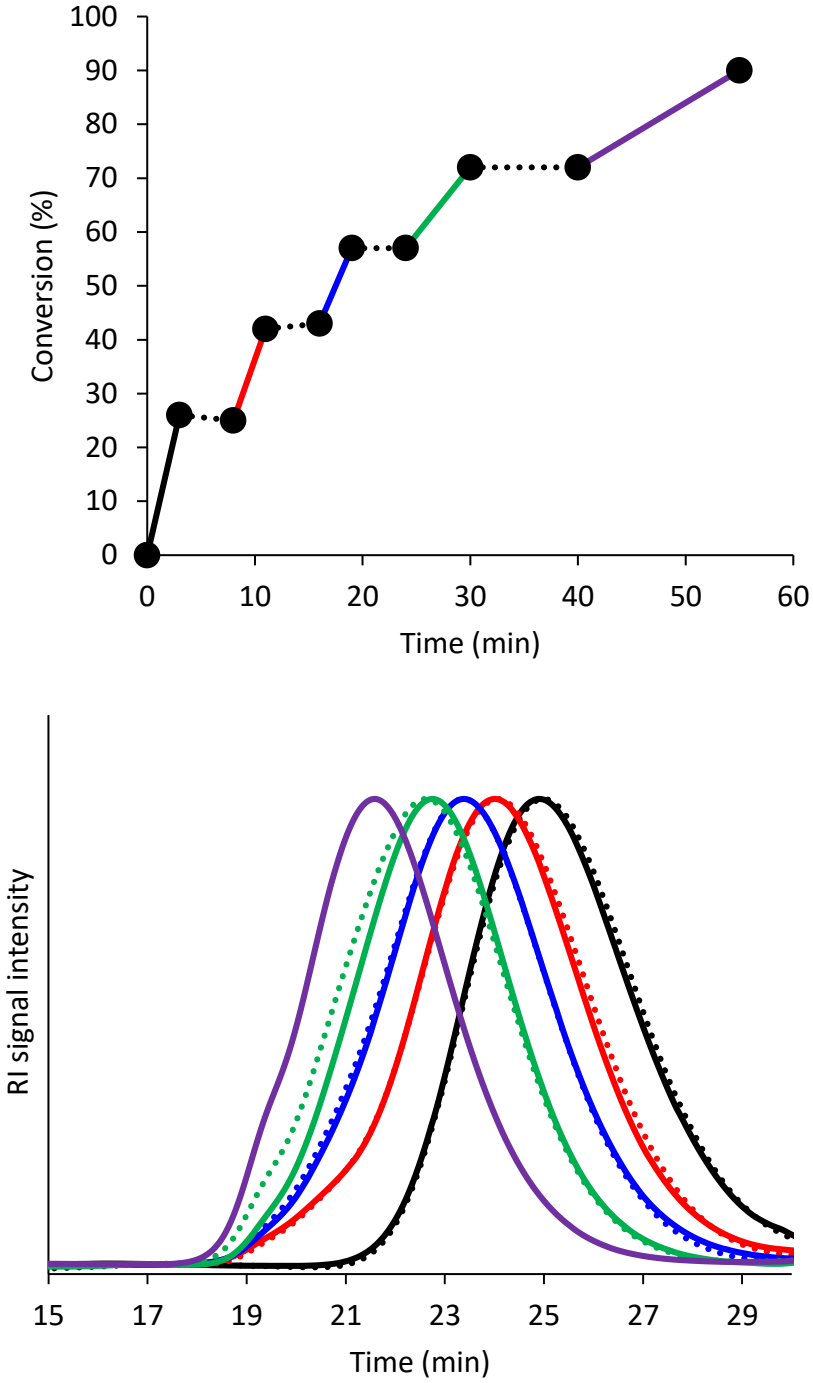


**Figure 1.8.** Top: Plot of % conversion of monomer vs time. Solid lines indicate periods of exposure to blue LED light. Dotted lines indicate periods in the dark. Data point labels indicate $M_n$ values (kDa). Initial conditions: **NB**:**1a** = 100:1, $[\mathbf{NB}]_0$ = 1.9 M. Bottom: GPC refractive index traces corresponding to data points from light cycling experiment. Solid lines indicate GPC traces taken immediately after light exposure, and dashed lines after dark exposure.

*1.3.c Expansion of Monomer Scope- Dicyclopentadiene*

Thus far, the monomer scope of MF-ROMP had been limited to unfunctionalized norbornene. Dicyclopentadiene and its derivatives were an attractive class of monomers for MF-ROMP due to the wide array of industrial applications of PDCPD. This new class of monomers was screened in homopolymerizations and in copolymerizations with norbornene.[14] The initial homopolymerization of *endo*-dicyclopentadiene (*endo*-DCPD) went to a low conversion of 15%, producing low-molecular weight, narrow-dispersity polymer ($M_n$ = 3.8 kDa, $Đ$ = 1.1). The PDCPD remained soluble and $^1$H NMR and GPC showed no signs of cross-linking. Additionally, a control experiment confirmed that cyclopentene does not undergo metathesis under MF-ROMP conditions. In contrast, while several methods to prepare linear, soluble PDCPD with metal ROMP initiators have been reported,[15] to many metal-mediated ROMP methods produce cross-linked PDCPD via olefin addition[15a-c] or olefin metathesis.[16] The MF-ROMP linear PDCPD was successfully cross-linked using thiol-ene click chemistry.

Efforts to optimize the homopolymerization of *endo*-DCPD by varying stoichiometry, temperature, and concentration increased conversion only to 20%. Random copolymerizations of *endo*-DCPD with norbornene were then evaluated at varying stoichiometries (Figure 1.6). While the amount of DCPD incorporated into the copolyemer was less than the theoretical, a linear correlation was observed between the mole fractions of DCPD loaded and DCPD incorporated. Molecular weight significantly decreased with increasing DCPD mole fraction, from 18.8 kDa at 10 mol % DCPD to 4.1 kDa at 90% DCPD. Interestingly, while DCPD conversions were low at high DCPD loadings DCPD conversions as high as 60% were observed at low DCPD mole fraction. This indicates that the lower reactivity of DCPD was not the cause of the low conversions at high DCPD loadings.

.

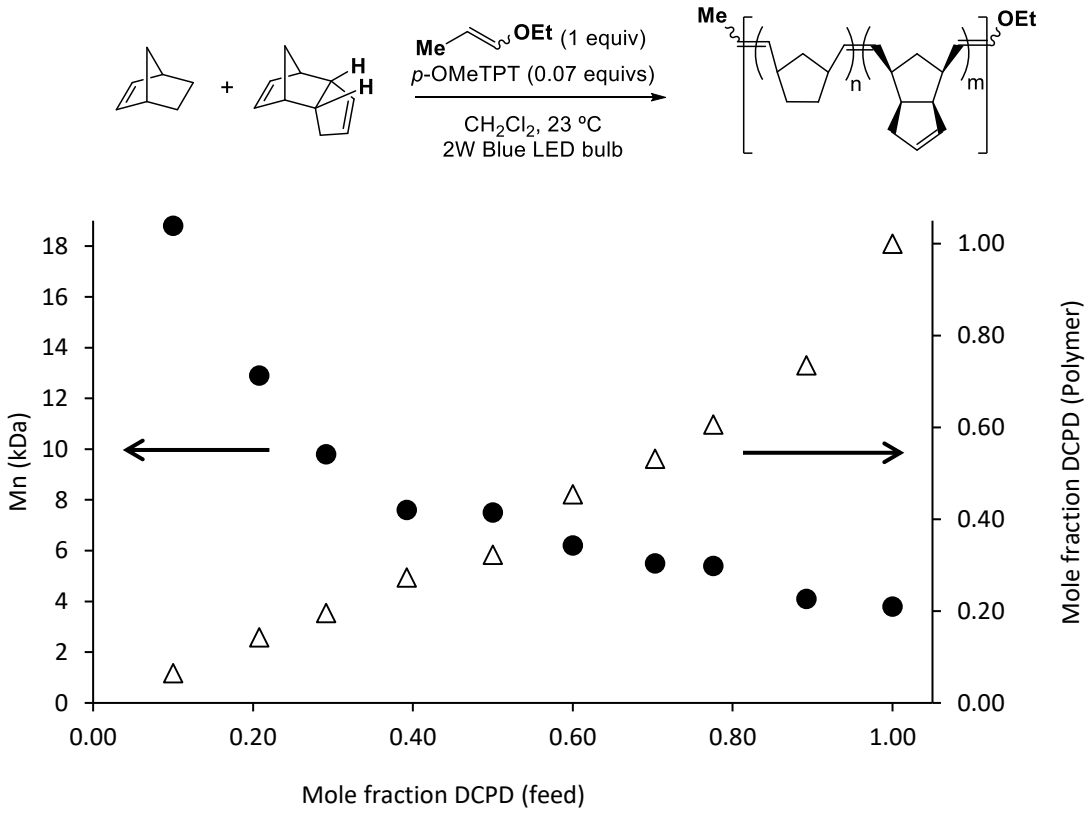


**Figure 1.9.** Top: Copolymerization of *endo*-dicyclopentadiene. Bottom: Plot of Mn (●) and DCPD incorporated into final polymer (△) vs DCPD loaded for DCPD/NB copolymerization.

Boydston and coworkers hypothesized that steric or electronic factors could limit conversions. They proposed that the *endo* orientation could undergo ring-opening metathesis to result in a propagating chain in which the propagating chain end is *syn* to the cyclopentene ring, diminishing the rate of monomer incorporation. Alternatively, the olefin of the cyclopentene ring may undergo a deleterious intramolecular reaction with the radical cation vinyl ether propagating chain end or with the cyclobutene radical cation.[17] To evaluate the impact of these factors on the polymerization of *endo*-DCPD, conversions were monitored over time for homopolymerizations of *endo*-DCPD, *exo*-dicyclopentadiene (*exo*-DCPD), *endo*-dihydrodicyclopentadiene (*endo*-

DCPD-$H_2$), and *exo*-dihydrodicyclopentadiene (*exo*-DCPD-$H_2$) (Figure 1.7). In contrast to metal-mediated ROMP, where *exo*-DCPD polymerizes substantially faster than *endo*-DCPD,[18] *endo*-DCPD and *exo*-DCPD MF-ROMP polymerizations reached the same conversion at similar rates. The relatively poor performance of *exo*-DCPD is attributed to intramolecular reactions of the cyclopentene olefin with the propagating radical cation.[17a-e] In contrast, *endo*-DCPD-$H_2$ reached moderate conversions of 50-60%. However, this conversion was likely limited by the polymer's poor solubility in the reaction solvent. The improved conversion of *endo*-DCPD-$H_2$ relative to *endo*-DCPD and *exo*-DCPD supports the hypothesis that intramolecular reactivity of the cyclopentene olefin with the vinyl ether radical cation plays a role in limiting conversion in MF-ROMP. The performance of *exo*-DCPD-$H_2$ was comparable to that of NB, reaching conversions of about 90%. This superior performance also indicates that intramolecular reactivity of the cyclopentene olefin limits conversion, and that steric hinderance in the *endo* isomer may also play a role in limiting conversion. Free cyclopentene spiked into the polymerization did not diminish conversions, which further supports the conclusion that intramolecular reactions of the cyclopentene olefin limit conversion.

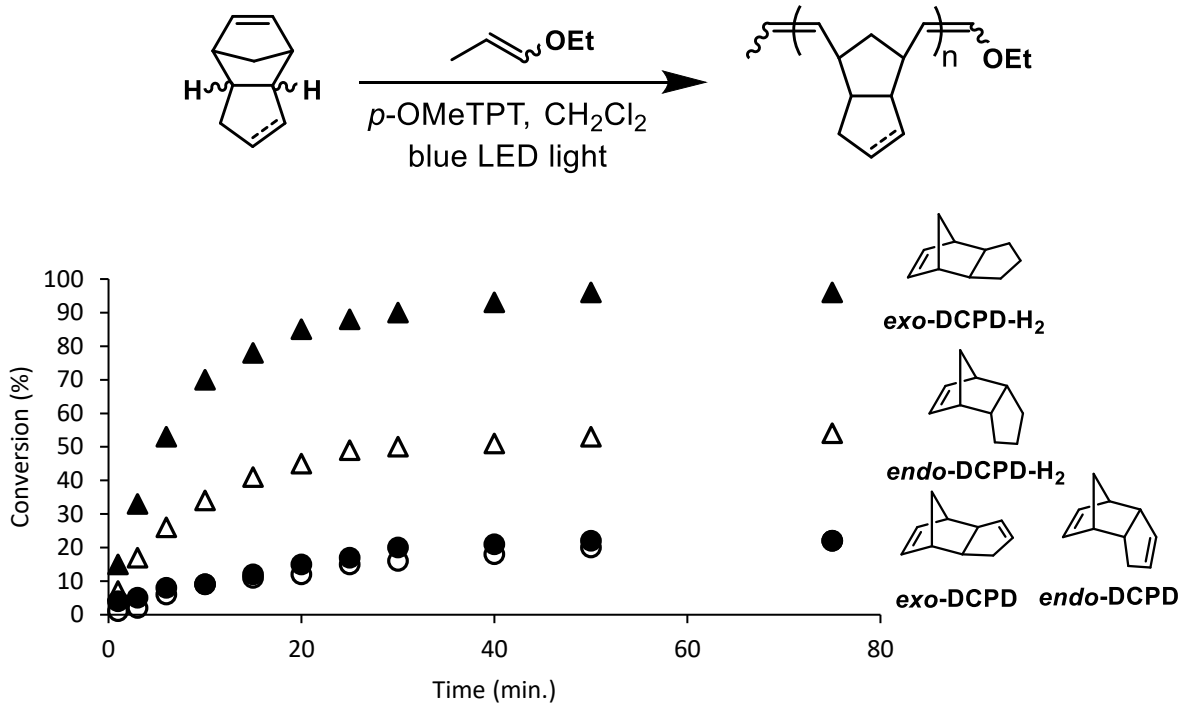


**Figure 1.10.** Plot of conversion vs time for monomers *endo*-DCPD (○), *exo*-DCPD (●), *endo*-DCPD-$H_2$ (△), and *exo*-DCPD-$H_2$ (▲) as determined by $^1$H NMR spectroscopy.

**Section 4: Summary**

Metal-mediated ROMP is a ground-breaking technology that has enabled advances in both industry and academia. Boydston and coworkers demonstrated the first metal-free approach to ROMP, which may offer both cost and purity advantages. Remarkably, photoredox-mediated MF-ROMP can be reversibly activated and deactivated with light cycling, enabling temporal control over the polymerization. Monomer scope to this point included both NB and the highly industrially relevant DCPD. Mechanistic investigations demonstrated that intramolecular reactivity with the with the propagating chain end can limit conversion. Several areas of ongoing investigation include exploring photo-oxidant systems for MF-ROMP, expanding the scope of MF-ROMP to produce functional ROMP polymers, evaluating MF-ROMP polymer structure,

and using chain transfer to control molecular weight. Current progress in these areas is discussed herein.

**Notes and References for Chapter 1**

[1] (a) Schrock, R. R. *Acc. Chem. Res*. **2014**, *47*, 2457−2466. (b) Sutthasupa, S.; Shiotsuki, M.; Sanda, F. *Polym. J*. **2010**, *42*, 905−915. (c) Bielawski, C. W.; Grubbs, R. H. *Prog. Polym. Sci*. **2007**, *32*, 1−29. (d) Rosebrugh, L. E.; Marx, V. M.; Keitz, B. K.; Grubbs, R. H. J. Am. Chem. Soc. **2013**, *135*, 10032−10035. (e) Jeong, H.; Kozera, D. J.; Schrock, R. R.; Smith, S. J.; Zhang, J.; Ren, N.; Hillmyer, M. A. *Organometallics*. **2013**, *32*, 4843−4850. (f) Forrest, W. P.; Axtell, J. C.; Schrock, R. R. *Organometallics*. **2014**, *33*, 2313−2325. g) Slugovc, C. *Macromol. Rapid. Commun.* **2004**, *25*, 1283-1297. g) Leitgeb, A.; Wappel, J.; Slugovc, C. *Polymer*. **2010**, *51*, 2927-2946.

[2] Mol, J. C. *J. Mol. Catal. A: Chem.* **2004**, *213*, 39.

[3] (a) Chauvin, Y. *Angew. Chem., Int. Ed*. **2006**, *45*, 3740−3747. (b) Schrock, R. R. *Angew. Chem., Int. Ed*. **2006**, *45*, 3748−3759. (c) Grubbs, R. H. *Angew. Chem., Int. Ed*. **2006**, *45*, 3760−3765.

[4] a) METTON Liquid Molding Resin ®. METTON Applications. https://www.metton.com/about-metton-lmr/applications#industrial (accessed Aug 1, 2018). b) Telene® Innovative Chemistry for Designers. Transportation Case Study. https://www.telene.com/ Case_Studies_Transportation.aspx.html (accessed Aug 1, 2018). c) Telene® Innovative Chemistry for Designers. Agriculture Case Study. https://www.telene.com/ Case_Studies_Agriculture.aspx.html (accessed Aug 1, 2018). d) Telene® Innovative Chemistry for Designers. Construction Case Study. https://www.telene.com/ Case_Studies_Construction.aspx.html (accessed Aug 1, 2018). e) Zeon. Products: RIM. http://www.zeon.co.jp/business_e/enterprise/rim/index.html (accessed Aug 1, 2018). f) Materia. The Next Generation of Thermoset Resins. http://www.materia-inc.com/products/thermoset-resins (accessed Aug 1, 2018). g) Materia. Proxima: Thermosets for Subsea Insulation. http://oilandgas.materia-inc.com/products/thermosets-for-subsea-insulation (accessed Aug 1, 2018).

[5] Sigma-Aldrich. Grubbs Catalyst 2nd Generation. https://www.sigmaaldrich.com/catalog/ product/aldrich/569747?lang=en&region=US (accessed Aug 1, 2018).

[6] Sigma-Aldirch. Ethyl-1-Propenyl Ether, Mixture of *cis* and *trans*. https://www.sigmaaldrich.com/catalog/product/aldrich/364045?lang=en&region=US (accessed Aug 1, 2018).

[7] Voughalis, G. C. *Chem. Eur. J.* **2012**, *18*, 8868-8880.

[8] a) Miura, T.; Kim, S.; Kitano, Y.; Tada, M.; Chiba, K. *Angew. Chem. Int. Ed.* **2006**, *45*, 1461-1463. b) Chiba, K.; Miura, T.; Kim, S.; Kitano, Y.; Tada, M. *J. Am. Chem. Soc.* **2001**, *123*, 11314-11315.

[9] a) Ogawa, K. A.; Goetz, A. E.; Boydston, A. J. *J. Am. Chem. Soc.* **2015**, *137*, 1400–1403. b) Ogawa, K. A.; Goetz, A. E.; Boydston, A. J. *Synlett*. **2016**, *27*, 203-214.

[10] a) Xu, J.; Jung, K.; Atme, A.; Shanmugam, S.; Boyer, C. *J. Am. Chem. Soc.* **2014**, *136*, 5508-5519. b) Xu, J.; Jung, K.; Corrigan, N. A.; Boyer, C. *Chem. Sci.* **2014**, *5*, 3568-3575. c) Xu, J.; Jung, K.; Boyer, C. *Macromolecules*. **2014**, *47*, 4217-4229. d) Shanmugam, S.; Xu, J.; Boyer, C. *Macromolecules*, **2014**, *47*, 4930-4942. e) Miyake, G. M.; Theriot, J. C. *Macromolecules*. **2014**, *47*, 8255-8261. f) Poelma, J. E.; Fors, B. P..; Meyers, G. F.; Kramer, J. W.; Hawker, C. J. *Angew. Chem. Int. Ed.* **2013**, *52*, 6844-6848. g) Fors, B. P.; Hawker, C. J. *Angew. Chem. Int. Ed.* **2012**,

*51*, 8850-8853. h) Dadashi-Silab, S.; Doran, S.; Yagci, Y. *Chem. Rev*. **2016**, *116*, 10212-10275. i) Shanmugam, S.; Xu, J.; Boyer, C. *J. Am. Chem. Soc*. **2015**, *137*, 9174−9185. j) Perkowski, A. J.; You, W.; Nicewicz, D. A. *J. Am. Chem. Soc*. **2015**, *137*, 7580−7583. k) Jung, K.; Xu, J.; Zetterlund, P. B.; Boyer, C. ACS Macro Lett. **2015**, *4*, 1139−1143. l) Xu, J.; Shanmugam, S.; Duong, H. T.; Boyer, C. Polym. Chem. **2015**, *6*, 5615−5624. (m) Chen, M.; MacLeod, M. J.; Johnson, J. A. ACS Macro Lett. **2015**, *4*, 566−569. (n) Melker, A.; Fors, B. P.; Hawker, C. J.; Poelma, J. E. *J. Polym. Sci., Part A: Polym. Chem*. **2015**, *53*, 2693−2698. (o) Chen, Y.; Hu, Z.; Xu, D.; Yu, Y.; Tang, X.; Guo, H. *Macromol. Chem. Phys*. **2015**, *216*, 1055−1060.

[11] a) Riener, M.; Nicewicz, D. A. *Chem. Sci.* **2013**, *4*, 2625-2629. b) Ischay, M. A.; Ament, M. S.; Yoon, T. P. *Chem. Sci.* **2012**, *3*, 2807-2811. c) Du, J.; Skubi, K. L.; Schultz, D. M.; Yoon, T. P. *Science*. **2014**, *344*, 392-396. d) Schultz, D. M.; Yoon, T. P. *Science*. **2014**, *343*, 1239176-1-1239176-8. e) Nicewicz, D. A.; Nguyen, T. M. *ACS Catal.* **2014**, *4*, 355-360.

[12] a) Sutterer, A.; Moeller, K. D. *J. Am. Chem. Soc*. **2000**, *122*, 5636−5637. b) Duan, S.; Moeller, K. D. *J. Am. Chem. Soc*. **2002**, *124*, 9368−9369. c) Liu, B.; Duan, S.; Sutterer, A. C.; Moeller, K. D. *J. Am. Chem. Soc*. **2002**, *124*, 10101−10111. d) Perkowski, A. J.; You, W.; Nicewicz, D. A. *J. Am. Chem. Soc*. **2015**, *137*, 7580−7583.

[13] Choi, T.-L.; Grubbs, R. H. *Angew. Chem., Int. Ed*. **2003**, *42*, 1743−1746.

[14] Goetz, A. E.; Boydston, A. J. *J. Am. Chem. Soc.* **2015**, *137*, 7572-7575.

[15] a) Davidson, T. A.; Wagener, K. B.; Priddy, D. B. *Macromolecules*. **1996**, *29*, 786−788. b) Davidson, T. A.; Wagener, K. B. *J. Mol. Catal. A: Chem*. **1998**, *133*, 67−74. c) Davidson, T. A.; Wagener, K. B. *Polymer Preprints.* **1996**, *37*, 323-324. d) Hayano, S.; Kurakata, H.; Tsunogae, Y.; Nakayama, Y.; Sato, Y.; Yasuda, H. *Macromolecules*. **2003**, *36*, 7422−7431. e) Yao, Z.; Wang, Z.; Yu, Y.; Zeng, C.; Cao, K. *Polymer*. **2017**, *119*, 98-106.

[16] Fisher, R. A.; Grubbs, R. H. *Makromol. Chem., Macromol. Symp*. **1992**, *63*, 271−277.

[17] a) Miyashi, T.; Konno, A. *J. Am. Chem. Soc*. **1988**, *110*, 3676− 3677. b) Parrish, J. D.; Ischay, M. A.; Lu, Z.; Guo, S.; Peters, N. R.; Yoon, T. P. *Org. Lett*. **2012**, *14*, 1640−1643. c) Gesmundo, N. J.; Nicewicz, D. A. *Beilstein J. Org. Chem*. **2014**, *10*, 1272−1281. d) Schenck, G. O.; Steinmetz, R. *Bull. Soc. Chim. Belg*. **1962**, *71*, 781−800. e) Schenck, G. O.; Steinmetz, R. *Chem. Ber*. **1963**, 96. f) Shida, T.; Momose, T.; Ono, N. J. Phys. Chem. 1985, 89, 815− 820.

[18] Rule, J. D.; Moore, J. S. *Macromolecules.* **2002**, *35*, 7878−7882.

# Chapter 2. Comparison of Pyrylium and Thiopyrylium Photooxidants in Metal-Free Ring-Opening Metathesis Polymerization[1]

## Section 1: Introduction

One of many factors likely to influence the equilibrium that governs chain end (de)activation is the nature of the photo-oxidant, which serves as a co-initiator and redox mediator throughout the polymerization.[1] Our initial investigations identified pyrylium salt **1a** (Figure 1) as an effective photo-oxidant in MF-ROMP, but extensive screening of different oxidants was not carried out.[2] It is reasonable to expect multiple variables, including excitation efficiency, excited state reduction potential, efficiency of intersystem crossing, and electron transfer via singlet versus triplet excited states each impact the ability of a photo-oxidant to initiate and moderate MF-ROMP. Unfortunately, predictive power with pyrylium-based systems is limited and often reaction-specific.[3] Therefore, systematic structural variation and evaluation of pyrylium and closely related thiopyrylium species is warranted.

## Section 2: Results and Discussion

### *2.2.a Pyrylium Efficacy*

To investigate, we evaluated a series of pyrylium and thiopyrylium photo-oxidants in the MF-ROMP of norbornene (Figure 1). The photo-oxidants (**1** – **4**) were easily prepared from reported procedures.[2c,4] Polymerizations were conducted in $CH_2Cl_2$ with norbornene as monomer

[1] Reproduced with permission from Pascual, L. M. M; Dunford, D. G.; Goetz, A. E.; Ogawa, K. A.; Boydston, A. J. "Comparison of Pyrylium and Thiopyrylium Photooxidants in Metal-Free Ring-Opening Metathesis Polymerization" *Synlett.* **2016**, *27*, 759. Copyright 2016 Georg Thieme Verlag KG.

(initial concentration = 1.8 M) and ethyl propenyl ether as initiator.[5] Each photo-oxidant was evaluated using an initial of ratio of monomer, initiator, and photo-oxidant of 2000:20:1, respectively. The solutions were irradiated with blue LEDs for 75 min, at which point monomer conversions were determined by $^1$H NMR analysis; key data are summarized in Table 1. In each case, maximum conversion appeared to be reached within the 75-min experiments.

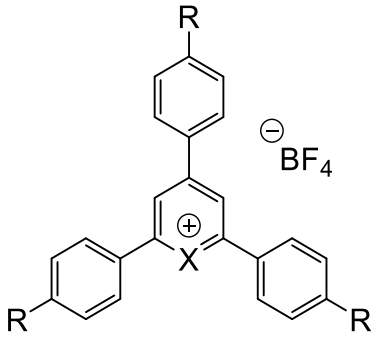


**1a**: X = O, R = OMe
**1b**: X = S, R = OMe
**2a**: X = O, R = Ph
**2b**: X = S, R = Ph
**3a**: X = O, R = Me
**3b**: X = S, R = Me
**4a**: X = O, R = H
**4b**: X = S, R = H

**Figure 2.1**. Structures of pyrylium and thiopyrylium salts used in this study.

**Table 2.1**. Results of MF-ROMP using pyrylium and thiopyrylium photo-oxidants.

| Photo-oxidant | $E^*_{red}$ (V vs. SCE)[a] | Conversion (%)[b] | $M_w$ (kDa)[c] | $Đ$[d] |
|---|---|---|---|---|
| **1a** | 1.89 | 75 ± 4 | 20.0 | 1.5 |
| **1b** | 1.86 | 84 ± 1 | 36.3 | 1.6 |
| **2a** | 2.02 | 31 ± 1 | 7.4 | 1.4 |
| **2b** | 2.02 | 52 ± 3 | 13.3 | 1.4 |
| **3a** | 2.23 | 12 ± 1 | 5.5 | 1.2[e] |
| **3b** | 2.20 | 26 ± 1 | 7.3 | 1.5 |
| **4a** | 2.46 | 9 ± 1 | n.d. | n.d. |
| **4b** | 2.41 | < 5 | n.d. | n.d. |

[a]Calculated excited state reduction potential based upon ground-state reduction potential determined by combination of cyclic voltammetry and photoluminescence blue-edge excitation energy (see Experimental). For previous examples of $E^*_{red}$, see Ref. 2c. [b]Conversion of norbornene to PNB as determined using $^1$H NMR spectroscopy to compare signals corresponding to norbornene and PNB; average of three runs, errors represent standard deviations. [c]Weight-average molecular weight determined by gel-permeation chromatography with in-line multi-angle laser light scattering detection for a representative experiment. [d]Molecular weight dispersity ($M_w/M_n$) determined by gel-permeation chromatography with in-line refractive index detection for a representative experiment. [e]Low $Đ$ likely due to fractionation.

Across the series of pyrylium salts, increasing $E_{red}$ corresponded to lower monomer conversion. Notably, the strongest oxidants in the series have $E_{red}$ values that may give rise to non-selective and deleterious reaction pathways. For example, higher oxidizing potentials may lead to oxidation of norbornene and PNB main chain olefins, as well as over-oxidation of the vinyl ether. Additionally, when a second portion of photo-oxidant was added to the reaction mixtures, we did not observe any further conversion of monomer. This indicated to us that any vinyl ether species had been consumed. Thus, judicious choice over the strength of photo-oxidant is critical as the strongest oxidants did not lead to the most successful polymerizations.

In each pyrylium/thiopyrylium pair for which successful MF-ROMP was observed (**1** – **3**), the thiopyrylium resulted in higher conversion than the similarly functionalized pyrylium salt. For example, **1b** emerged as a promising photo-oxidant and slightly outperformed **1a**, which was used in our previous studies. Although conversion decreased moving through the series, **2b** and **3b** reached higher conversion than **2a** and **3a**, respectively.

To directly compare the highest performing photo-oxidants (**1a** and **1b**) over the course of the polymerization, we monitored the conversion over time when each photo-oxidant was employed (Figure 2). The two photo-oxidants consistently led to equally high conversion, but it was clear that during the polymerization the thiopyrylium **1b** led to higher conversion at the same time intervals in comparison with **1a**. The ability to reach a critical conversion in shorter time may prove particularly advantageous in applications requiring gelation or crosslinking, for example.

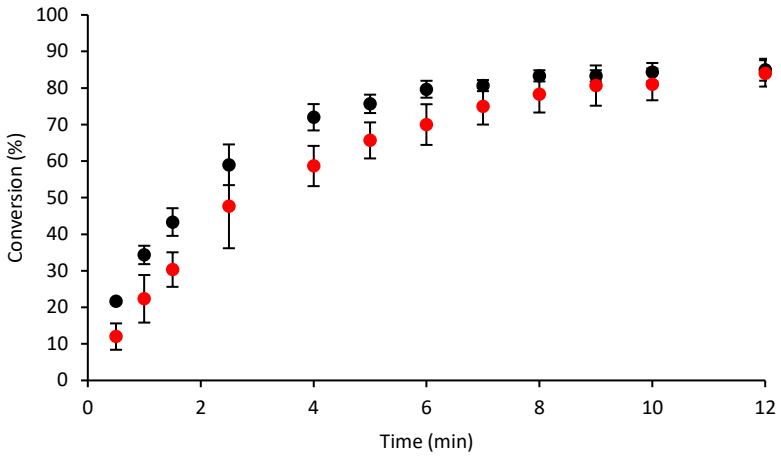


**Figure 2.2**. Plot of conversion versus time using photo-oxidants 1a (red) and 1b (black) in MF-ROMP of norbornene. Data points represent an average of three runs, error bars = one standard deviation.

Molecular weights of isolated PNB were generally consistent across the series of photo-oxidants (Table 1) when taking into account the specific monomer conversion in each experiment. Molecular weight dispersity (*Đ*) was also similar for each experiment. Collectively, these results suggested to us that the *relative* rates of initiation and propagation are not strongly influenced by the nature of the photo-oxidant, as would be expected from the similar oxidation potentials between the initiator and chain end vinyl ethers. One apparent exception, however, was the higher molecular weight obtained when **1b** was employed.

*2.2.b Photophysical Properties of Photo-oxidants*

Analysis of the UV-vis absorption spectrum of each photo-oxidant (**1** – **4**) revealed varying degrees of overlap with the wavelength output of the blue LEDs used to drive the polymerizations (Figure 3). Specifically, the blue light output spanned from ca. 430 – 490 nm,

with $\lambda_{max}$ = 458 nm. Photo-oxidants **1** and **2** each displayed good energy overlap with the blue LED output, with **2a** having the greatest molar absorptivity in that range of wavelengths. Notably, use of **2a** resulted in relatively low yield in comparison with the other photo-oxidants. On the other hand, **2b** has considerably lower molar absorptivity in the region of overlap with the blue LED output and yet led to higher conversion than **2a**. These results further highlight the challenges of correlating single physicochemical properties of the photo-oxidant with MF-ROMP reaction efficiency. It may be expected that moving to shorter wavelengths could entice greater reaction efficiency from **3** and **4**, however this would also compromise the inherent advantages of using visible instead of ultraviolet light.

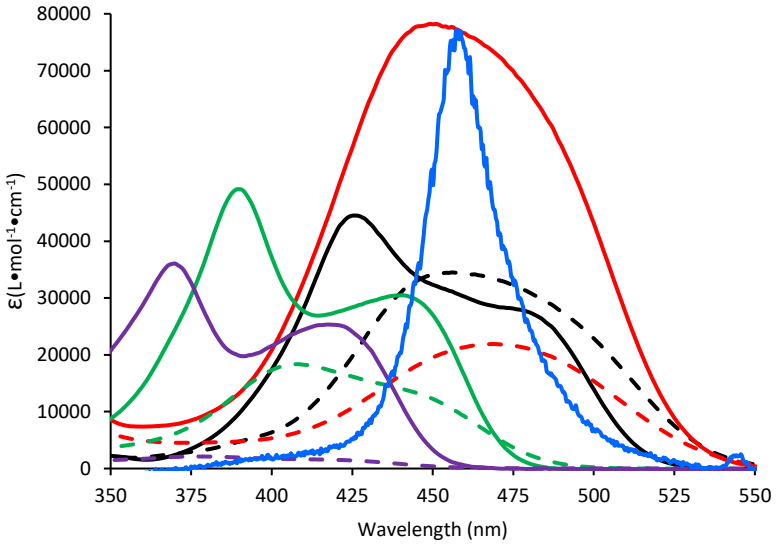


**Figure 2.3**. Overlay of UV/vis absorption spectra of photo-oxidants **1 – 4** and optical output from blue LEDs used for MF-ROMP. Photo-oxidants: **1** (black), **2** (red), **3** (green), **4** (purple); solid lines are pyrylium salts, dashed lines are thiopyrylium salts. Blue LED output intensity (solid blue line) is arbitrarily scaled for visual comparison.

## Section 3: Conclusions

In conclusion, we have evaluated a series of pyrylium and thiopyrylium salts which revealed discernible trends in efficacy toward facilitating MF-ROMP. Throughout the series, thiopyrylium variants led to higher conversion of monomer than their corresponding pyrylium counterparts. Notably, more strongly oxidizing mediators did not result in higher conversion within the series, and clear correlations between photophysical properties of the (thio)pyrylium salts and efficiency in MF-ROMP could not be drawn. We observed higher rate of polymerization from the most effective thiopyrylium photo-oxidant than from any of the pyrylium species in the series. These results suggest to us that continued examination of photo-oxidants for MF-ROMP may be most fruitful from pursuing milder photo-oxidants based upon thiopyrylium structures.

## Section 4: Experimental

### *2.4.a General Considerations*

Dichloromethane ($CH_2Cl_2$) and tetrahydrofuran (THF) were obtained from a solvent purification system. $^1H$ and $^{13}C$ NMR spectra were recorded on Bruker AVance 300 MHz or 500 MHz spectrometers. Chemical shifts are reported in delta (δ) units, expressed in parts per million (ppm) downfield from tetramethylsilane using the residual protio-solvent as an internal standard ($CDCl_3$, $^1H$: 7.26 ppm; DMSO-$d_6$, $^1H$: 2.49 ppm and $^{13}C$: 39.5 ppm). Gel permeation chromatography (GPC) was performed using a GPC setup consisting of: a Shimadzu pump, 3 in-line columns, and Wyatt light scattering and refractive index detectors with tetrahydrofuran (THF) as the mobile phase. Number-average molecular weights ($M_n$) and weight-average molecular weights ($M_w$) were calculated from light scattering and refractive index data. All

polymerizations were carried out under an inert atmosphere of nitrogen in standard borosilicate glass vials purchased from Fisher Scientific with magnetic stirring unless otherwise noted. Irradiation of photochemical reactions was done using a 2 W Miracle blue LED indoor gardening bulb. The output of the blue LED bulb was measured using an Ocean Optics USB2000 spectrometer. The (thio)pyrylium tetrafluoroborate salts were prepared according to literature procedure.[2c,4] Norbornene was sublimed prior to use. All other reagents and solvents were obtained from commercial sources and used as received unless otherwise noted.

*2.4.b Cyclic Voltammetry*

Inside a glovebox under $N_2$ atmosphere, 1.0 mmol (67 mM) of photo-oxidant and 320 mg (0.200 M) $LiClO_4$ were dissolved in 15 mL of anhydrous acetonitrile ($CH_3CN$) from the solvent still in a 3-neck round bottom flask equipped with a stir bar. The flask was sealed with septa pierced with a glassy carbon working electrode (3 mm), a Pt basket counter electrode (Premier Lab Supply), and a 0.1 M $Ag/AgNO_3$ reference electrode (0.1 M $AgNO_3$ in dry $CH_3CN$). The cell was removed from the glovebox and equipped with a $N_2$ balloon. The mixture was stirred prior to cyclic voltammetry measurements. Cyclic voltammograms (CVs) were obtained using a BASi Epsilon potentiostat. Ferrocene (0.15 mmol) was added as an internal standard after each voltammogram and a subsequent CV was taken.

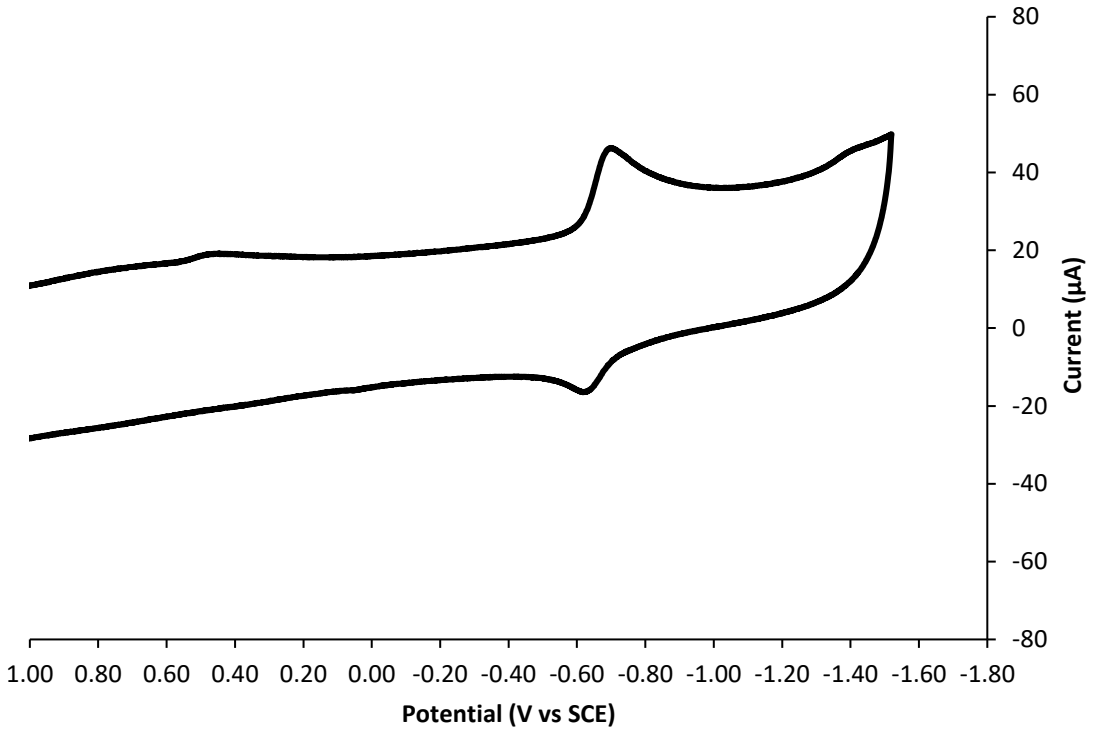


**Figure 2.4**. Cyclic voltammogram of photo-oxidant **1a**.

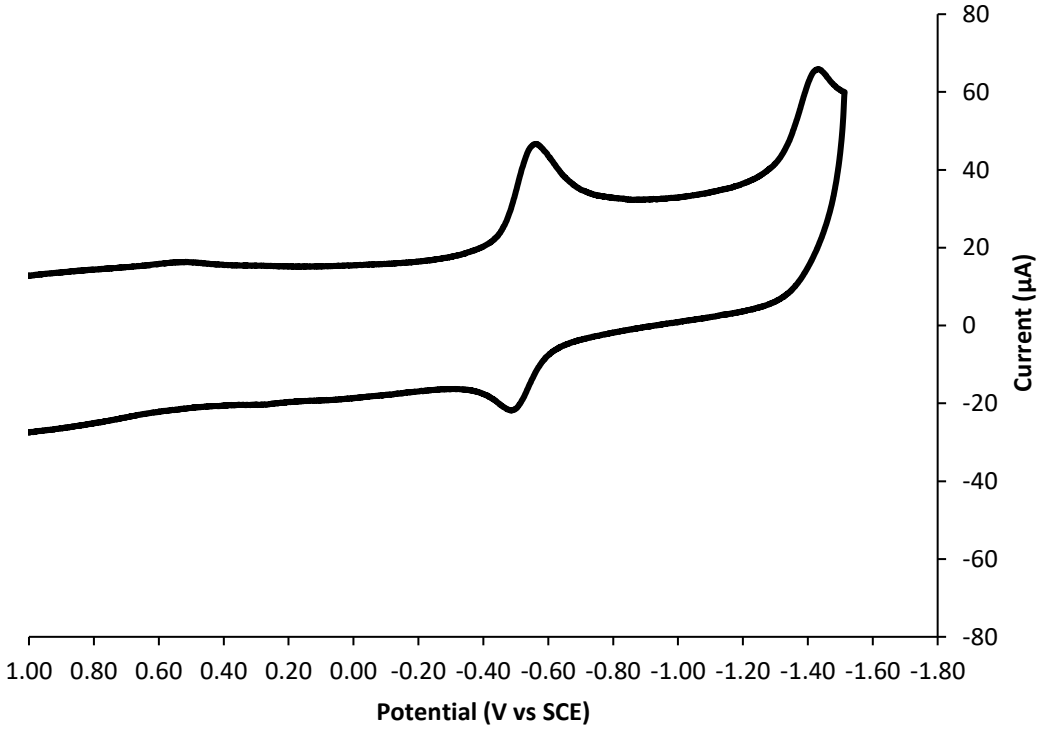


**Figure 2.5**. Cyclic voltammogram of photo-oxidant **1b**.

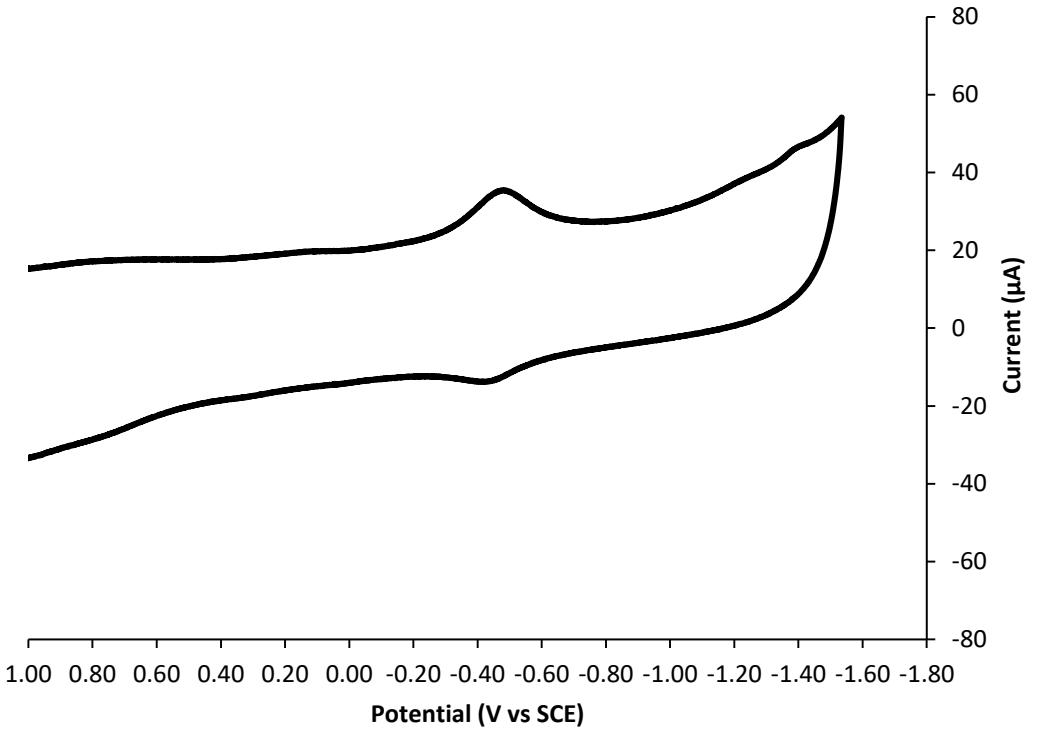


**Figure 2.6**. Cyclic voltammogram of photo-oxidant **2a**.

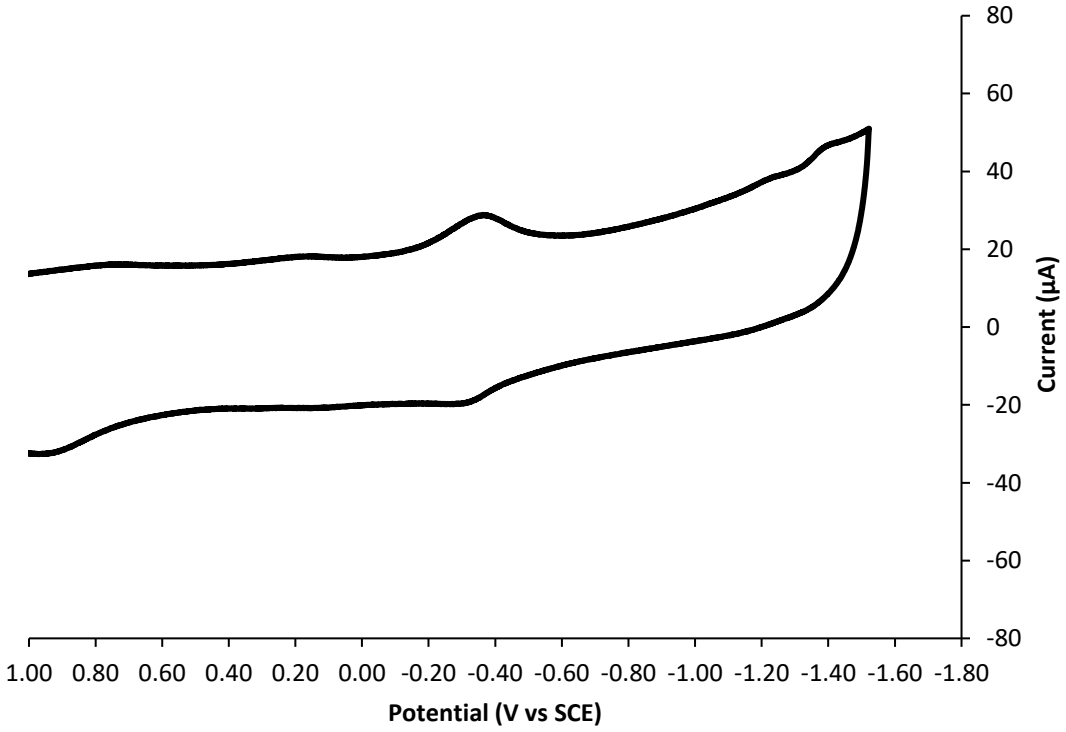


**Figure 2.7**. Cyclic voltammogram of photo-oxidant **2b**.

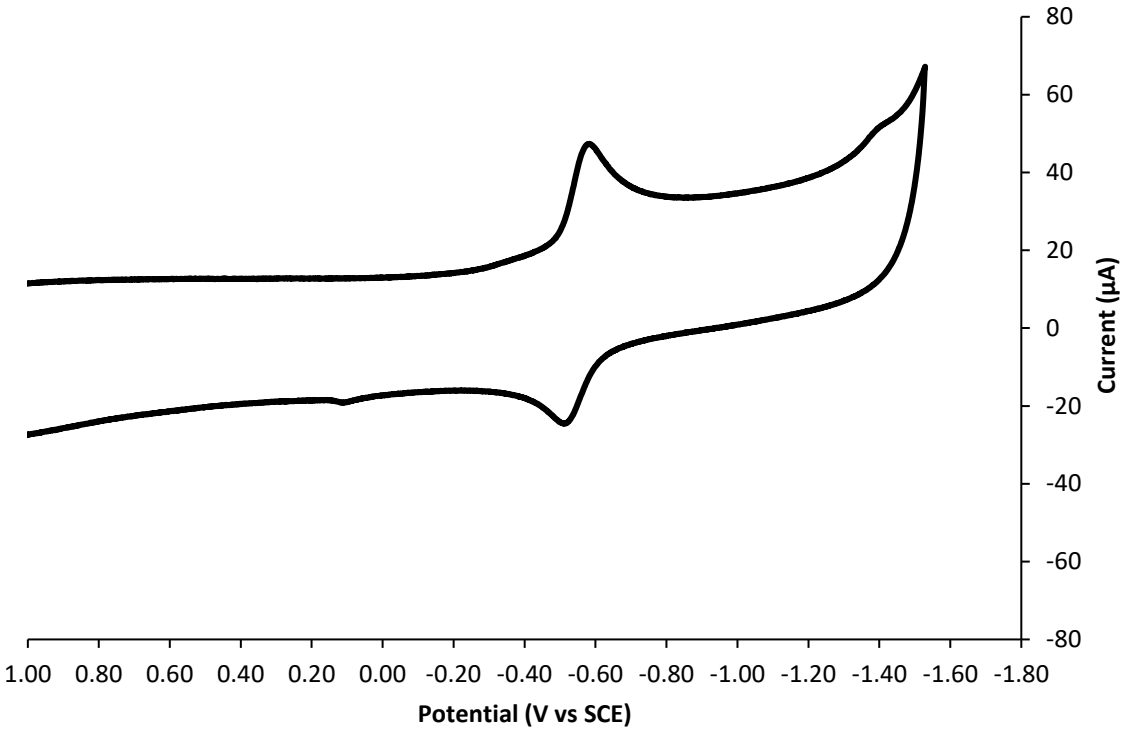


**Figure 2.8**. Cyclic voltammogram of photo-oxidant **3a**.

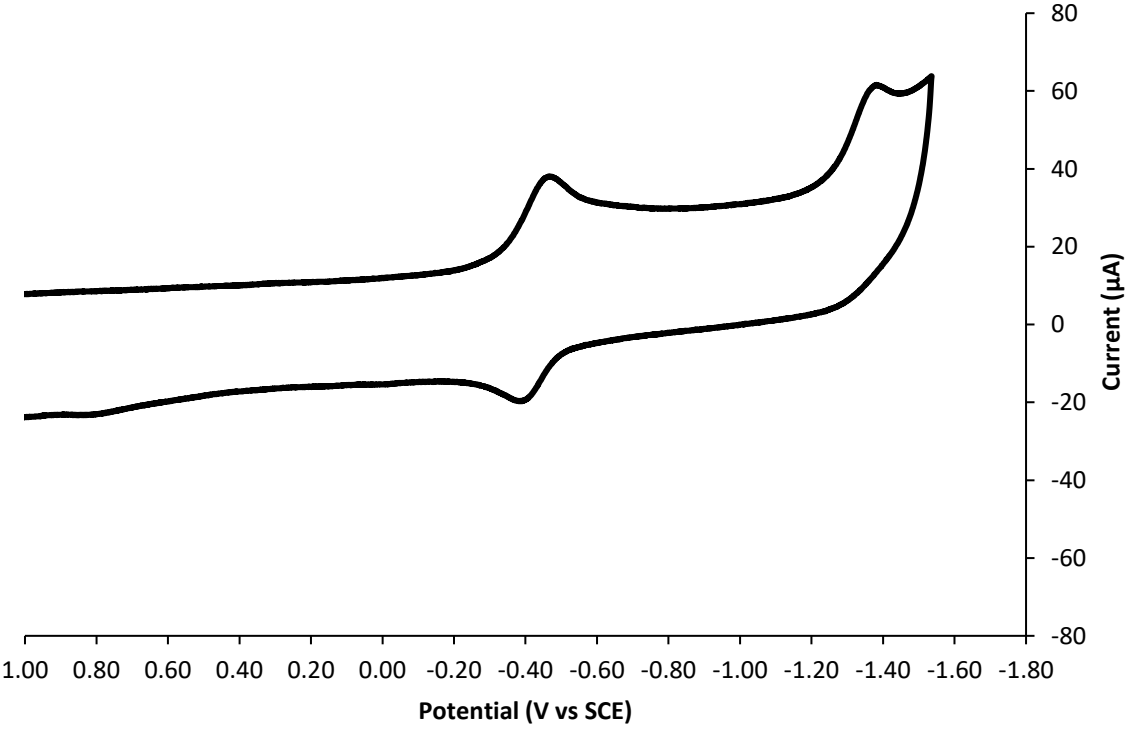


**Figure 2.9**. Cyclic voltammogram of photo-oxidant **3b**.

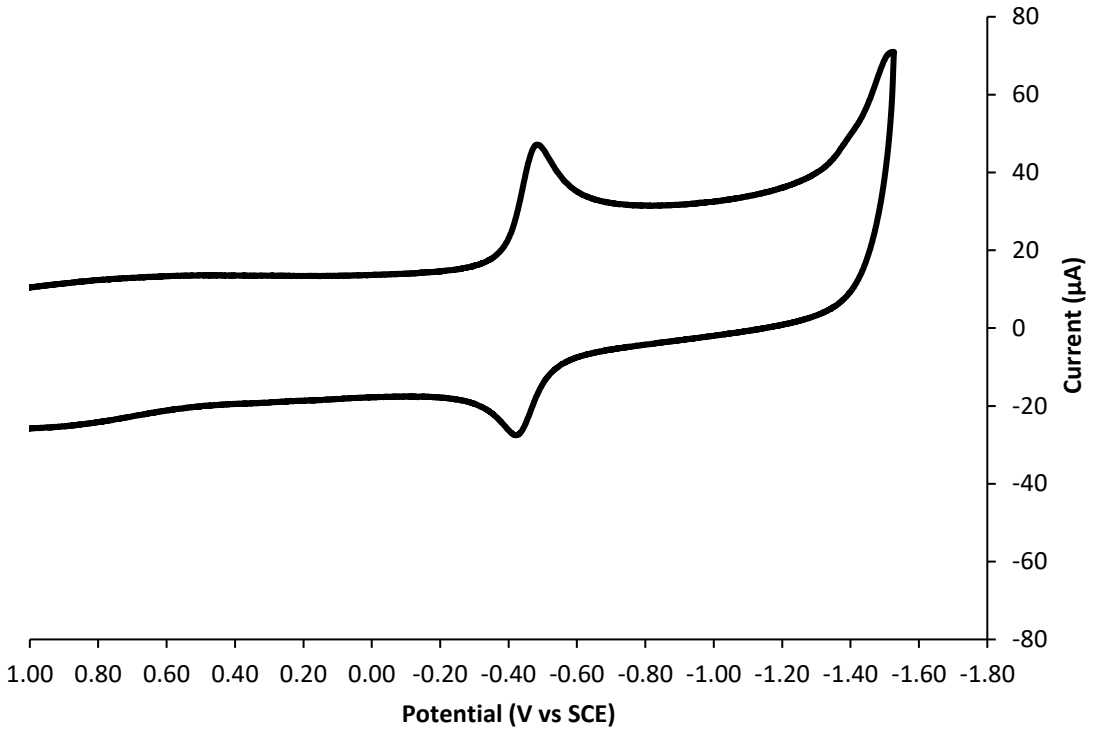


**Figure 2.10**. Cyclic voltammogram of photo-oxidant **4a**.

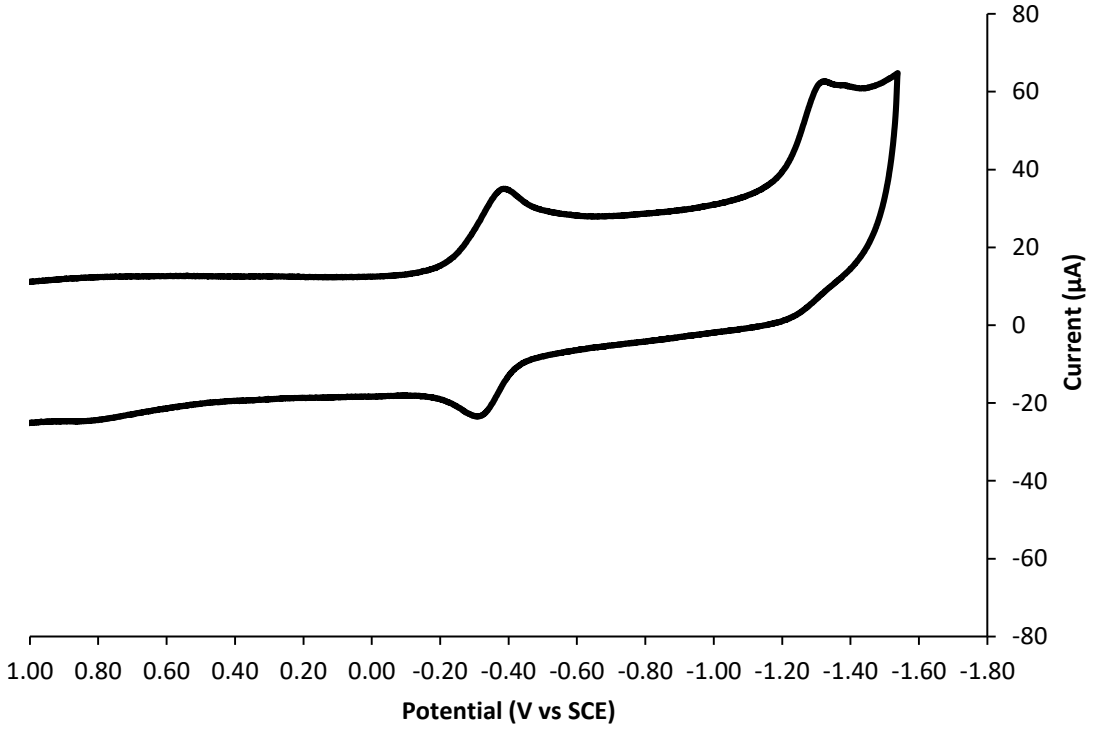


**Figure 2.11**. Cyclic voltammogram of photo-oxidant **4b**.

*2.4.c Photoluminescence Data and Excited State Reduction Potential Calculations for Photo-oxidants*

A Horiba Fluorolog FL3 was used to obtain photoluminescence spectra of 1 µg/mL solutions of each photo-oxidant in acetonitrile. The blue-edge wavelength was determined as the shortest wavelength at which 10% of the maximum emission intensity was observed. This value was used to calculate an excitation energy for each photo-oxidant.

**Table 2.2**. Excitation wavelengths for photoluminescence of photo-oxidants.

| photo-oxidant | excitation wavelength (nm) |
|---|---|
| **1a** | 420 |
| **1b** | 450 |
| **2a** | 450 |
| **2b** | 470 |
| **3a** | 395 |
| **3b** | 410 |
| **4a** | 365 |
| **4b** | 375 |

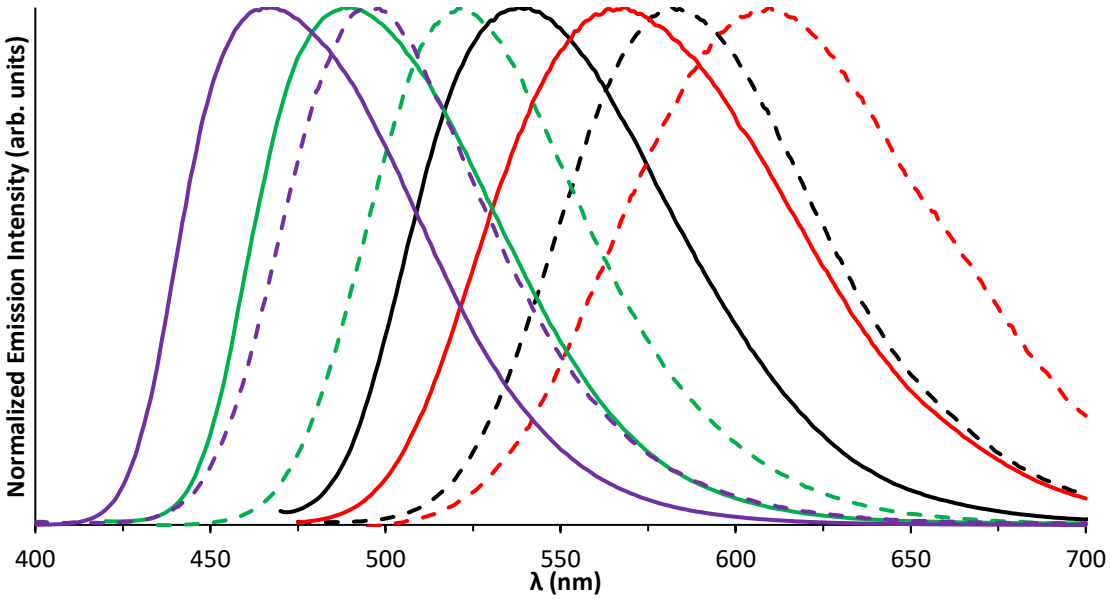


**Figure 2.12.** Normalized photoluminescence spectra of photo-oxidants **1** – **4** in acetonitrile: **1** (black), **2** (red), **3** (green), **4** (purple); solid lines are pyrylium salts, dashed lines are thiopyrylium salts.

**Table 2.3.** Ground and excited state reduction potentials for photo-oxidants.

| photo-oxidant | $E_{red}$ (V vs SCE)[a] | blue edge (nm)[b] | excitation energy (eV) | $E^*_{red}$ (V vs SCE)[c] | $E^*_{red}$ (V vs SCE) from Ref. 1[d] |
|---|---|---|---|---|---|
| **1a** | -0.661 | 486 | 2.55 | 1.89 | 1.74 |
| **1b** | -0.524 | 521 | 2.38 | 1.86 | 1.80 |
| **2a** | -0.451 | 501 | 2.47 | 2.02 | 1.83 |
| **2b** | -0.322 | 530 | 2.34 | 2.02 | - |
| **3a** | -0.547 | 446 | 2.78 | 2.23 | 2.03 |
| **3b** | -0.427 | 471 | 2.63 | 2.20 | - |
| **4a** | -0.452 | 426 | 2.91 | 2.46 | 2.29 |
| **4b** | -0.348 | 449 | 2.76 | 2.41 | 2.35 |

[a]Ground state reduction potential measured by cyclic voltammetry. [b]Shortest wavelength at which 10% of the maximum emission intensity was observed. [c]Excited state reduction potential = $E_{red}$ + excitation energy. [d]These values were calculated using the photoluminescence $\lambda_{max}$.

*2.4.d Polymerization of norbornene*

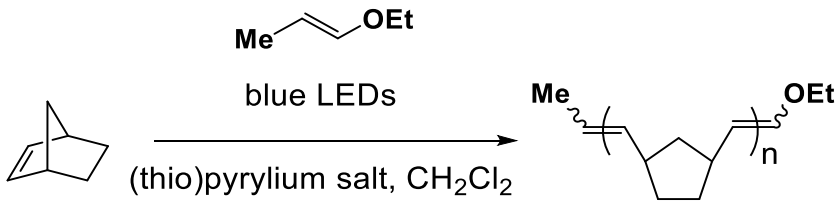



**Figure 2.13.** Polymerization setup for MF-ROMP of NB. The reaction mixture was stirred and irradiated for 75 min at a distance of 1 cm using a 2-W (total output) blue LED light source.

**Table 2.4.** Percent conversion of NB to PNB via MF-ROMP.

| entry | 1a | 1b | 2a | 2b | 3a | 3b | 4a | 4b |
|---|---|---|---|---|---|---|---|---|
| trial 1 | 80 | 85 | 32 | 55 | 12 | 26 | 9 | < 5 |
| trial 2 | 73 | 84 | 31 | 53 | 13 | 25 | 10 | < 5 |
| trial 3 | 73 | 84 | 30 | 49 | 12 | 26 | 8 | < 5 |
| average | 75 | 84 | 31 | 52 | 12 | 26 | 9 | < 5 |
| std. dev. | 4 | 1 | 1 | 3 | 1 | 1 | 1 | n/a |

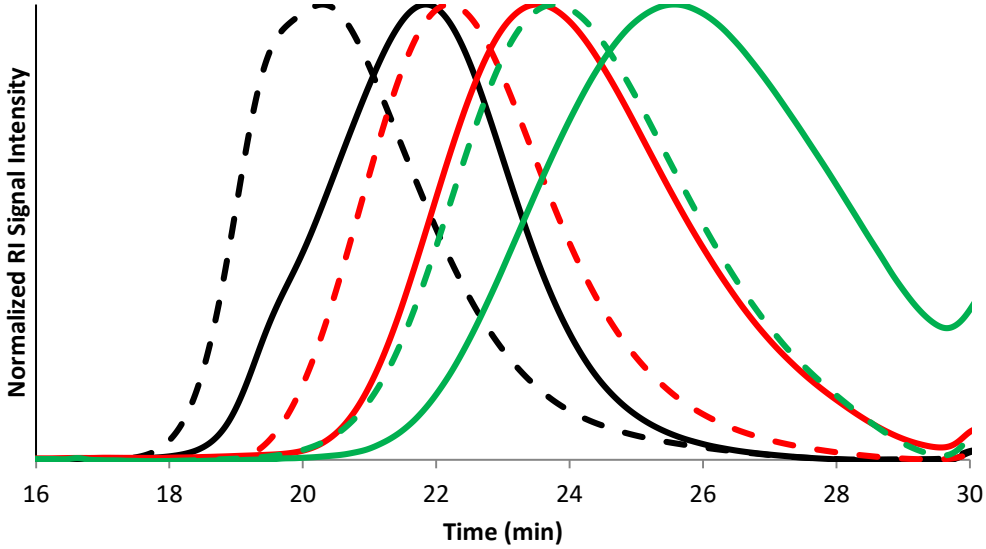


**Figure 2.14.** GPC traces of PNB produced via MF-ROMP using photo-oxidants **1** (black), **2** (red), and **3** (green); solid lines are pyrylium salts, dashed lines are thiopyrylium salts.

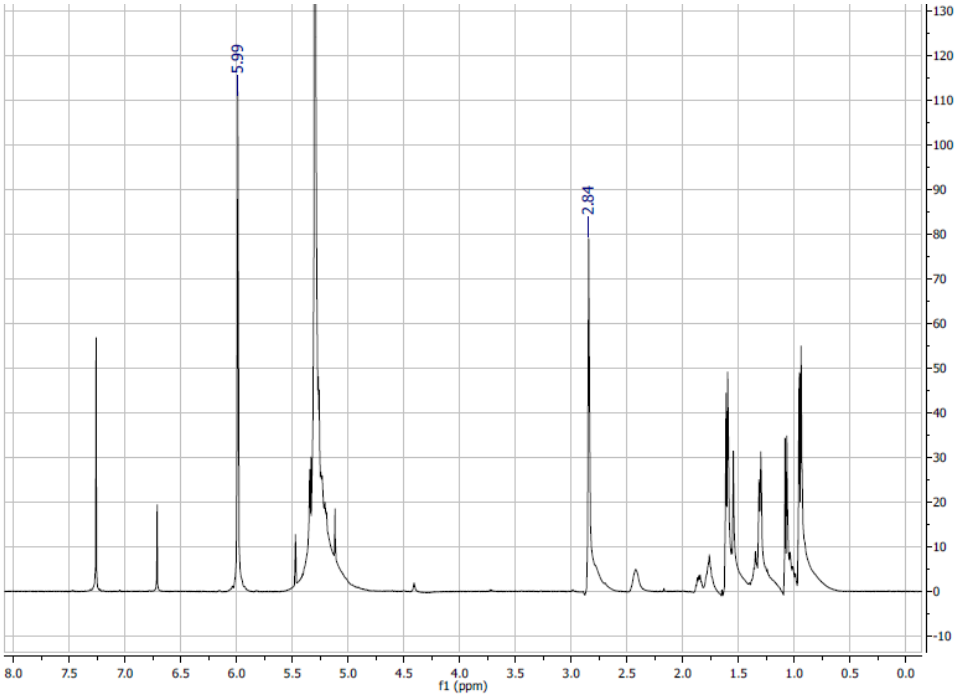


**Figure 2.15.** $^{1}$H NMR spectrum of a reaction aliquot showing unreacted NB (δ 5.99 and 2.84 ppm).

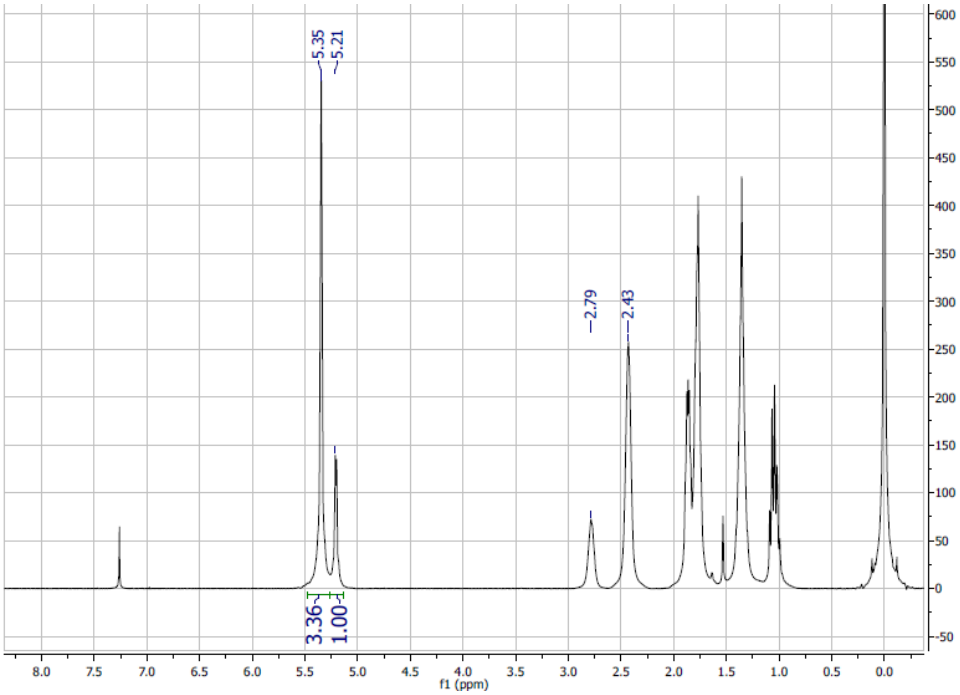


**Figure 2.16.** $^{1}$H NMR spectrum of purified PNB. The internal olefin peaks at 5.35 and 5.21 ppm correspond to a *trans*:*cis* ratio of 3.4:1.

**Notes and References to Chapter 2**

(1) (a) Francke, R.; Little, R. D. *Chem. Soc. Rev.* **2014**, *43*, 2492. (b) Schultz, D. M.; Yoon, T. P. *Science* **2014**, *343*, 1239716. (c) Nicewicz, D. A.; Nguyen, T. M. *ACS Catalysis* **2014**, *4*, 355. (d) Du, J.; Skubi, K. L.; Schultz, D. M.; Yoon, T. P. *Science* **2014**, *344*, 392. (e) Riener, M.; Nicewicz, D. A. *Chem. Sci.* **2013**, *4*, 2625. (f) Lu, Z.; Yoon, T. P. *Angew. Chem. Int. Ed.* **2012**, *51*, 10329.

(2) (a) Goetz, A. E.; Boydston, A. J. *J. Am. Chem. Soc.* **2015**, *137*, 7572. (b) Ogawa, K. A.; Goetz, A. E.; Boydston, A. J. *J. Am. Chem. Soc.* **2015**, *137*, 1400. (c) Martiny, M.; Steckhan, E.; Esch, T. *Chem. Ber.* **1993**, *126*, 1671.

(3) (a) Miranda, M. A.; Izquierdo, M. A.; Pérez-Ruiz, R. *J. Phys. Chem. A* **2003**, *107*, 2478. (b) Miranda, M. A.; García, H. *Chem. Rev.* **1994**, *94*, 1063.

(4) Heyes, D; Menon, R. S; Watt, I. F; Wiseman, J; Kubinski, P. *J. Phys. Org. Chem*. **2002**, *15*, 689.

(5) A 2-dram vial was equipped with a magnetic stir bar and then a (thio)pyrylium salt (1.0 equiv) was added. The vial was then transferred into a nitrogen-filled glovebox. To this vial was then added norbornene (424 mg, 4.50 mmol, 2000 equiv) and $CH_2Cl_2$ (2 mL). Then, ethyl propenyl ether (5 µL, 0.045 mmol, 20 equiv) was added via syringe. The vial was then sealed with a PTFE-lined screw cap, transferred out of the glovebox to a fume hood, and irradiated with 2-W blue LEDs for 75 min. The LEDs were placed ca. 1 cm from the vial. After 75 min, the vial was opened and a small amount (ca. 5 mg) of hydroquinone was added. A small aliquot was then taken for $^1$H NMR analysis to determine conversion to polymer. The remaining contents of the vial were diluted with $CH_2Cl_2$ and passed through a thin plug of neutral alumina using $CH_2Cl_2$ as eluent to remove any (thio)pyrylium salt. The filtrate was then concentrated to a volume of ca. 5 mL and then added dropwise into an excess of methanol (60 mL), which resulted in precipitation of the PNB. The solids were collected by vacuum filtration, washed with cold methanol, and then dried under reduced pressure.

# Chapter 3. Expanded Functionality of Polymers Prepared Using Metal-Free Ring-Opening Metathesis Polymerization[1]

## Section 1: Introduction

Ring-opening metathesis polymerization (ROMP) is a common technique for the preparation of functional polymers from strained cycloalkene monomers (Figure 3.1).[1] Whereas the initial ill-defined catalyst systems (typically comprised of Al, Ti, and W species) were limited to alkyl functionality, the development and continual improvement of well-defined W-, Mo-, and Ru-complexes over the past 30 years has resulted in a wide array of polar functional groups that can be introduced within the polymer structure.[2] The ability to tolerate such diverse functionality contributes greatly to the attractiveness of ROMP for preparing functional polymers and materials.

Recently, our lab disclosed a metal-free variant of ROMP (MF-ROMP) that relied on a unique photoredox-based mechanism, wherein an enol ether initiator is oxidized to form an active radical cation species.[3] Similar to other types of photoredox polymerizations,[4] this method allowed for temporal control over the polymerization[5] and offered the potential advantage of avoiding any transition metal species. Unfortunately, the initial monomer scope for this MF-ROMP appeared to be limited. Our initial disclosure focused solely on norbornene, and a subsequent report demonstrated varying levels of success with dicyclopentadiene-type monomers (Figure 3.1).[3b] Given the high reactivity of the radical cation intermediates, we hypothesized that certain polar functional groups may be incompatible with these polymerization conditions. We became interested in exploring the functional group tolerance for this new

[1] Reproduced with permission from Pascual, L. M. M; Dunford, D. G.; Goetz, A. E.; Ogawa, K. A.; Boydston, A. J. "Comparison of Pyrylium and Thiopyrylium Photooxidants in Metal-Free Ring-Opening Metathesis Polymerization" *Synlett.* **2016**, *27*, 759. Copyright 2016 Thieme Gruppe.

method with the goal of identifying functionalized monomers that could be successfully polymerized.

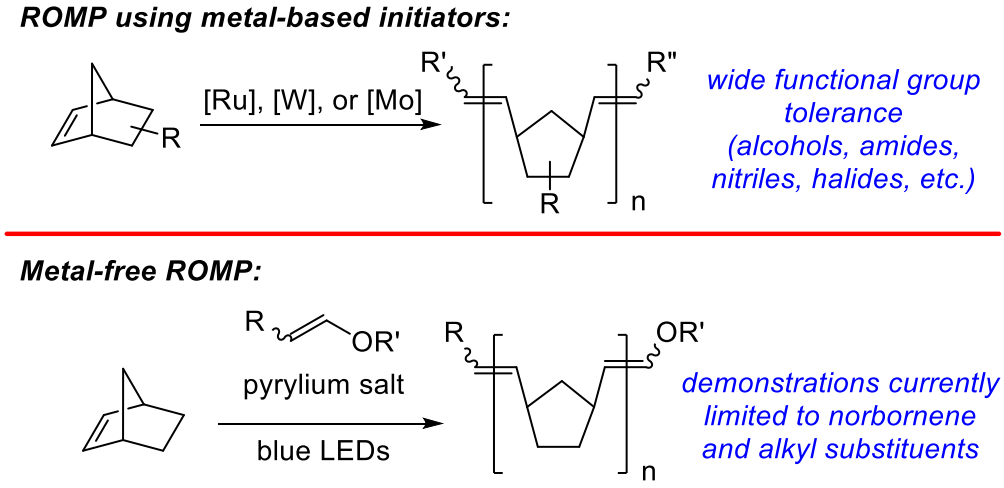


**Figure 3.1.** Metal-mediated and MF-ROMP functional group tolerance.

## Section 2: Results and Discussion

*3.2.a Additive Screenings*

As a simple method to probe functional group compatibility with our polymerization conditions, we initially examined the effect of small molecule additives on the polymerization of norbornene (**1**) using our previously reported photoredox conditions. We examined two feed ratios for the additives: a 1:1 molar ratio relative to initiator (each at 1 equiv) and a 1:1 molar ratio relative to monomer (each at 100 equiv). When introduced at a 1:1 feed ratio relative to initiator, water and methanol were each found to reduce the maximum conversion of norbornene (1), reaching 53% and 40%, respectively (Table 1). As we progressed from methanol to more sterically hindered alcohols, the negative impact on the polymerization was diminished. Specifically, we observed 68% conversion when iso-propanol was introduced, and tert-butanol appeared to have no impact on the polymerization at the low feed ratio. This trend is likely due

primarily to the relative nucleophilicity of the respective alcohols, as radical cation intermediates have been shown to be susceptible to nucleophilic attack from alcohols, and a larger influence is seen for the less sterically hindered additives.[4e,6] Moving to the higher feed ratio (1:1 with monomer), which more closely resembles homo- or copolymerization with functionalized monomers, we found that *tert*-butanol completely precluded polymerization. Notably, electron-deficient hexafluoroisopropanol (HFIP) and sterically hindered methyl tert-butyl ether (MTBE) each had little impact on norbornene conversion.

**Table 3.1.** Effect of additives on polymerization of **1** to polynorbornene (**2**).

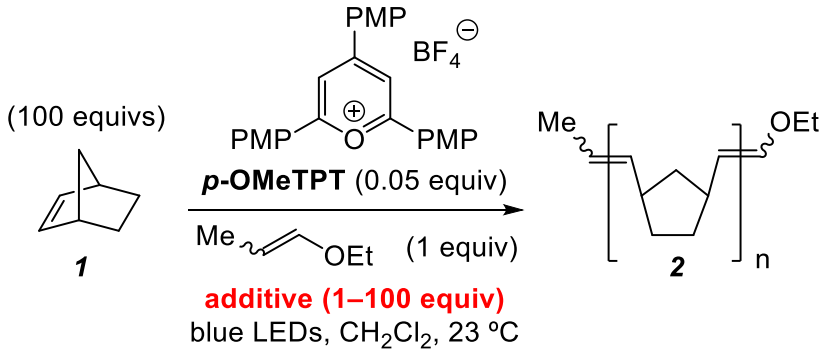


| Additive | Equivalents[a] | Conversion (%)[b] |
|---|---|---|
| none | - | 80 |
| $H_2O$ | 1 | 53 |
| MeOH | 1 | 40 |
| *i*-PrOH | 1 | 68 |
| *t*-BuOH | 1 | 80 |
| *t*-BuOH | 100 | 0 |
| HFIP | 100 | 72 |
| MTBE | 100 | 78 |

[a]Relative to enol ether initiator. [b]Determined using $^1$H-NMR spectroscopy by comparison of monomer and polymer peaks. PMP = *p*-methoxyphenyl. All reactions times = 90 min.

The observed 53% conversion to polynorbornene (**2**) in the presence of small amounts of water (1:1 with initiator, 310 ppm by wt) encouraged us to explore the polymerization efficiency

under ambient atmosphere. Therefore, we compared the results of polymerizations that were set up inside a glovebox under $N_2$ atmosphere using solvent obtained from purification columns with those set up under ambient conditions using solvent that was dried over molecular sieves. Importantly, we found that failure to dry the $CH_2Cl_2$ over molecular sieves led to highly variable conversions depending upon the source of solvent used, which suggested to us that water sensitivity is a general concern. The solubility of water in $CH_2Cl_2$ is reported to be ca. 1540 ppm by wt, thus allowing for concentrations well above our controlled addition of water to dry $CH_2Cl_2$.[7] The simple protocol of drying $CH_2Cl_2$ over molecule sieves, however, can achieve water concentrations below 1 ppm by wt.[8]

Surprisingly, we found that the reactions set up under ambient conditions achieved higher average conversion (87 ± 2%) than those set up and sealed under nitrogen atmosphere (80 ± 1%).[9] The discernible improvement when circumventing drybox use or other rigorous conditions was found to be reproducible and offers a significant technical advantage. The exact nature of the benefit gained by exposing the reaction to air is unknown. It is worth noting that O2 has been used as a terminal oxidant with various transition-metal photoredox catalysts and could help regenerate photochemically active pyrylium species.[10] However, previous studies have shown that related pyranyl radicals do not appear to undergo oxidation by $O_2$.[11] In our experiments, further increasing the oxygen content by purging the vial headspace with $O_2$ prior to irradiation with blue light resulted in a modest decrease in conversion (70 ± 4%).[12]

*3.2.b Copolymerizations*

We next returned focus toward exploration of functional group compatibility. Having identified some level of tolerance toward alcohols and ethers with the polymerization conditions,

we investigated monomers with similar functionality (Figure 3.2). Initially, we targeted direct incorporation of alcohol functional groups via homopolymerizations of 5-norbornene-2-methanol (**3**) and the related tertiary alcohol monomer **4**. Unfortunately, neither monomer led to any detectable amount of polymer. We next prepared a series of monomers (**5a−e**) derived from **3**, which were each employed as mixtures of *endo* and *exo* diastereomers. In homopolymerizations, monomers **5a−d** each failed to provide polymer. However, protection of the alcohol with a bulky *tert*-butyldimethylsilyl (TBS) group (**5e**) resulted in successful conversion (50%) to poly(**5e**), which was isolated in 20% yield (Mw = 18.8 kDa, Đ = 1.2). Notably, polymerization of the purely *exo* isomer (*exo*-5e) led to modest improvement in the conversion (62%).

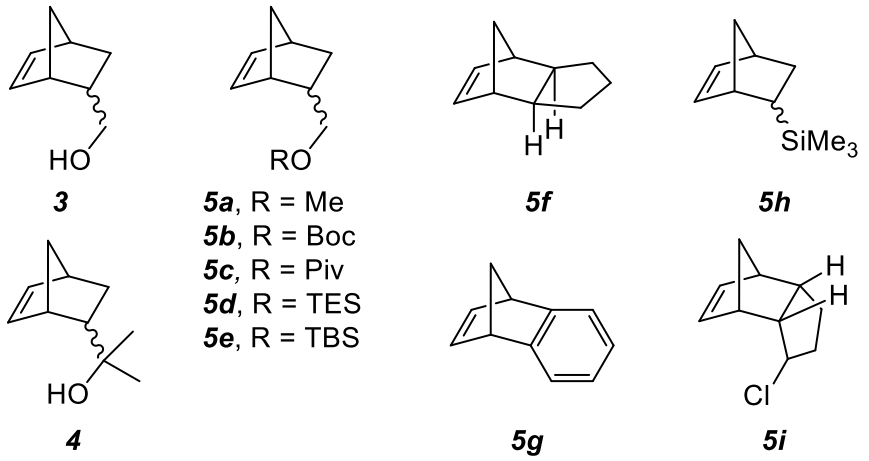


**Figure 3.2.** Functionalized monomers used in this study.

We recognized that the compatibility of monomer **5e** with the polymerization conditions could allow for the incorporation of alcohol functionality through copolymerization with monomers such as **1**. We have previously demonstrated the ability to copolymerize norbornene with endo-dicyclopentadiene (DCPD) using our metal-free conditions; however, significant

decreases in conversion were observed if the DCPD loading was greater than 10 mol % with respect to **1**.[3b] In contrast, we found that much higher loadings of **5e** could be successfully incorporated without a significant decrease in conversion or isolated yield (Table 3.2). Using feed ratios in which monomer **5e** comprised 25−75 mol % of the mixture resulted in successful polymerizations and good isolated yields of the resulting polymer. In each case, the amount of the TBS ether-containing monomer incorporated into the polymer chain was approximately 5−10% less than the feed ratio. Following precipitation of the polymer, removal of the TBS group was accomplished by treating a THF solution of the polymer with a fluoride source such as TBAF.[13]

**Table 3.2.** Copolymerization of **1** and **5e** at varying feed ratios.

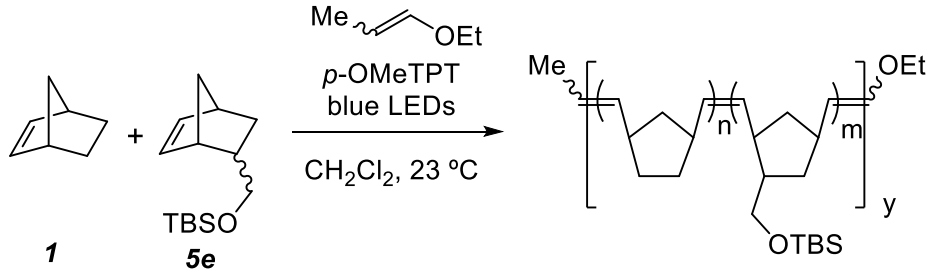


| 1:5e (feed) | Conversion (Isolated Yield)[a] | 1:5e (polymer)[b] | $M_w$ (kDa)[c] | $Đ$ |
|---|---|---|---|---|
| 75:25 | 78% (71%) | 80:20 | 27.0 | 1.5 |
| 50:50 | 69% (60%) | 57:43 | 30.0 | 1.3 |
| 25:75 | 60% (58%) | 34:66 | 28.0 | 1.3 |
| 0:100 | 50% (20%) | 0:100 | 18.8 | 1.2 |

[a]Determined by $^1$H-NMR spectroscopy of a reaction aliquot. Yield in parenthesis after isolation of polymer. [b]Determined by $^1$H-NMR spectroscopy of the isolated polymer. [c]Weight-average molecular weight determined by gel-permeation chromatography with in-line multiangle laser-light scattering detection. Molecular weight dispersity ($Đ$) = $M_w/M_n$. All reaction times = 90 min.

Based upon the results in Table 3.2, we further investigated the incorporation of **1** versus **5e** (1:1 feed ratio) over the course of the polymerization. At various time points, aliquots were

removed and analyzed by $^{1}$H NMR spectroscopy and GPC (Figure 3). The crude aliquots were used to assess conversion of monomers and molecular weight data prior to precipitation of the polymer. In parallel, a sample of precipitated polymer at each time point was used to assess the composition of the polymer (ratio of **1**:**5e**) and comparative GPC data. Overall, the GPC traces of crude and precipitated samples were similar between the two sets, and each was monomodal.[13] At 5 min into the polymerization, the ratio of **1**:**5e** was found to be 60:40, whereas all time points later in the polymerization gave polymer with 44−48% incorporation of **5e**. The gradually changing, but non-zero, amount of **5e** that was incorporated throughout the polymerization would be consistent with a statistical microstructure displaying slight gradation in the ratio of **1**:**5e**.

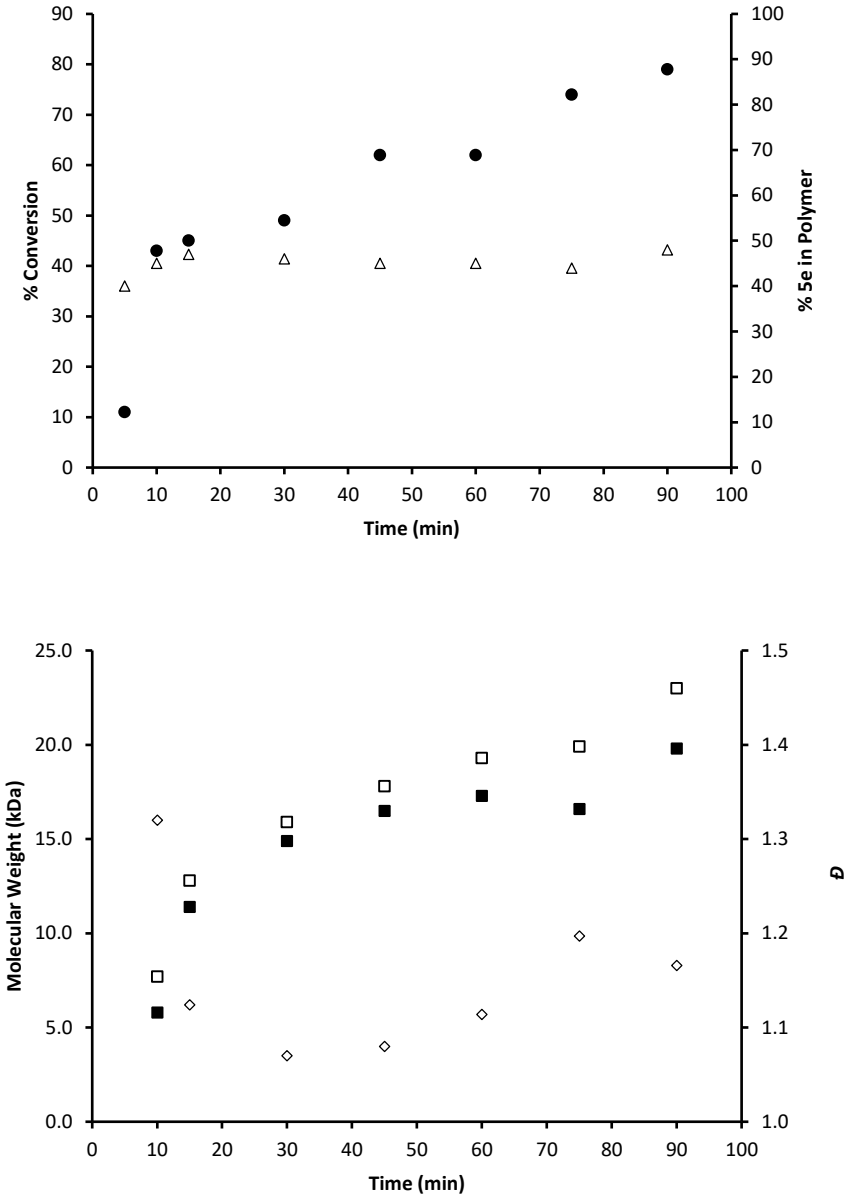


**Figure 3.3.** Data from copolymerization of **1** and **5e** with an initial 1:1 feed ratio. (top) Conversion determined by $^{1}$H-NMR analysis of crude *reaction* aliquots (black circles) and % of **5e** in isolated polymer determined by $^{1}$H-NMR analysis of precipitated samples (white triangles). (bottom) Molecular weight data obtained from isolated polymer samples during copolymerization (white squares = $M_w$, black squares = $M_n$, white diamonds = Đ.

Encouraged by the successful copolymerization of **5e**, we investigated monomers **3**, **4**, **5a−c**, and **5f−i**, each in copolymerizations with **1** (Table 3.3). Monomers **3** and **4** each completely precluded any polymerization when loaded in a 1:3 feed ratio relative to 1. In contrast, alcohol derivatives **5a−c** and monomers **5f−h** each underwent successful copolymerization, albeit with varying conversion and incorporation of **5** across the series. Copolymerization of **5a** and **5c** each with **1** was unremarkable, whereas use of Boc-protected monomer **5b** led to gelation during the polymerization and bimodal molecular weight distributions as determined by GPC analysis. Switching solvent from $CH_2Cl_2$ to $CHCl_3$ remedied the gelation and resulted in less bimodality in the GPC trace. Analysis of the **1**/ **5b** copolymer by thermogravimetric analysis revealed a 4.2 wt % loss at an onset temperature of 213 °C, consistent with thermolysis of the Boc group (theor. wt loss = 3.7%).[14] Monomer **5f** was previously found to perform exceptionally well in homopolymerizations using MF-ROMP and not surprisingly gave a high isolated yield of the copolymer with **1**.[3b] Furthermore, the incorporation of this monomer perfectly matched the feed ratio that was used, giving a polymer with a 3:1 ratio of **1**:**5f** units. While monomer **5f** lacks functionality seen in the other monomers, the rigidity of this comonomer leads to copolymers with higher $T_g$ values than pure 2 and allows for easy control over this parameter by adjusting the ratio between the two monomers. Monomers **5g** and **5h** each successfully copolymerized with **1** but at relatively low conversions and isolated yields. Consistent with their poor polymerization efficiency, neither **5g** nor **5h** yielded successful homopolymerization.

**Table 3.3.** Copolymerization of **1** and **5**.

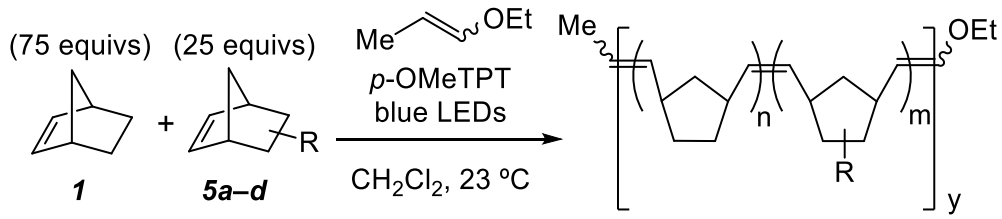


| Co-monomer | Conversion (Isolated Yield)[a] | 1:5 (polymer)[b] | $M_w$ (kDa)[c] | $Đ$ |
|---|---|---|---|---|
| **5a** | 77% (34%) | 82:18 | 20.3 | 1.4 |
| **5b ($CH_2Cl_2$)** | 70% (30%) | 88:12 | 95.0 | 3.7 |
| **5b ($CHCl_3$)** | 68% (36%) | 93:7 | 18.9 | 1.7 |
| **5c** | 74% (55%) | 89:11 | 37.2 | 2.2 |
| **5f** | 95% (74%) | 75:25 | 22.7 | 1.5 |
| **5g** | 47% (9%) | 90:10 | 5.3 | 1.3 |
| **5h** | 34% (19%) | 74:26 | 7.9 | 1.2 |
| **5i** | (87% wrt **1**) | 100:0 | 24.0 | 1.5 |

[a]Determined by $^1$H-NMR spectroscopy of a reaction aliquot. Yield in parenthesis after isolation of polymer. [b]Determined by $^1$H-NMR spectroscopy of the isolated polymer. [c]Weight-average molecular weight determined by gel-permeation chromatography with in-line multiangle laser-light scattering detection. Molecular weight dispersity ($Đ$) = $M_w/M_n$. All reaction times = 90 min.

Interestingly, chloro-substituted monomer **5i** was found to undergo successful homopolymerizations but did not result in copolymer formation when used in combination with **1**. Specifically, homopolymerization of **5i** gave 54% conversion to polymer (32% isolated yield) with $M_w$ = 27.7 kDa (Đ = 1.6). Attempted copolymerization with **1** led only to homopolymerization of **1** with **5i** remaining unreacted during the course of the polymerization. To investigate, we compared the polymerization of **1** with that of **5i** in NMR-scale experiments (Figure 3.4). Polymerization of **1** clearly proceeds at a higher rate than that of **5i**, reaching >90% conversion within 5 min versus 24% conversion of **5i** at the same time point. Moreover, the sigmoidal nature of the conversion versus time plot for **5i** is consistent with gradual initiation over a relatively longer period than in the case of **1**. These results suggested to us that

polymerization of **1** simply outpaces incorporation of **5i** during attempted copolymerizations and that incorporation of **5i** onto the active chain end of **2** is particularly inhibited.

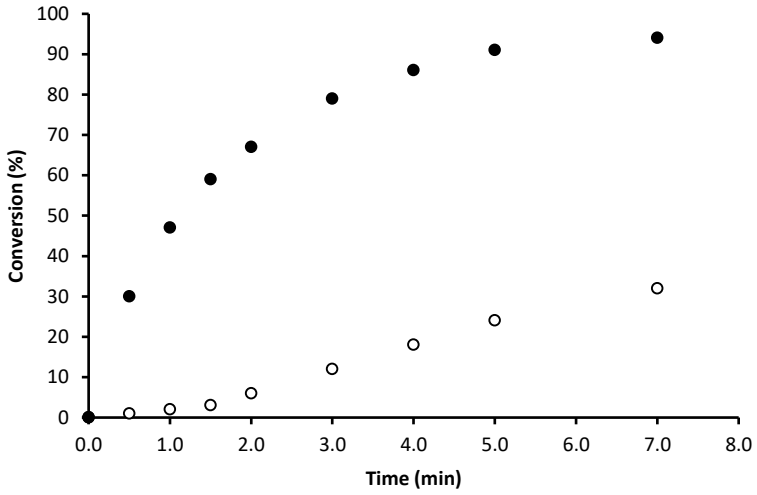


**Figure 3.4.** Conversion versus time for NMR-scale polymerization of **1** (black circles) and **5i** (white circles).

**Section 3: Conclusions**

In conclusion, we have found that a series of protected alcohols, which includes ether, ester, carbonate, and silyl ether functional groups, can be used as monomers in photoredox-driven MF-ROMP. Additionally, benzannulated, silane-functionalized, and chloro-substituted monomers were also found to participate in MF-ROMP, giving homo- and copolymers with various functionality and physical properties. Finally, the exploration of small molecule additives has revealed that the polymerization is sensitive to water but that polymerizations can be readily conducted under ambient conditions with minimal reagent purification, which has strong operational advantages. We hope that these studies will lead to an even more detailed

mechanistic understanding to help further improve the scope and applicability of this polymerization method.

## Section 4: Experimental

### *3.4.a General Considerations*

For reactions set up inside the glovebox $CH_2Cl_2$ was obtained from a solvent purification system and stored inside the glovebox. For reactions set up outside the glovebox, $CH_2Cl_2$ was dried over 4 Å molecular sieves before use. All polymerizations were carried out in standard borosilicate glass vials purchased from Fisher Scientific with magnetic stirring unless otherwise noted. Irradiation of photochemical reactions was done using a 2 W Miracle blue LED indoor gardening bulb purchased from Amazon. Norbornene (**1**) was sublimed prior to use. The alcohols used for the additive studies were dried over 4 Å molecular sieves prior to use. Pyridine and THF were obtained from a solvent purification system. All other reagents and solvents were obtained from commercial sources and used as received unless otherwise noted. $^{1}H$ and $^{13}C$ NMR spectra were recorded on Bruker AVance 300 MHz or 500 MHz spectrometers. Chemical shifts are reported in delta (δ) units, expressed in parts per million (ppm) downfield from tetramethylsilane using the residual protio-solvent as an internal standard ($CDCl_3$, $^{1}H$: 7.26 ppm and $^{13}C$: 77.0 ppm). Data are reported as follows: chemical shift, multiplicity (s = singlet, d = doublet, dd= doublet of doublets, br = broad, m = multiplet), coupling constants (Hz) and integration. Gel permeation chromatography (GPC) was performed using a GPC setup consisting of: a Shimadzu pump, 3 in-line columns, and Wyatt light scattering and refractive index detectors with tetrahydrofuran (THF) as the mobile phase. Number-average molecular weights ($M_n$) and weight-average molecular weights ($M_w$) were calculated from light scattering. $T_g$

values were determined using either a Perkin-Elmer DMA 8000 or a TA instruments Discovery DSC. For DMA, analysis was performed on powdered samples held within material pockets supplied by Perkin-Elmer. Samples were analyzed using the SingleCantilever Geometry Fixture with the following settings: heating rate = 3.0 ºC/min, frequency = 1 Hz, static force = 1.0 N. Reported $T_g$ values refer to the temperature corresponding to the peak of the tan delta curve. For Tg values below room temperature, samples were analyzed by DSC at a rate of 10 ºC/min. The pyrylium tetrafluoroborate salt was prepared according to literature procedure.[15] TGA analysis was performed using a TA Instruments Q50 TGA.

*3.4.b Monomer Preparation*

Monomers **3**, **5a**, and **5e** were prepared using known procedures starting from the commercially available mixture of 5-norbornene-2-carboxylic acid diastereomers.[16,17,18] Monomers **5f**, **5g**, and **5h** were prepared using reported procedures.[19,20,21] Compound **5h** was obtained as a 1.8:1 mixture of *endo*:*exo* diastereomers.[22]

*Preparation of tertiary alcohol* **4**.

**Scheme 3.1**. Synthesis of tertiary alcohol-functionalized monomer (**4**).

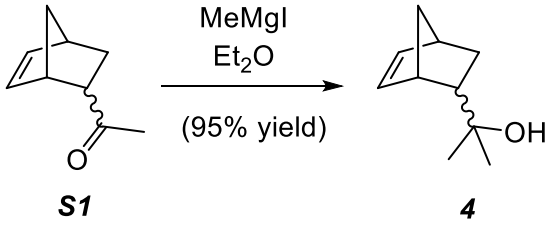


To a solution of **S1** (2.75 mL, 20.29 mmol) in $Et_2O$ (100 mL) at 0°C was added a solution of MeMgI (35 mL, 1.06 M, 36.95 mmol). The reaction mixture was stirred for 2 h and then

saturated $NH_4Cl$ (aq) solution and water (50 mL each) were added to the mixture. The mixture was extracted with EtOAc (2 × 60 mL) and the combined organics were then washed with brine (50 mL), and then dried over $MgSO_4$. Purification of the desired product by flash chromatography on silica gel (1:1 hexanes:$Et_2O$ eluent) provided 2.92 g (95% yield) of alcohol **4**. Spectral data matched those previously reported.[23]

*Preparation of carbonate* **5b**.

**Scheme 3.2**. Synthesis of Boc carbonate-functionalized NB monomer (**5b**).

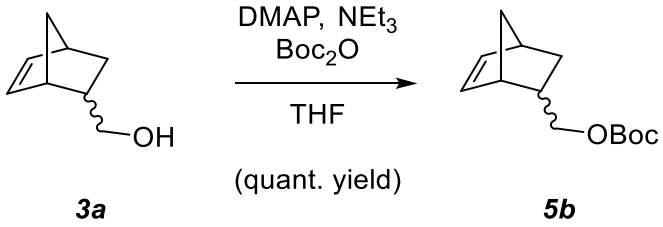


To a solution of alcohol **3a** (2.48 g, 19.97 mmol, 1 equiv) in THF (20 mL) was added triethylamine (8.5 mL, 60.98 mmol, 3 equiv), DMAP (245.1 mg, 2.01 mmol, 0.1 equiv), and di-*tert*-butyl dicarbonate (8.62 g, 39.50 mmol, 2 equiv). After 17 hours, water (5 mL) and $Et_2O$ (75 mL) were added. This mixture was washed successively with $H_2O$ (40 mL), 5% HCl (40 mL), sat. aq. $NaHCO_3$ (50 mL), and brine (50 mL). The organic layer was dried over $MgSO_4$. The crude product was purified by flash chromatography (9:1 hexane:$Et_2O$ eluent) to give the desired product (4.47 g, quantitative yield) as a 4.2:1 ratio of diastereomers. $^1$H-NMR (major isomer) ($CDCl_3$, 300 MHz) 6.21–6.15 (*m*, 1H), 5.98 (*dd*, J = 5.6, 2.6, 1H), 3.95–3.65 (*m*, 2H), 2.94 (*s*, 1H), 2.84 (*s*, 1H), 2.53–2.37 (*m*, 1H), 1.94–1.82 (*m*, 1H), 1.50 (*s*, 9H), 1.32–1.23 (*m*, 2H), 0.62–0.53 (m, 1H); $^{13}$C-NMR (major isomer) ($CDCl_3$, 75 MHz) 153.8, 137.7, 132.3, 81.0, 70.5, 49.5,

43.9, 42.3, 37.9, 29.0, 27.9; MS-ESI (m/z) [M + $NH_4^+$] calcd for $C_{13}H_{24}NO_3$, 242.2, found, 242.2.

*Preparation of pivalate* **5c**.

**Scheme 3.3**. Synthesis of pivalate ester-functionalized NB (**5c**).

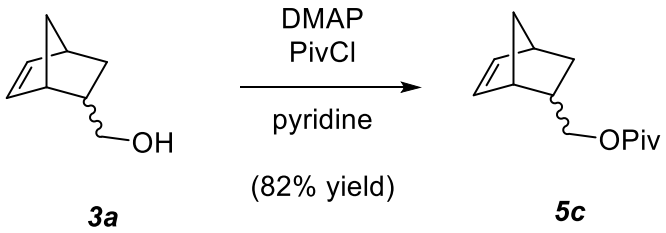


To a flask containing a stir bar was added alcohol **3a** (1.56 g, 12.56 mmol, 1 equiv), pyridine (62 mL), and DMAP (308.6 mg, 2.53 mmol, 0.2 equiv). The pivaloyl chloride (1.9 mL, 15.44 mmol, 1.2 equiv) was added dropwise, and the reaction stirred for 4.5 hours. Water (100 mL) was added and the reaction extracted with EtOAc (2 x 75 mL). The combined organic layers were washed consecutively with 1 M HCl (2 x 50 mL), 1 M NaOH (50 mL), saturated aq. $NaHCO_3$ (50 mL), brine (50 mL), and then dried over $MgSO_4$. The crude product was purified by flash chromatography (12:1 hexane:EtOAc eluent) to give the desired product (2.17 g, 82%) as a 3.9:1 *endo*:*exo* mixture of diastereomers. $^1$H-NMR (major isomer) ($CDCl_3$, 300 MHz) 6.14 (*dd*, J = 5.4, 2.8, 1H), 5.92 (*dd*, J = 5.4, 2.6, 1H), 3.84 (*dd*, J = 10.7, 6.8, 1H), 3.62 (*app. t*, J = 10.2, 1H), 2.84 (*d*, J = 17.0, 1H), 2.52–2.33 (*m*, 1H), 1.88–1.76 (*m*, 1H), 1.48–1.31 (*m*, 3H), 1.20 (*s*, 9H), 0.55 (*ddd*, J = 11.6, 4.0, 2.5, 1H); $^{13}$C-NMR ($CDCl_3$, 125 MHz) 178.5, 137.5, 132.3, 67.8, 49.4, 44.0, 42.3, 38.9, 37.9, 28.9, 27.3; MS-ESI (m/z) [M + $Na^+$] calcd for $C_{13}H_{20}O_2Na$, 231.1; found 231.0.

*Preparation of TES ether* **5d**.

**Scheme 3.4**. Synthesis of TES ether-functionalized NB (**5d**).

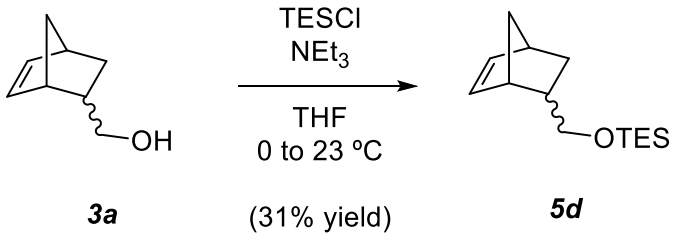


To a flame dried flask was added THF (11 mL) and triethylamine (1.50 mL, 10.5 mmol, 1.3 equiv). The reaction was cooled to 0°C and triethylsilyl chloride (1.80 mL, 10.5 mmol, 1.3 equiv) was added rapidly. A solution of 5-norbornene-2-methanol (1.00 g, 8.06 mmol, 1.0 equiv) in THF (8 mL) was added dropwise and the reaction mixture was warmed to room temperature. After 2 hrs. water (20 mL) was added and the mixture extracted with hexanes (4 x 20 ml). The combined organic layers were then washed with water (40 mL), brine (40 mL) and dried over $MgSO_4$. The solvent was evaporated to give the crude product as a yellow oil which was passed through a silica plug using hexanes to give **3c** as an oil (0.602 g, 31%). Spectral data matched those previously reported.[24]

*Preparation of chlorinated monomer* **5i**.

**Scheme 3.5**. Synthesis of 2-chloro-2,3-dihydro-*endo*-dicyclopentadiene (**5i**).

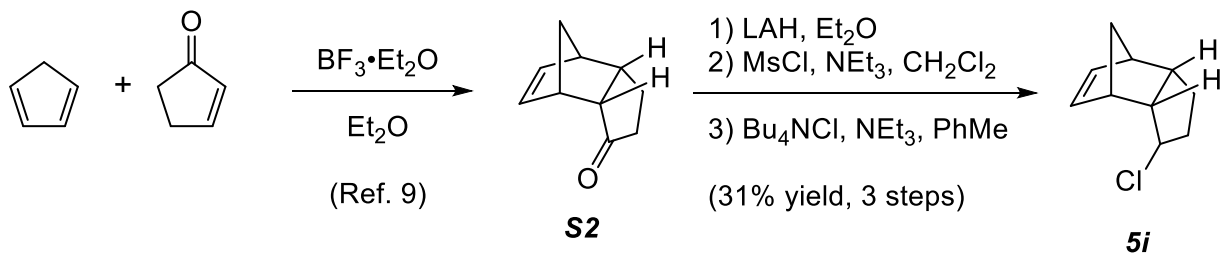

Monomer **5i** was prepared from Diels-Alder adduct **S2**, which was obtained using a known procedure.11 To a flask containing a slurry of lithium aluminum hydride (1.80 g, 47.4 mmol) in $Et_2O$ (150 mL) at 0 ºC was added over 5 minutes **S2** (4.62 g, 31.17 mmol, 1 equiv) as a solution in 10 mL $Et_2O$. The reaction was allowed to gradually warm to room temperature. After 90 minutes, the flask was cooled to 0ºC, and MeOH (20 mL) was added gradually (add *MeOH slowly with a vent needle present on the flask to avoid pressure buildup*) followed by 30% aq. Rochelle's salt (75 mL). After stirring for an additional 60 minutes, the solution was extracted with $Et_2O$ (3 x 75 mL), and the combined organic layers dried over $MgSO_4$. Evaporation under reduced pressure afforded the crude alcohol, which was used directly in the next step.

To a solution of the crude alcohol and triethylamine (6.5 mL, 46.64 mmol, 1.5 equiv) in $CH_2Cl_2$ (130 mL) at 0 ºC was added methanesulfonyl chloride (2.7 mL, 34.88 mmol, 1.1 equiv) dropwise over 2 minutes. After 3.5 hours, the reaction mixture was transferred to a separatory funnel was washed successively with $H_2O$ (60 mL), 10% aq. HCl (60 mL), sat. aq. $NaHCO_3$ (75 mL), and brine (75 mL). The organic layer was then dried over $MgSO_4$. Evaporation under reduced pressure afforded the crude mesylate, which was further purified by flash chromatography (1:1 hexane:$Et_2O$) to give the desired mesylate (4.51 g, 63% yield, 2 steps) which was used directly in the next step.

To a flame-dried flask containing anhydrous tetrabutylammonium chloride (8.2 g, 29.5 mmol, 1.5 equiv), toluene (50 mL), and triethylamine (6 mL, 43.05 mmol, 2.2 equiv) was added the mesylate as a solution in toluene (2 mL). The flask was placed in an oil bath at 50 ºC for 22 hours. After cooling to room temperature, the reaction mixture was diluted with $Et_2O$ (75 mL)

and washed with $H_2O$ (4 x 100 mL) and brine (100 mL) and the organic layer dried over $MgSO_4$. Evaporation under reduced pressure afforded the crude product, which was purified by flash chromatography (hexane eluent) to afford chloride **5i** (1.63 g, 49% yield) as a colorless oil. $^1$HNMR (CDCl3, 300 MHz) 6.21–6.09 (*m*, 2H), 3.70 (*app. q*, J = 5.9, 1H), 2.96 (*s*, 1H), 2.89–2.81 (*m*, 2H), 2.78 (*s*, 1H), 2.15–2.07 (*m*, 1H), 1.91–1.76 (*m*, 2H), 1.59 (*d*, J = 8.2, *1*H), 1.44 (*d*, J = 8.2, 1H), 1.08–1.00 (*m*, 1H); $^{13}$C-NMR ($CDC_{l3}$, 75 MHz) 137.2, 135.8, 62.0, 57.7, 53.4, 47.0, 46.2, 44.7, 41.1, 27.0; GC-MS (m/z) calcd for $C_{10}H_{13}Cl$, 168.1; found 168.1.

*3.4.c Polymerization Procedures*

*General Procedure for Polymerizations Set Up Inside the Glovebox*

A 2 dram vial containing a magnetic stirbar and p-OMeTPT (1.1 mg, 0.002 mmol, 0.05 equivs) was taken into a glovebox maintained under nitrogen atmosphere. To this vial was added norbornene (**1**, 424 mg 4.5 mmol, 100 equiv). Dichloromethane (2 mL) was added, followed by ethyl propenyl ether (5 µL, 0.045 mmol, 1 equiv). The vial was capped, removed from the glovebox, and irradiated with blue LEDs (λ = 450–480 nm, 2 W) for 90 minutes. A small scoop of hydroquinone was added to the vial and an aliquot taken for analysis to determine conversion. The contents of the vial were then diluted with $CH_2Cl_2$ and filtered over neutral alumina to remove any remaining p-OMeTPT. This $CH_2Cl_2$ mixture was concentrated down to ~5 mL and added slowly to MeOH (70 mL) causing the polymer to precipitate. The solids were collected by filtration, washed with MeOH and acetone, and dried under reduced pressure to give the final polymer.

*General Procedure for (Co)Polymerizations Set Up Outside the Glovebox*

To a 2 dram vial containing a magnetic stirbar was added p-OMeTPT (1.1 mg, 0.002 mmol, 0.05 equivs) followed by norbornene and any comonomers (total 4.5 mmol, 100 equiv). Dichloromethane (2 mL) was added, followed by ethyl propenyl ether (5 µL, 0.045 mmol, 1 equiv). The vial was capped and irradiated with blue LEDs (λ = 450–480 nm, 2 W) for 90 minutes. A small scoop of hydroquinone was added to the vial and an aliquot taken for analysis to determine conversion of each monomer. The contents of the vial were then diluted with $CH_2Cl_2$ and filtered over neutral alumina to remove any remaining p-OMeTPT. This $CH_2Cl_2$ mixture was concentrated down to approximately 5 mL and added slowly into MeOH (70 mL) causing the polymer to precipitate. The solids were collected by filtration, washed successively with MeOH and acetone, and then dried under reduced pressure to give the final polymer.

*Method for Determining Conversion for (Co)polymerizations*

Conversions were approximated using $^1$H-NMR spectroscopy ($CDCl_3$) by comparing the relative integrations of the following signals. In cases where monomer and polymer signals overlapped, the polymer integration was determined by subtracting the monomer signals from the total integration:

*Polymerization of norbornene*: The monomer peak at 5.99 ppm was integrated against the region from 3.0–2.3 ppm, which contained signals corresponding 2H from the monomer and 2H from the polymer.

*Copolymerization of methyl ether monomer* **5a** *and norbornene*: The norbornene monomer signal at 5.99 ppm (2H) and the methyl ether monomer signals from 6.2–5.90 (2H) were integrated against the region from 3.15–2.30 ppm, which contains signals corresponding to 2H from norbornene monomer, 5H from methyl ether monomer, and 4H from the polymer.

*Copolymerization of Boc carbonate monomer* **5b** *and norbornene*: The norbornene monomer signal at 5.99 ppm (2H) and the Boc monomer signal from 6.20–5.90 (2H) were integrated against the region from 3.0–2.25 ppm, which contained signals corresponding to 2H from norbornene monomer, 3H from Boc carbonate monomer, and 4H from the polymer.

*Copolymerization of pivalate monomer* **5c** *and norbornene*: The norbornene monomer peak at 5.99 ppm (2H) and pivalate monomer peaks at 6.2–5.9 ppm (2H) were integrated against the region from 3.0–2.2 ppm, which contains signals corresponding to 2H from norbornene monomer, 3H from pivalate monomer, and 4H from the polymer.

*Polymerization of TBS ether monomer* **5e**: The monomer peaks at 6.15–5.9 ppm (2H) were integrated against the region from 3.0–2.3 ppm, which contains signals corresponding to 2H from the monomer and 2H from the polymer.

*Copolymerization of TBS ether monomer* **5e** *and norbornene*: The monomer peaks at 6.15–5.9 ppm (4H total) were integrated against the region from 3.0–2.3 ppm, which contains signals corresponding to 4H from the monomers, and 4H from the polymer.

*Copolymerization of exo-dihydroDCPD monomer* **5f** *and norbornene*: The norbornene monomer peaks at 5.99 ppm (2H) and the *exo*-dihydroDCPD monomer peak at 6.1 ppm (2H) were integrated against the region from 1.25–0.90 ppm, which contains signals corresponding to 3H from norbornene monomer, 2H from *exo*-dihydroDCPD monomer and 2H from the polymer.

*Copolymerization of benzannulated monomer* **5g** *and norbornene*: The norbornene monomer peak at 5.99 ppm (2H) and the benzannulated monomer peak at 6.8 ppm (2H) were integrated against the region from 1.22–0.95 ppm, which contains signals corresponding to 3H from norbornene monomer and 2H from the polymer.

*Copolymerization of TMS monomer* **5h** *and norbornene*: The monomer peaks at 6.15–5.90 ppm (4H total) were integrated against the region from 1.25–0.8 ppm, which contains signals corresponding to 6H from the monomers and 3H from the polymer.

*Polymerization of chlorinated monomer* **5i**: For larger scale polymerization in $CH_2Cl_2$ (NMR analysis in $CDCl_3$), the monomer peaks at 6.17 ppm (2H) were integrated against the region from 4.3–3.65 ppm, which contains signals corresponding to 1H from the monomer and 1H from the polymer. For NMR-scale kinetics experiment in $CD_2Cl_2$, olefinic regions for monomer and polymer were directly compared.

*3.4.d Polymerization and Copolymerization Data*

**Table 3.4.** Comparison of Norbornene Polymerizations Setup Inside vs. Outside of Glovebox

| Atmosphere | Run 1 | Run 2 | Run 3 | Run 4 | Run 5 | Run 6 | Avg. |
|---|---|---|---|---|---|---|---|
| **$N_2$** | 82% | 79% | 78% | 80% | 80% | 81% | 80 ± 1% |
| **Ambient air** | 88% | 85% | 89% | 86% | 88% | 85% | 87 ± 2% |
| **$O_2$** | 72% | 65% | 73% | - | - | - | 70 ± 4% |

*Example Removal of TBS Ether from Copolymer*

**Scheme 3.6**. Removal of TBS Ether from copolymer.

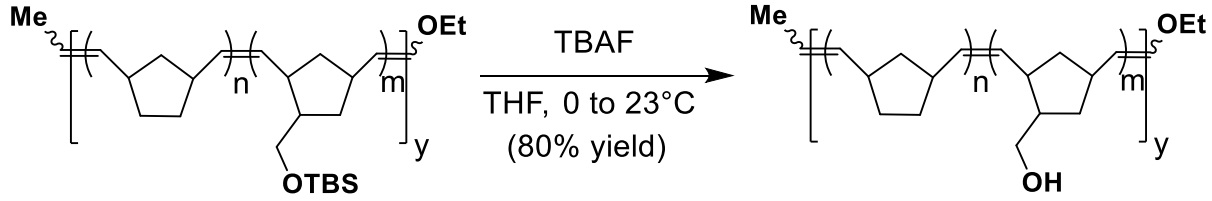


To a solution of the TBS ether-containing copolymer (169.7 mg, TBS content = 20% by $^1$H NMR) in THF (15 mL) at 0ºC was added TBAF (1.0 M in THF, 850 μL, 0.85 mmol) dropwise. The reaction was removed from the ice bath and allowed to gradually warm to room temperature. After 3.5 hours, the reaction mixture was concentrated to ~5 mL under reduced pressure, and then added dropwise to MeOH (50 mL) causing the polymer to precipitate. The solids were collected by filtration, washed with MeOH and acetone and dried under reduced pressure to give the final polymer (109.9 mg, 80% yield, TBS content = 3% by $^1$H NMR spectroscopy).

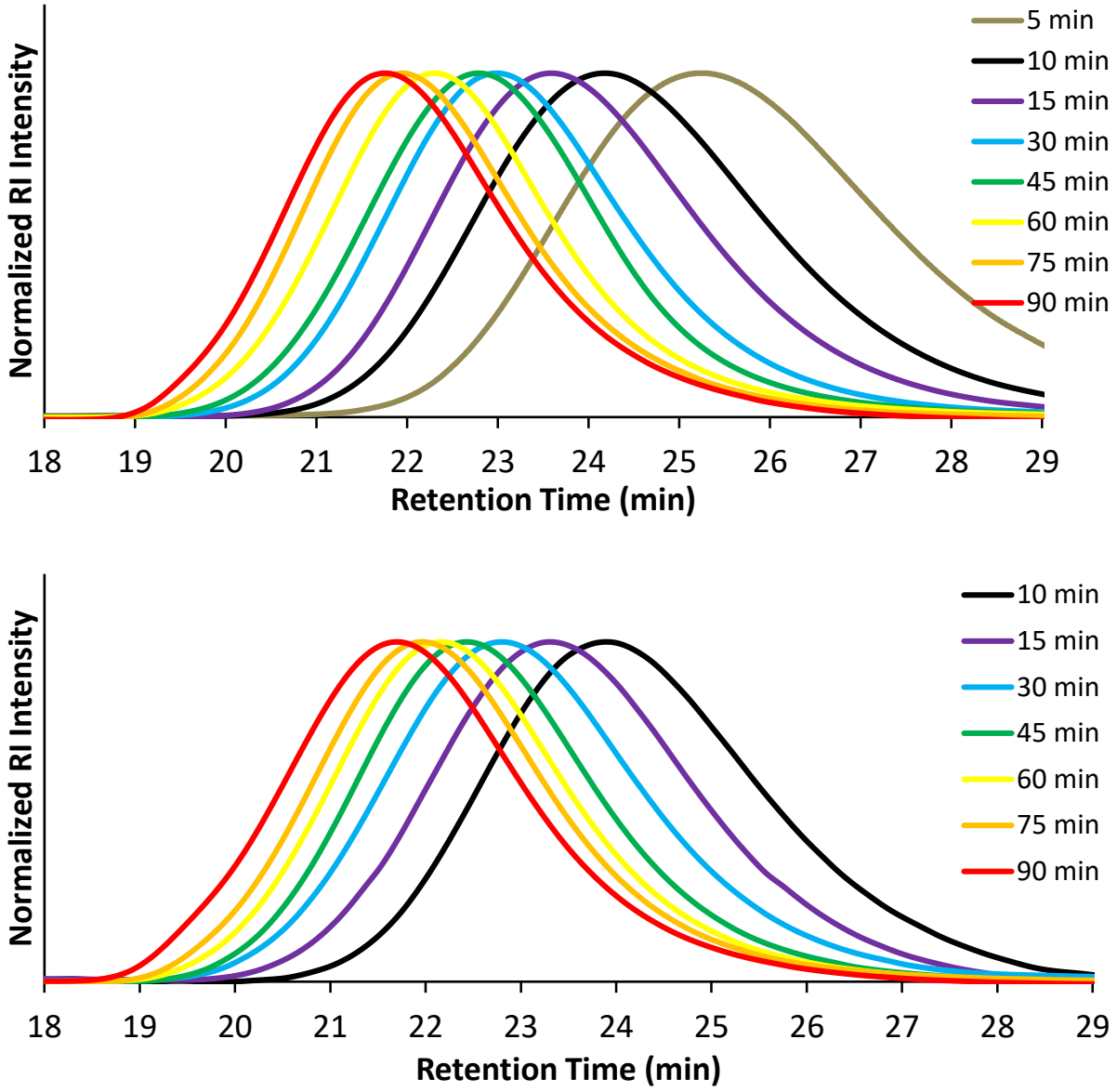


**Figure 3.5.** GPC traces taken during the copolymerization of **1** and **5e** with an initial 1:1 feed ratio. (top) GPC traces of crude aliquots. (bottom) GPC traces of polymer samples isolated by precipitation into MeOH at each time point.

**Table 3.5.** GPC data from copolymerization of **1** and **5e** relating to Figure 3.5.

| | Crude polymer data | | | Precipitated polymer data | | |
|---|---|---|---|---|---|---|
| **Time (min)** | $M_w$ **(kDa)** | $M_n$ **(kDa)** | $Đ$ | $M_w$ **(kDa)** | $M_n$ **(kDa)** | $Đ$ |
| 10 | 11.7 | 9.4 | 1.3 | 7.7 | 5.8 | 1.3 |
| 15 | 11.7 | 9.9 | 1.2 | 12.8 | 11.4 | 1.1 |
| 30 | 12.8 | 11.1 | 1.2 | 15.9 | 14.9 | 1.1 |
| 45 | 14.9 | 12.8 | 1.2 | 17.8 | 16.5 | 1.1 |
| 60 | 16.8 | 14.6 | 1.2 | 19.3 | 17.3 | 1.1 |
| 75 | 22.3 | 20.8 | 1.1 | 19.9 | 16.6 | 1.2 |
| 90 | 21.9 | 18.9 | 1.2 | 23.0 | 19.8 | 1.2 |

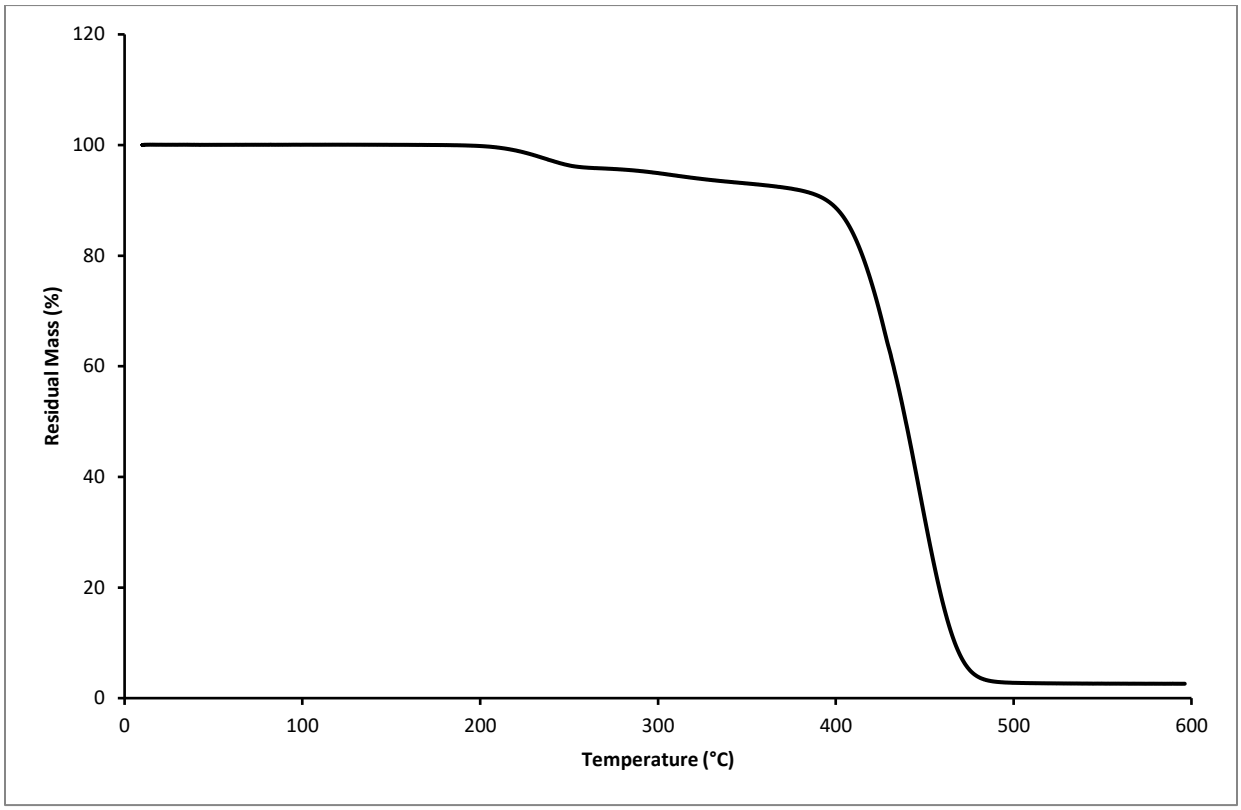


**Figure 3.6.** Thermogravimetric analysis of poly(**1**-*co*-**5b**). Heating rate = 10°C/min, $N_2$ atmosphere.

*3.4.e $^{1}H$ NMR and GPC Data*

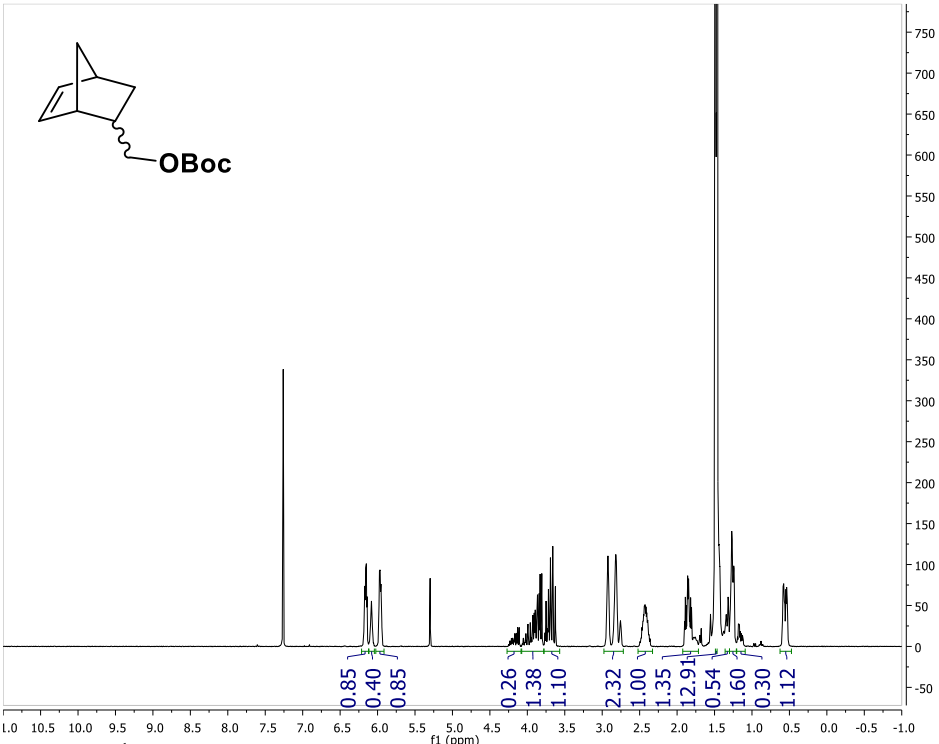


**Fig. 3.7.** $^{1}H$ NMR of Boc carbonate-functionalized NB (**5b**).

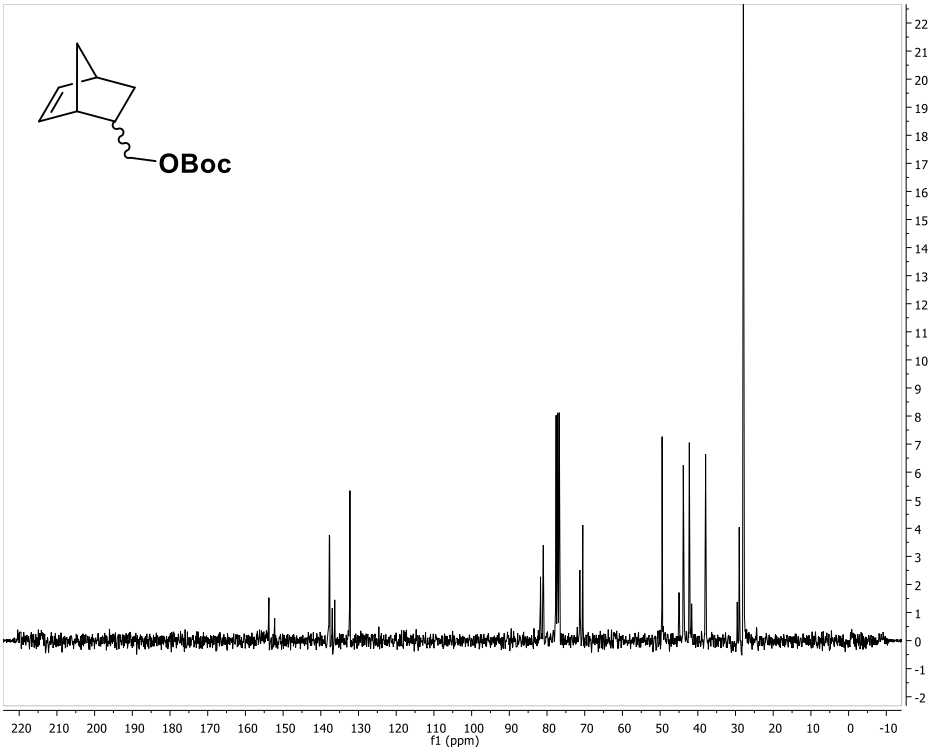


**Fig. 3.8.** $^{13}C$ NMR of Boc carbonate-functionalized NB (**5b**).

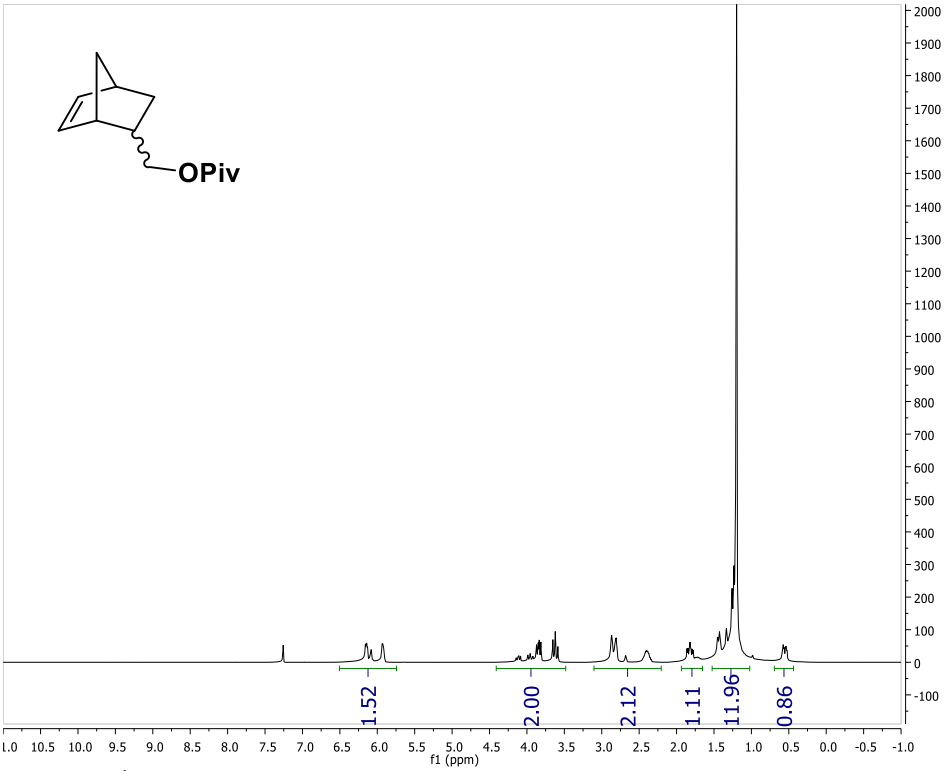


**Fig. 3.9.** $^{1}$H NMR of pivalate ester-functionalized NB (**5c**).

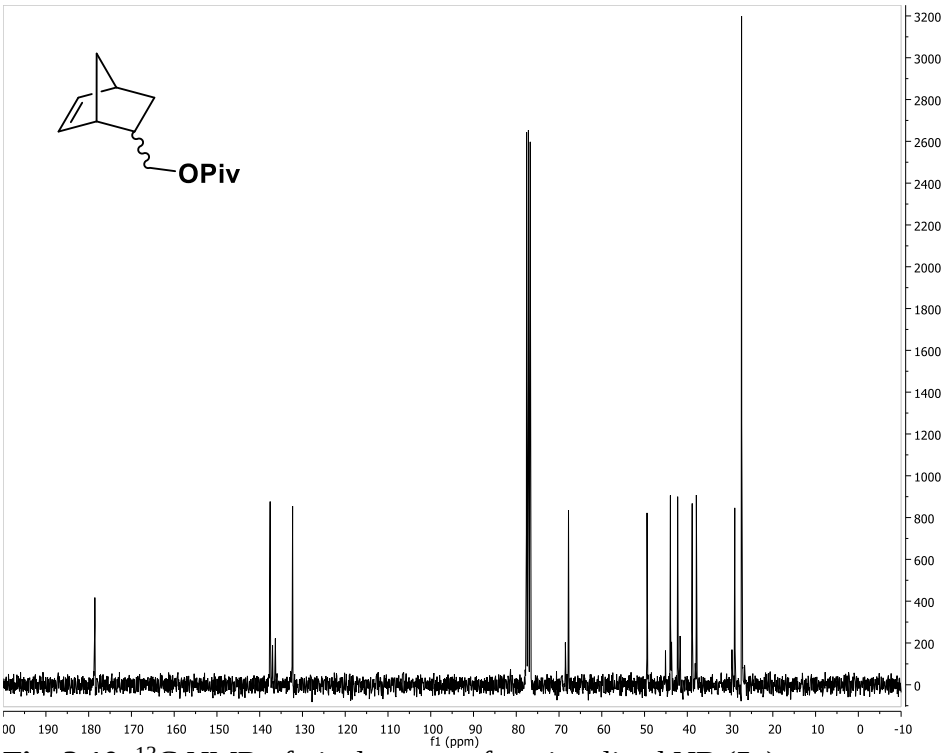


**Fig. 3.10.** $^{13}$C NMR of pivalate ester-functionalized NB (**5c**).

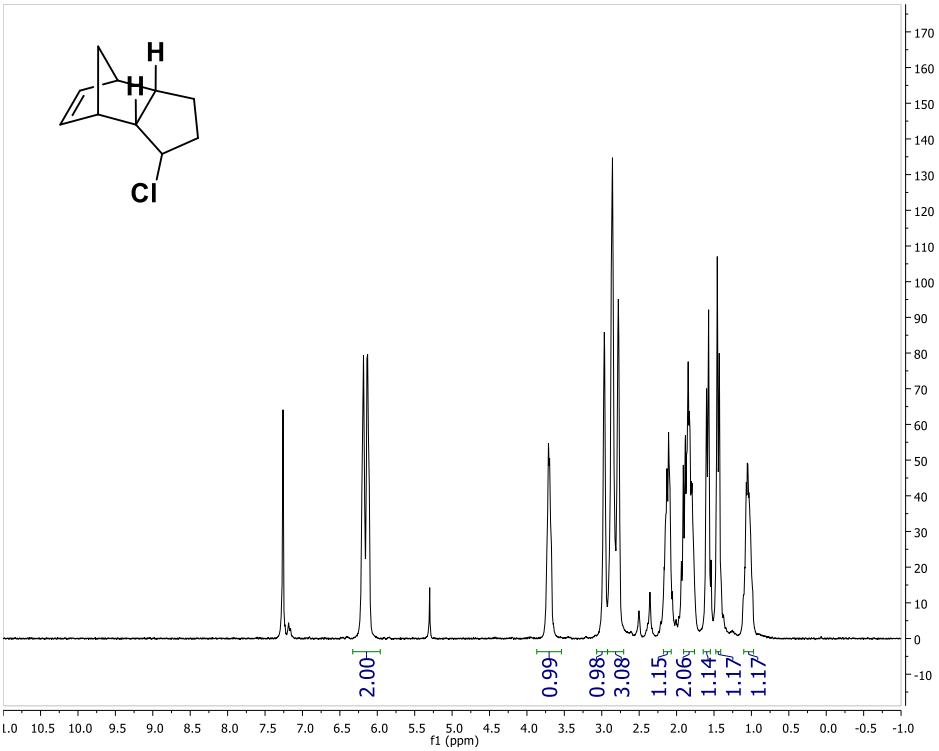


**Fig. 3.11.** $^{1}$H NMR of 2-chloro-2,3-dihydro-*endo*-dicyclopentadiene (**5i**).

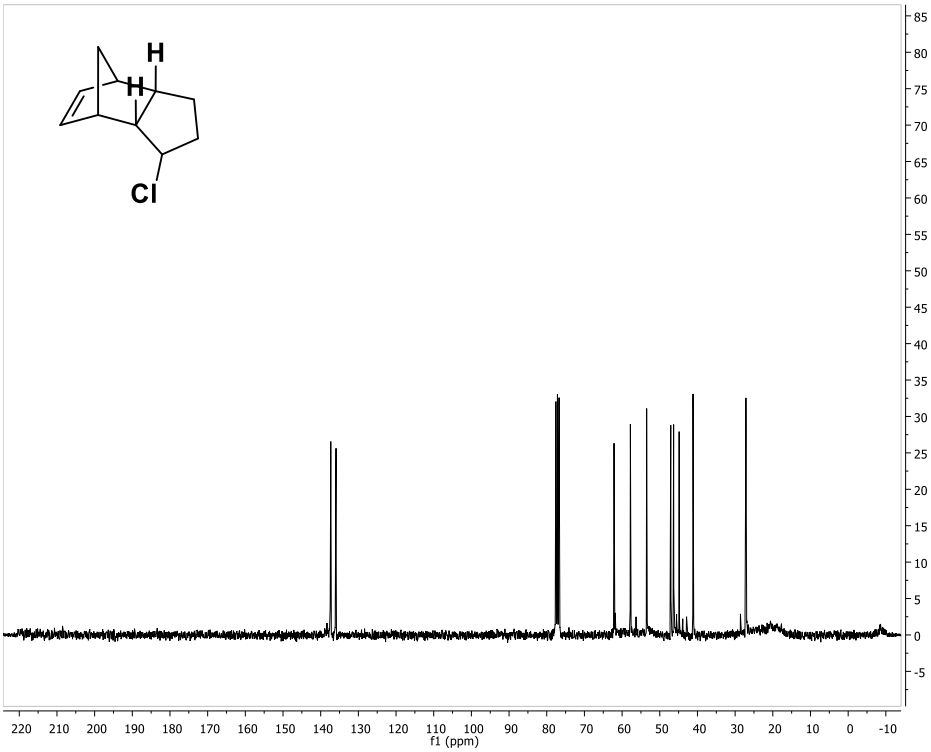


**Fig. 3.12.** $^{13}$C NMR of 2-chloro-2,3-dihydro-*endo*-dicyclopentadiene (**5i**).

Copolymers of Norbornene and TBS Ether Monomer **5e** – The ratio was determined by $^{1}$H-NMR spectroscopy by comparing the peaks corresponding to the olefins with the peaks corresponding to the methylene adjacent to the TBS Ether.

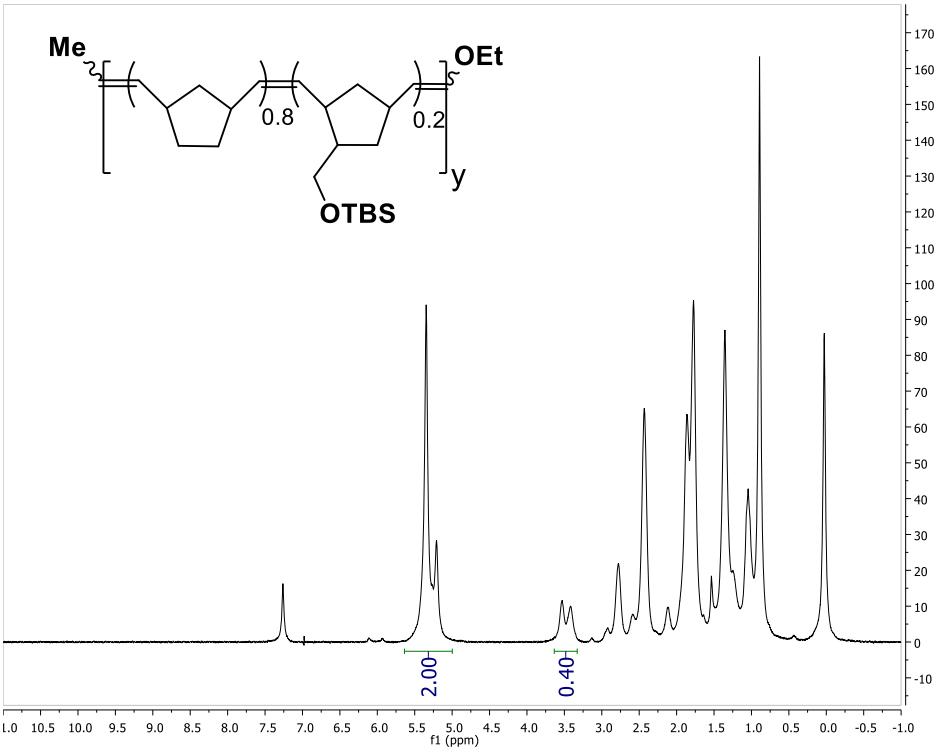


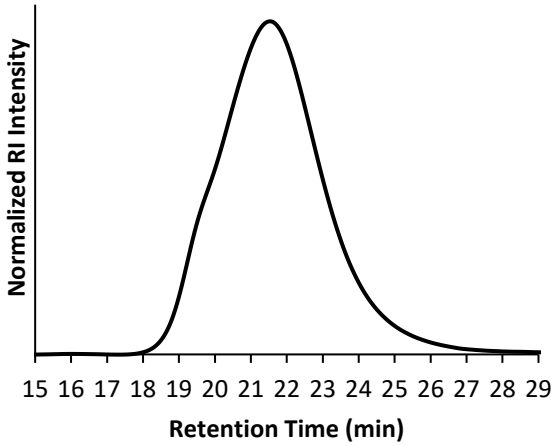


$M_n$ = 17.7 kDa; $M_w$ = 27.0 kDa; $Đ$ = 1.5; $T_g$ = 29 ºC (DMA)

**Fig. 3.13.** Copolymer of NB (**1**) and TBS ether-functionalized NB (0.8:0.2) (**5e**) top: $^{1}$H NMR; bottom: GPC refractive index

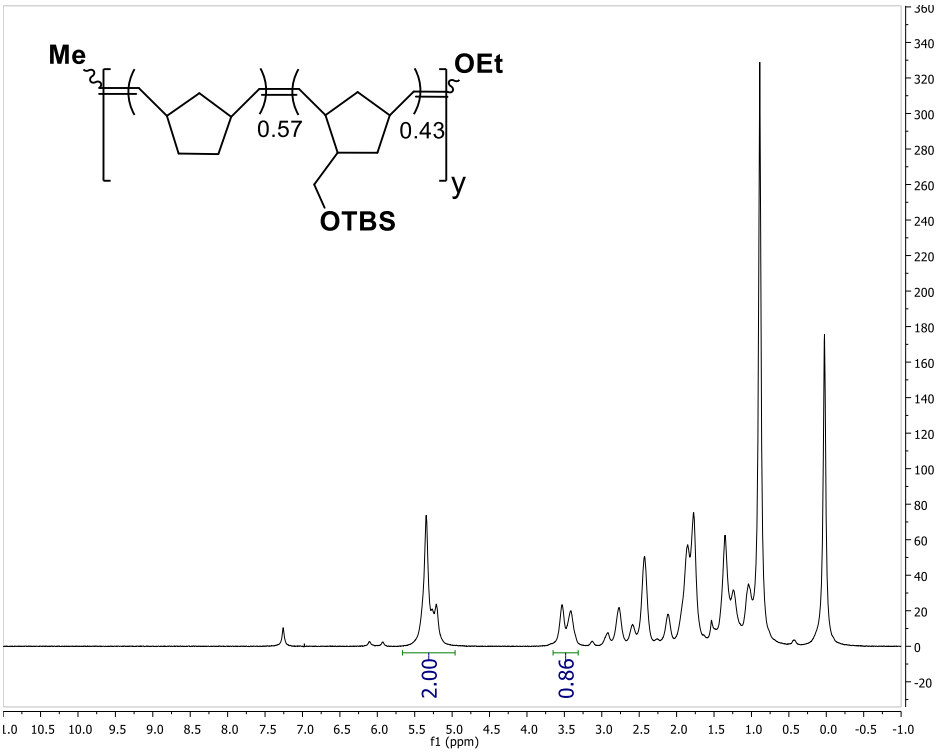


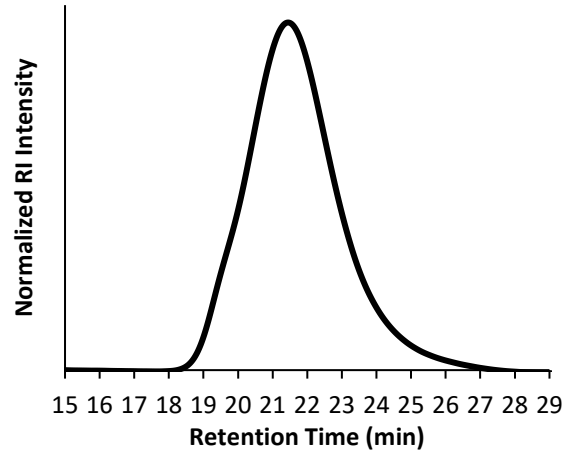


$M_n$ = 23.4 kDa; $M_w$ = 30.0 kDa; $Đ$ = 1.3; $T_g$ = –14.4 ºC (DSC)

**Fig. 3.14.** Copolymer of NB (**1**) and TBS ether-functionalized NB (**5e**) (0.57:0.43) top: $^1$H NMR; bottom: GPC refractive index

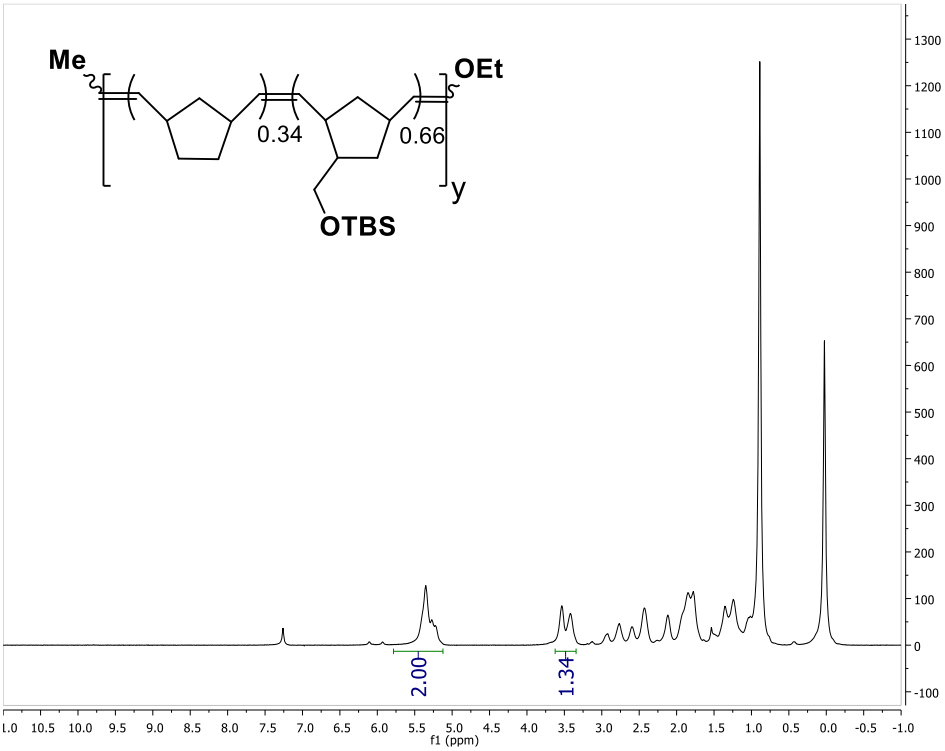


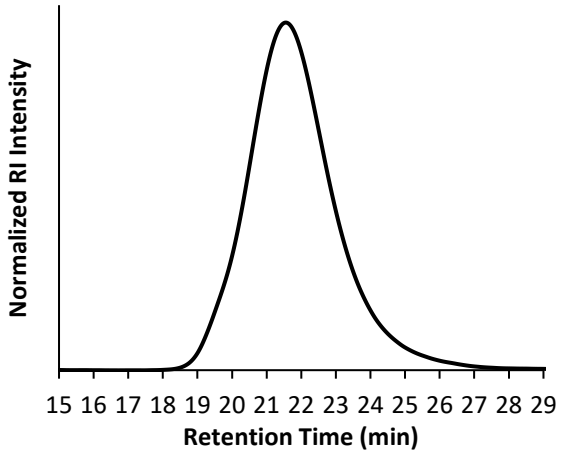


$M_n$ = 21.3 kDa; $M_w$ = 28.0 kDa; $Đ$ = 1.3; $T_g$ = –3.9 ºC (DSC)

**Fig. 3.15.** Copolymer of NB (**1**) and TBS ether-functionalized NB (**5e**) (0.34:0.66) top: $^1$H NMR; bottom: GPC refractive index

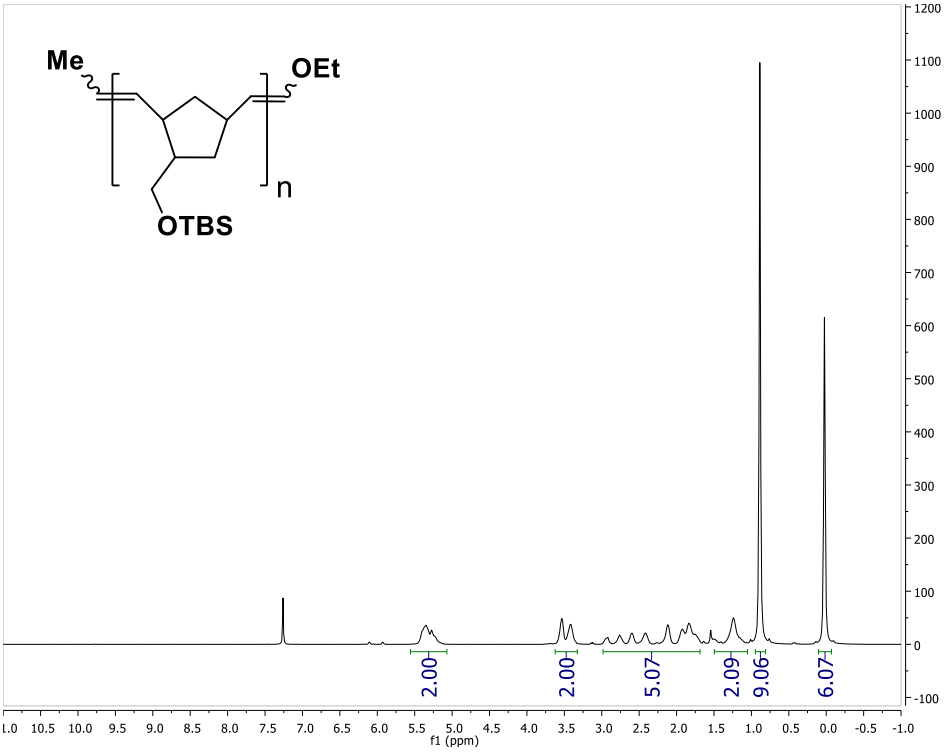


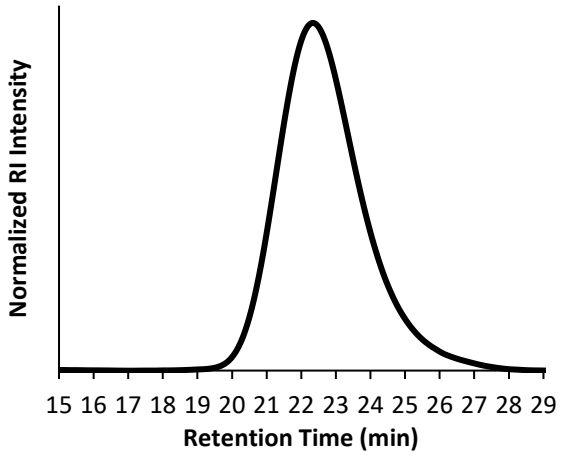


$M_n$ = 15.4 kDa; $M_w$ = 18.8 kDa; $Đ$ = 1.2

**Fig. 3.16.** Homopolymer of TBS ether-functionalized NB (**5e**)
top: $^1$H NMR; bottom: GPC refractive index

*<u>Removal of TBS Group from Copolymer</u> – The amount of TBS ether remaining was determined by $^1$H-NMR spectroscopy by comparing the peaks corresponding to the olefins with the peak at 0.0 ppm corresponding to the 2 $CH_3$ groups of the TBS ether.*

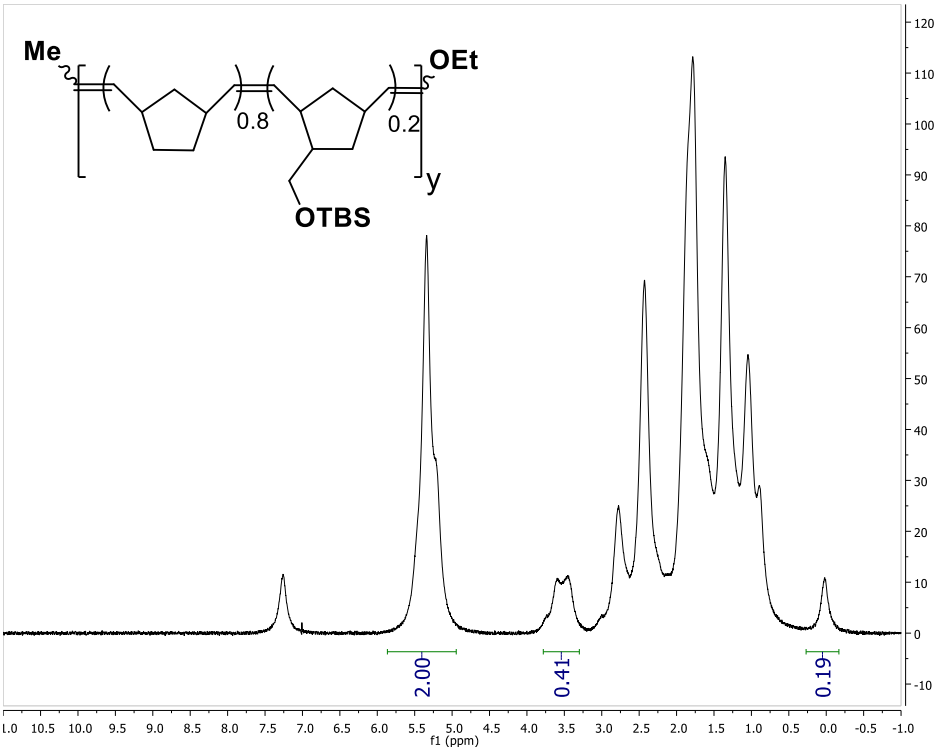


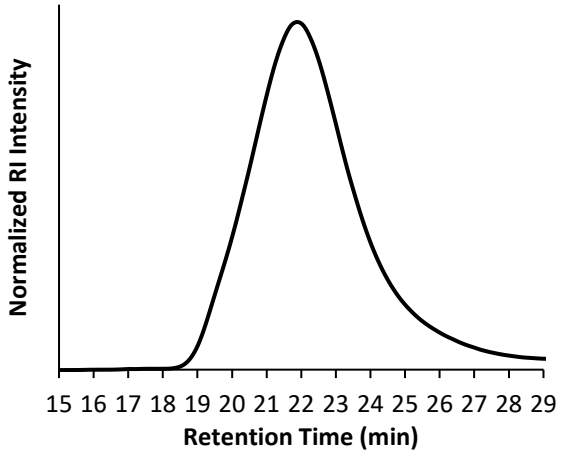


$M_n$ = 20.2 kDa; $M_w$ = 25.5 kDa; $Đ$ = 1.3; $T_g$ = 47 ºC

**Fig. 3.17.** Deprotected copolymer of NB (**1**) and TBS ether-functionalized NB (0.8:0.2) (**5e**) top: $^1$H NMR; bottom: GPC refractive index

*<u>Copolymer of Norbornene and methyl ether monomer **5a**</u> – The ratio was determined by $^{1}$H-NMR spectroscopy by comparing the peaks corresponding to the olefins with the peaks corresponding to the methoxy group.*

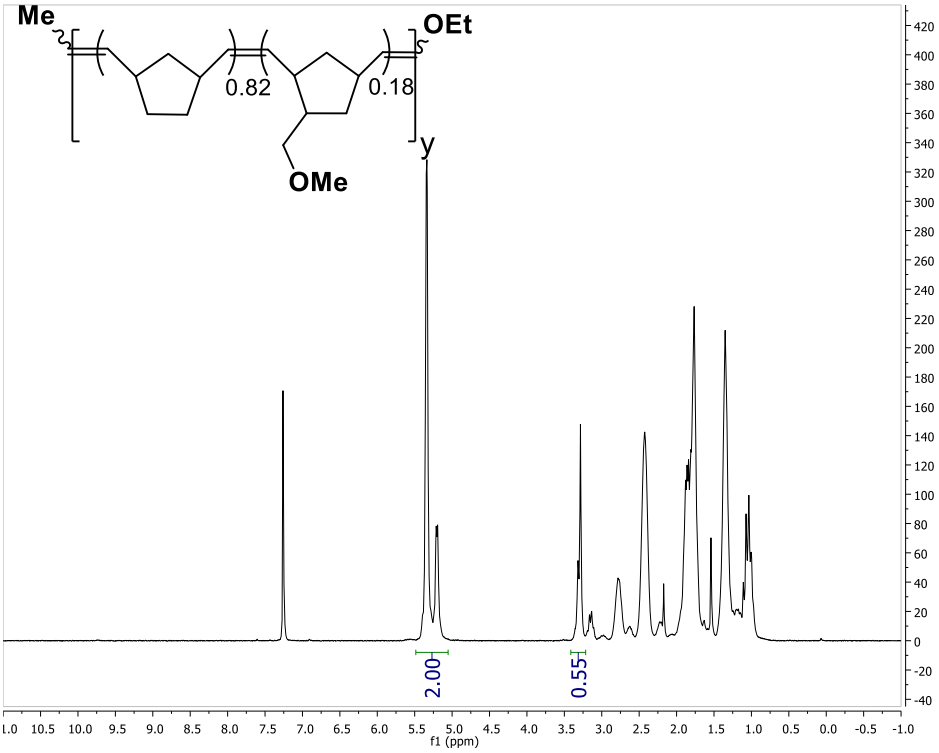


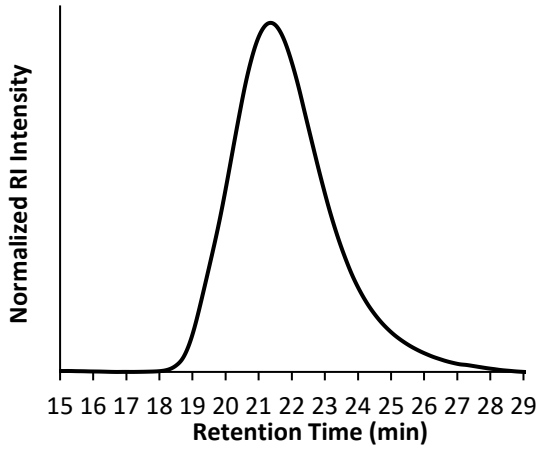


$M_n$ = 15.1 kDa, $M_w$ = 20.3 kDa; $Đ$ = 1.4; $T_g$ = 45 ºC (DMA)

**Fig. 3.18.** Copolymer of NB (**1**) and methyl ether-functionalized NB (0.82:0.18) (**5a**) top: $^{1}$H NMR; bottom: GPC refractive index

*<u>Copolymer of Norbornene and Boc carbonate monomer **5b**</u> – The ratio was determined by $^{1}$H-NMR spectroscopy by comparing the peaks corresponding to the olefins with the peaks corresponding to the methylene adjacent to the carbonate.*

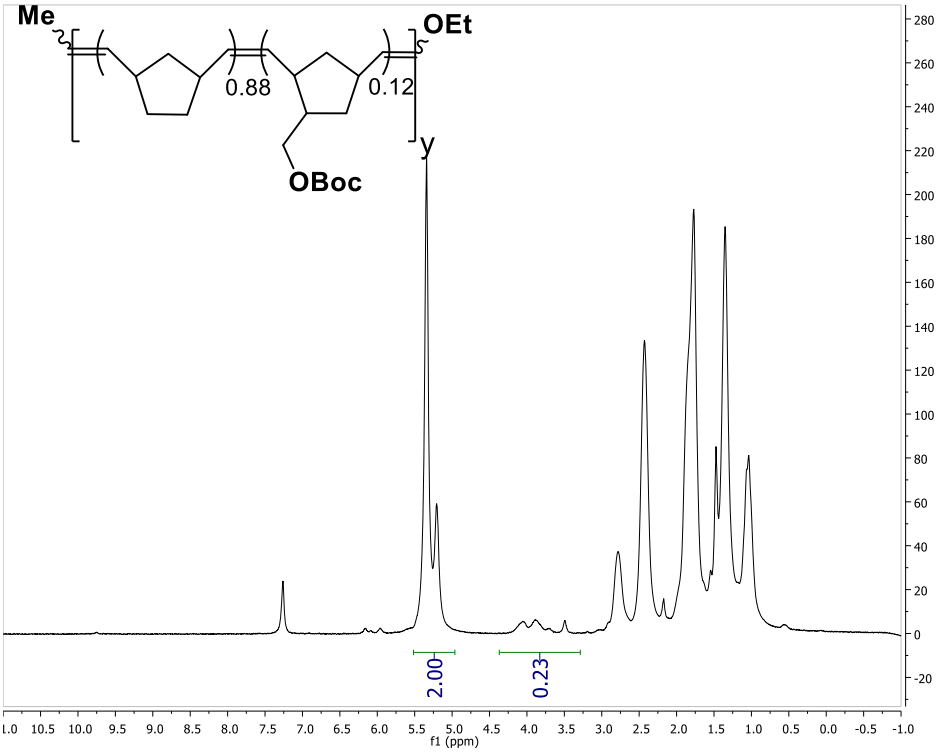


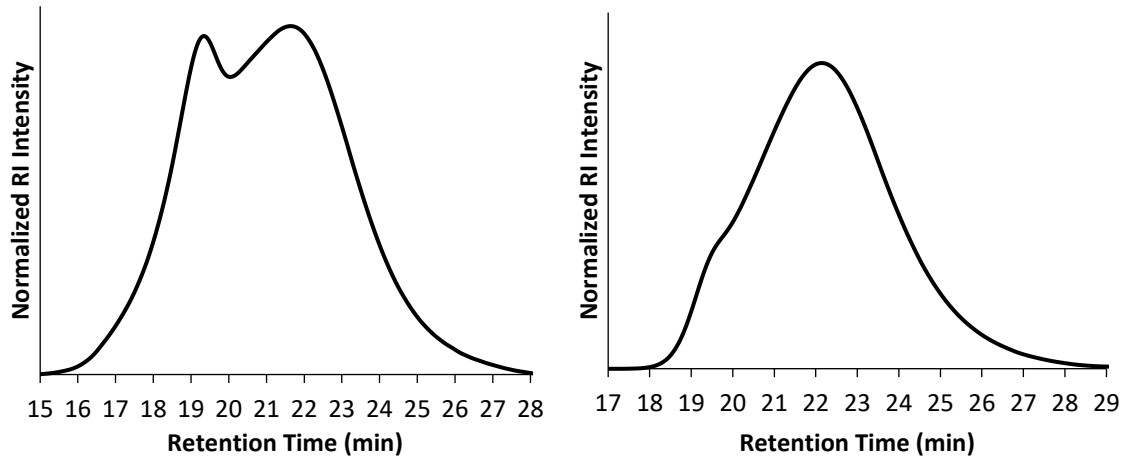


(left) Polymerization in $CH_2Cl_2$: $M_n$ = 25.7 kDa; $M_w$ = 95.0 kDa; $Đ$ = 3.7; $T_g$ = 51ºC (DMA)
(right) Polymerization in $CHCl_3$: $M_n$ = 11.3 kDa; $M_w$ = 18.9 kDa; $Đ$ = 1.7; $T_g$ = 51ºC (DMA)

**Fig. 3.19.** Copolymer of NB (**1**) and methyl Boc carbonate-functionalized NB (0.93:0.07) (**5b**) top: $^{1}$H NMR; bottom: GPC refractive index of polymerization in $CH_2Cl_2$ (left) and $CHCl_3$ (right).

*<u>Copolymer of Norbornene and Pivalate Monomer **5c**</u> - The ratio was determined by $^{1}$H-NMR spectroscopy by comparing the peaks corresponding to the olefins with the peaks corresponding to the methylene adjacent to the pivalate ester.*

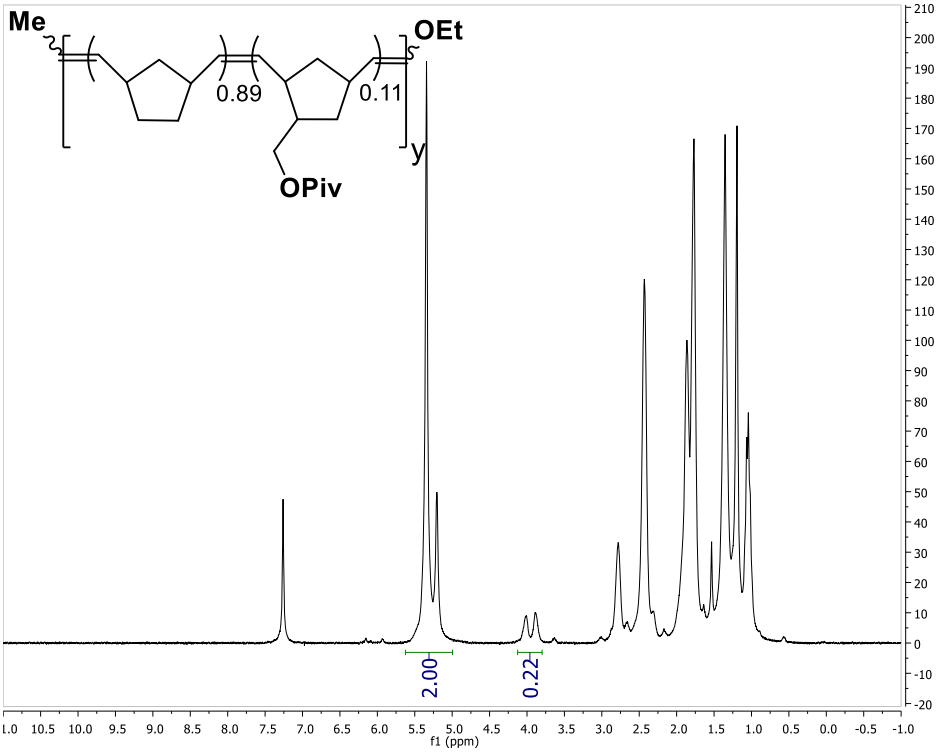


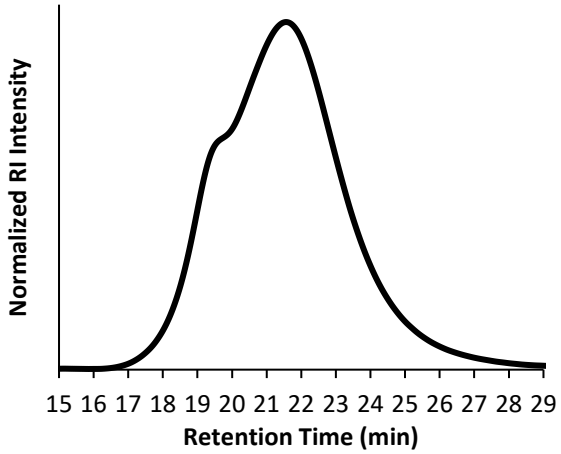


$M_n$ = 16.9 kDa; $M_w$ = 37.2 kDa; $Đ$ = 2.2; $T_g$ = 36 ºC (DMA)

**Fig. 3.20.** Copolymer of NB (**1**) and pivalate ester-functionalized NB (0.89:0.11) (**5c**) top: $^{1}$H NMR; bottom: GPC refractive index.

*<u>Copolymer of Norbornene and exo-DihydroDCPD Monomer **5f**</u> - The ratio was determined by $^{1}$H-NMR spectroscopy by comparing the peaks corresponding to the olefins with the peak at 1.05 ppm, which corresponds to a single hydrogen in polynorbornene.*

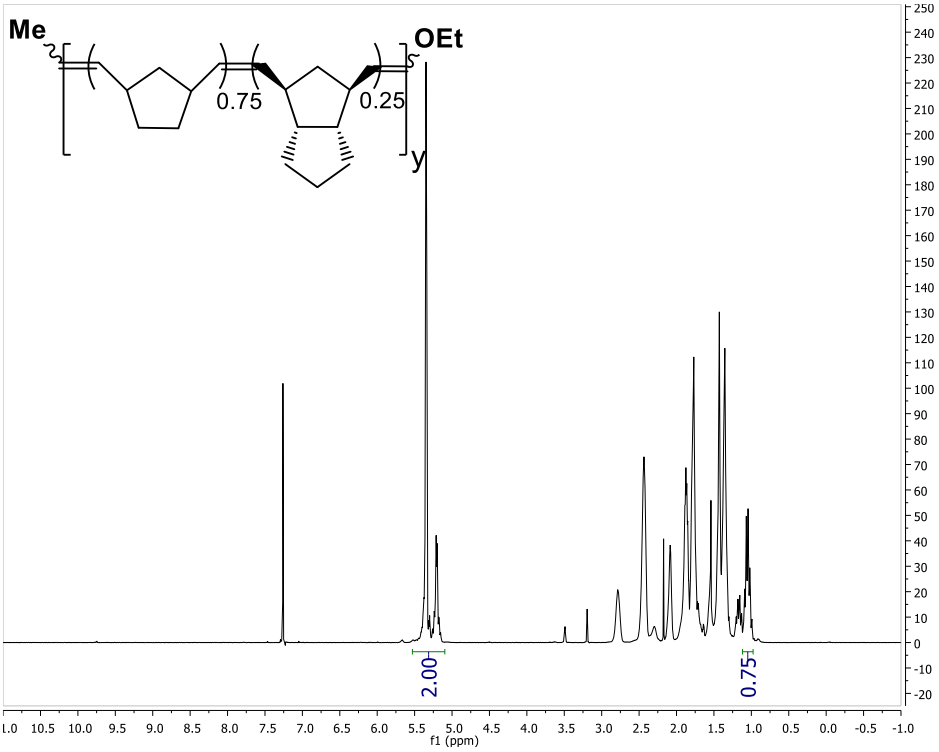


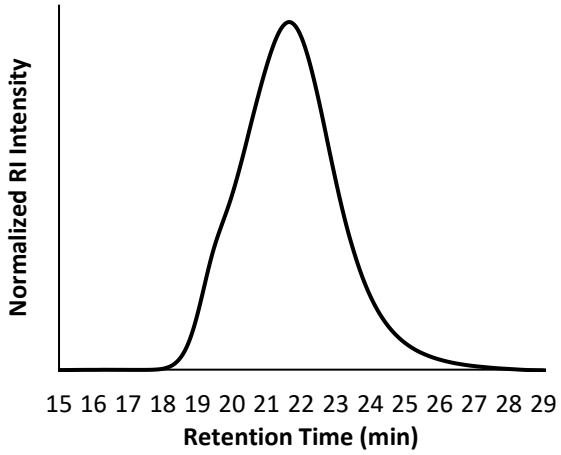


$M_n$ = 15.4 kDa; $M_w$ = 22.7 kDa; $Đ$ = 1.5; $T_g$ = 74 ºC (DMA)

**Fig. 3.21.** Copolymer of NB (**1**) and *exo*-dihydrodicyclopentadiene (0.75:0.25) (**5f**) top: $^{1}$H NMR; bottom: GPC refractive index.

*<u>Copolymer of Norbornene and Benzannulated Monomer **5g**</u> - The ratio was determined by $^{1}$H-NMR spectroscopy by comparing the peaks corresponding to the olefins with the aromatic peaks.*

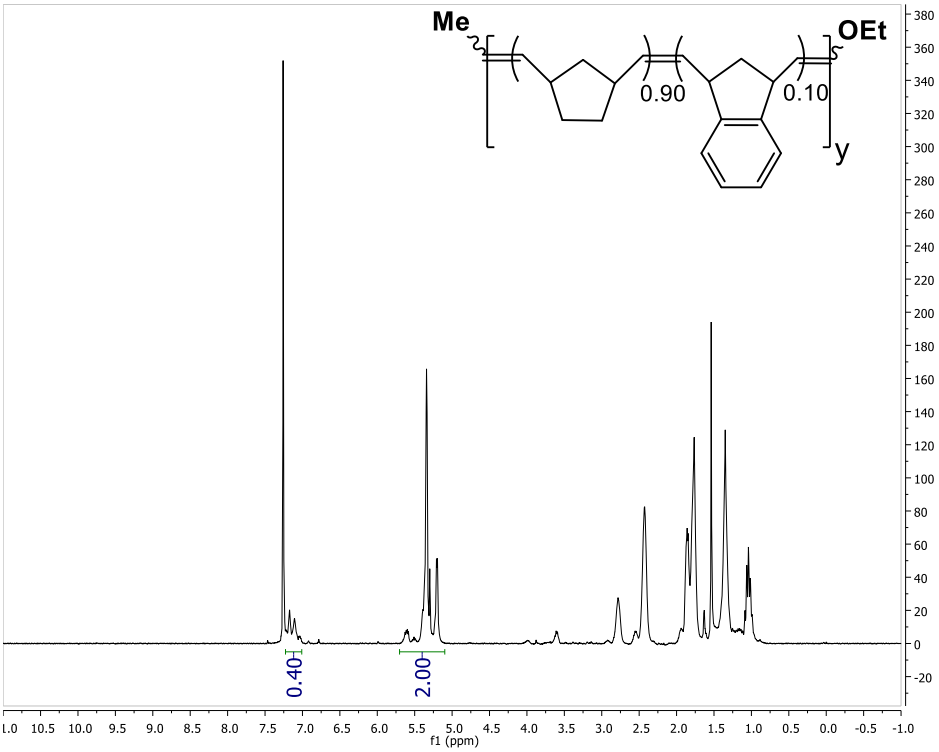


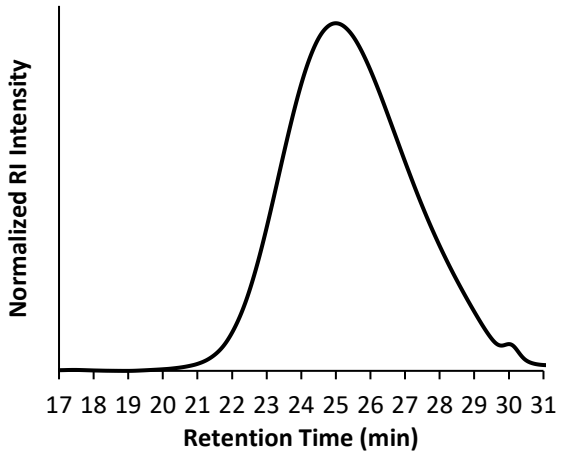


$M_n$ = 4.2 kDa; $M_w$ = 5.3 kDa; $Đ$ = 1.3; $T_g$ = 42 ºC (DMA)

**Fig. 3.22.** Copolymer of NB (**1**) and benzannulated NB (**5g**) (0.90:0.10)
top: $^{1}$H NMR; bottom: GPC refractive index.

*<u>Copolymer of Norbornene and Silyl Monomer **5h**</u> - The ratio was determined by $^{1}$H-NMR spectroscopy by comparing the peaks corresponding to the olefins with the peak corresponding to the TMS group.*

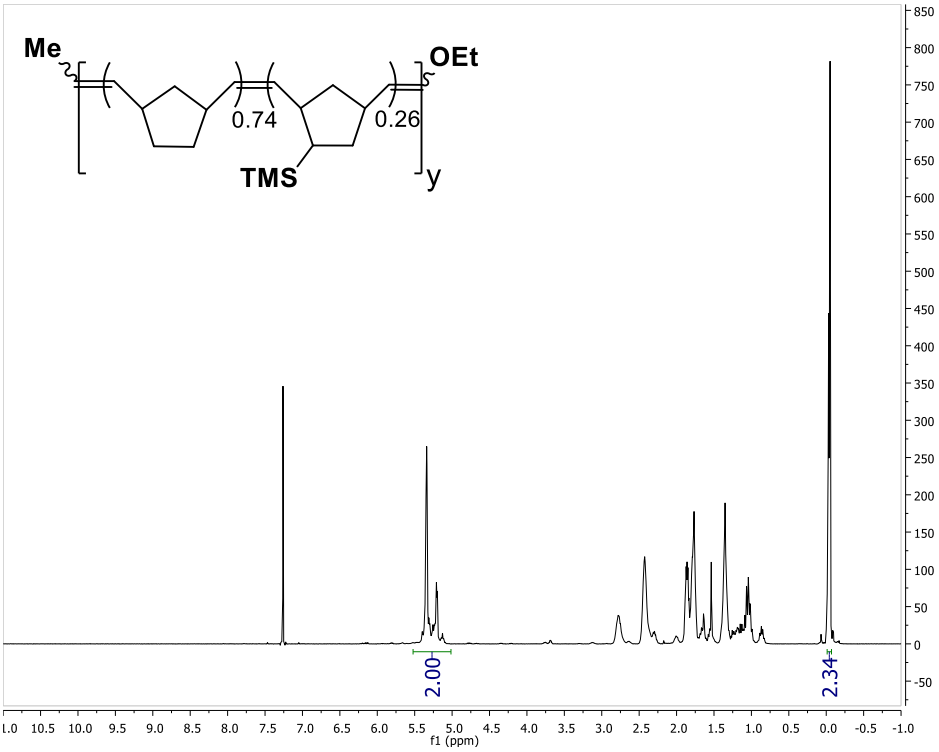


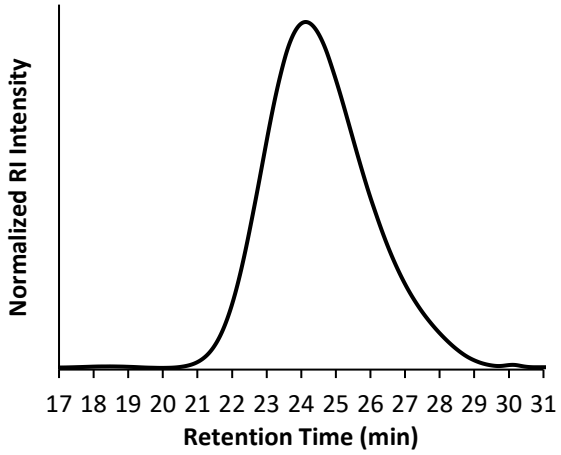


$M_n$ = 6.5 kDa; $M_w$ = 7.9 kDa; $Đ$ = 1.2; $T_g$ = 55 ºC (DMA)

**Fig. 3.23.** Copolymer of NB (**1**) and TMS-functionalized NB (**5h**) (0.74:0.26)
top: $^{1}$H NMR; bottom: GPC refractive index.

*Homopolymer 2-chloro-2,3-dihydro-endo-dicyclopentadiene* ***5h***

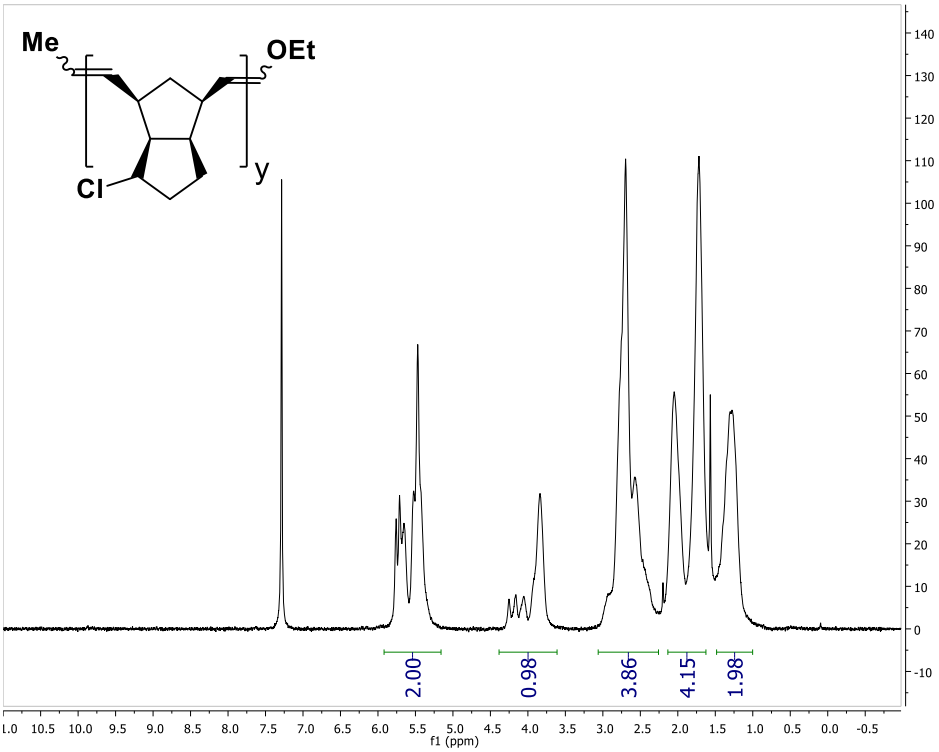


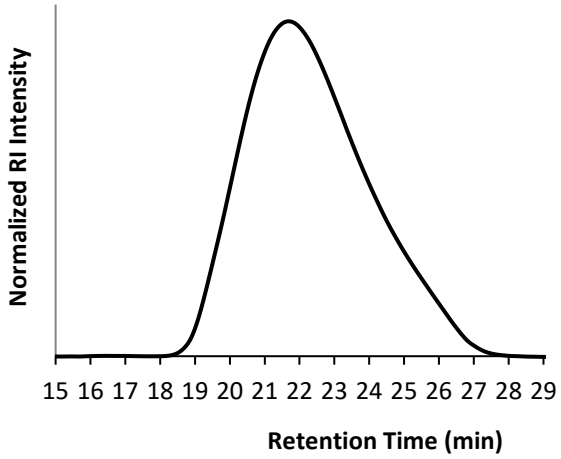


$M_n$ = 17.8 kDa, $M_w$ = 27.7 kDa; $Đ$ = 1.6; $T_g$ = 170 ºC (DMA)

**Fig. 3.24.** Homopolymer of 2-chloro-2,3-dihydro-endo-dicyclopentadiene (**5i**) top: $^1$H NMR; bottom: GPC refractive index.

**Notes and References for Chapter 3**

[1] a) Schrock, R. R. *Acc. Chem. Res.* **2014**, *47*, 2457–2466. b) Bielawski, C. W.; Grubbs, R. H. *Prog. Polym. Sci.* **2007**, *32*, 1–29.
[2] a) Leitgeb, A.; Wappel, J.; Slugovc, C. *Polymer* **2010**, *51*, 2927–2946. b) Sutthasupa, S.; Shiotsuki, M.; Sanda, F. *Polym. J.* **2010**, *42*, 905–915. c) Slugovc, C. *Macromol. Rapid Commun.* **2004**, *25*, 1283–1297.
[3] a) Ogawa, K. A.; Goetz, A. E.; Boydston, A. J. *J. Am. Chem. Soc.* **2015**, *137*, 1400–1403. b) Goetz, A. E.; Boydston, A. J. *J. Am. Chem. Soc.* **2015**, *137*, 7572–7575. c) Pascual, L. M. M.; Dunford, D. G.; Goetz, A. E.; Ogawa, K. A.; Boydston, A. J. *Synlett* 10.1055/s-0035-1561330.
[4] a) Dadashi-Silab, S.; Doran, S.; Yagci, Y. *Chem. Rev.* 10.1021/acs.chemrev.5b00586. b) Treat, N. J.; Sprafke, H.; Kramer, J. W.; Clark, P. G.; Barton, B. E.; Read de Alaniz, J.; Fors, B. P.; Hawker, C. J. *J. Am. Chem. Soc.* **2014**, *136*, 16096–16101. c) Miyake, G. M.; Theriot, J. C. *Macromolecules* **2014**, *47*, 8255–8261. d) Shanmugam, S.; Xu, J.; Boyer, C. *J. Am. Chem. Soc.* **2015**, *137*, 9174–9185. e) Perkowski, A. J.; You, W.; Nicewicz, D. A. *J. Am. Chem. Soc.* **2015**, *137*, 7580–7583. f) Shanmugam, S.; Xu, J.; Boyer, C. *J. Am. Chem. Soc.* **2015**, *137*, 9174–9185. g) Jung, K.; Xu, J.; Zetterlund, P. B.; Boyer, C. *ACS Macro Lett.* **2015**, *4*, 1139–1143. h) Xu, J.; Shanmugam, S.; Duong, H. T.; Boyer, C. *Polym. Chem.* **2015**, *6*, 5615–5624. i) Chen, M.; MacLeod, M. J.; Johnson, J. A. *ACS Macro Lett.* **2015**, *4*, 566–569. j) Melker, A.; Fors, B. P.; Hawker, C. J.; Poelma, J. E. *J. Polym. Sci., Part A: Polym. Chem.* **2015**, *53*, 2693–2698. k) Chen, Y.; Hu, Z.; Xu, D.; Yu, Y.; Tang, X.; Guo, H. *Macromol. Chem. Phys.* **2015**, *216*, 1055–1060.
[5] a) Ogawa, K. A.; Goetz, A. E.; Boydston, A. J. *Synlett* **2016**, *27*, 203–214. b) Teator, A. J.; Lastovickova, D. N.; Bielawski, C. W. *Chem. Rev.* **2016**, *116*, 1969-1992. c) Eivgi, O.; Lemcoff, G. *Synthesis*. **2018**, *50*, 49-63.
[6] a) Sutterer, A.; Moeller, K. D. *J. Am. Chem. Soc.* **2000**, *122*, 5636–5637. b) Duan, S.; Moeller, K. D. *J. Am. Chem. Soc.* **2002**, *124*, 9368–9369. c) Liu, B.; Duan, S.; Sutterer, A. C.; Moeller, K. D. *J. Am. Chem. Soc.* **2002**, *124*, 10101–10111.
[7] Chen, J.; Fritz, J. S. *J. Chromatogr.* **1989**, *482*, 279–287.
[8] Williams, D. B. G.; Lawton, M. *J. Org. Chem.* **2010**, *75*, 8351–8354.
[9] Average of 6 trials.
[10] a) Condie, A. G.; Gonzalez-Gomez, J. C.; Stephenson, C. R. J. *J. Am. Chem. Soc.* **2010**, *132*, 1464–1465. b) Lin, S.; Ischay, M. A.; Fry, C. G.; Yoon, T. P. *J. Am. Chem. Soc.* **2011**, *133*, 19350–19353.
[11] Akaba, R.; Sakuragi, H.; Tokumaru, K. *J. Chem. Soc. Perkin Trans. 2* **1991**, 291–297.
[12] Average of 3 trials.
[13] See Experimental section for details.
[14] Jiang, Y.; Fréchet, J. M. J.; Willson, C. G. *Polym. Bull*. **1987**, *17*, 1−6.
[15] Martiny, M.; Steckhan, E.; Esch, T. *Chem. Ber.* **1993**, *126*, 1671–1682.
[16] Nakazaki, M.; Naemura, K.; Kondo, Y. *J. Org. Chem.* **1976**, *41*, 1229–1233.
[17] Haigh, D. M.; Kenwright, A. M.; Khosravi, E. *Tetrahedron* **2004**, *60*, 7217–7224.
[18] Mayo, P. Orlova, G.; Goddard, J. D.; Tam, W. *J. Org. Chem.* **2001**, *66*, 5182–5191.
[19] Goetz, A. E.; Boydston, A. J. *J. Am. Chem. Soc.* **2015**, *137*, 7572–7575.
[20] Goll, J. M.; Fillion, E. *Organometallics* **2008**, *27*, 3622–3625.
[21] Cunico, R. F. *J. Org. Chem.* **1971**, *36*, 929–932.
[22] Driver, T. G.; Franz, A. K.; Woerpel, K. A. *J. Am. Chem. Soc.* **2002**, *124*, 6524-6525.

[23] Wendt, R. A.; Fink, G. *Macromol. Chem. Phys.* **2000**, *201*, 1365–1373.
[24] Masjedizadeh, M. R.; Dannecker-Doerig, I.; Little, R. D. *J. Org. Chem.* **1990**, *55*, 2742–2752.

# Chapter 4: Investigation of Tacticity and Living Characteristics of Photoredox-Mediated Metal-Free Ring-Opening Metathesis Polymerization[1]

## Section 1: Introduction

Polymer microstructure and monomer sequence can each have significant impact on property and function.[1,2] In ring-opening metathesis polymerization (ROMP), microstructural control provides opportunities to modulate the olefin geometry (*cis* versus *trans*) as well as the stereochemical relationship between adjacent repeat units (*meso* versus *racemic*), as depicted in Figure 4.1.[3] The evolution of well-defined W, Mo, and Ru alkylidene initiators has led to highly controlled polymer stereochemistry, including the ability to achieve thermodynamically disfavored high cis olefin content coupled with highly tactic polymer.[4] The nature of the structurally diverse metal complexes is such that stereochemical retention or inversion is possible upon addition of monomer units to the active chain end, providing opportunities for control over polymer tacticity.

We recently discovered a method of ROMP that diverges from metal-mediated approaches by employing a vinyl ether initiator, which is activated toward monomer incorporation via one-electron oxidation.[5] Although the polymers obtained from the metal-free approach are superficially the same as those produced via metal-mediated ROMP, the mechanistic distinctions between the two pose unanswered questions regarding synthetic capabilities and structural control from the former. As a first step toward understanding the stereochemical outcomes of metal-free ROMP, we have investigated the olefin geometry and

[1] Reproduced with permission from Pascual, L. M. M.; Goetz, A. E.; Roehrich, A. M.; Boydston, A. J. "Investigation of Tacticity and Living Characteristics in Metal-Free Ring-Opening Metathesis Polymerization" *Macromol. Rapid Commun.* **2017**, *38*, 1600766. Copyright 2017 John Wiley & Sons, Inc.

tacticity of three common polymers: polynorbornene (pNB), polydicyclopentadiene (pDCPD), and polydihydrodicyclopentadiene (pDCPD-$H_2$).

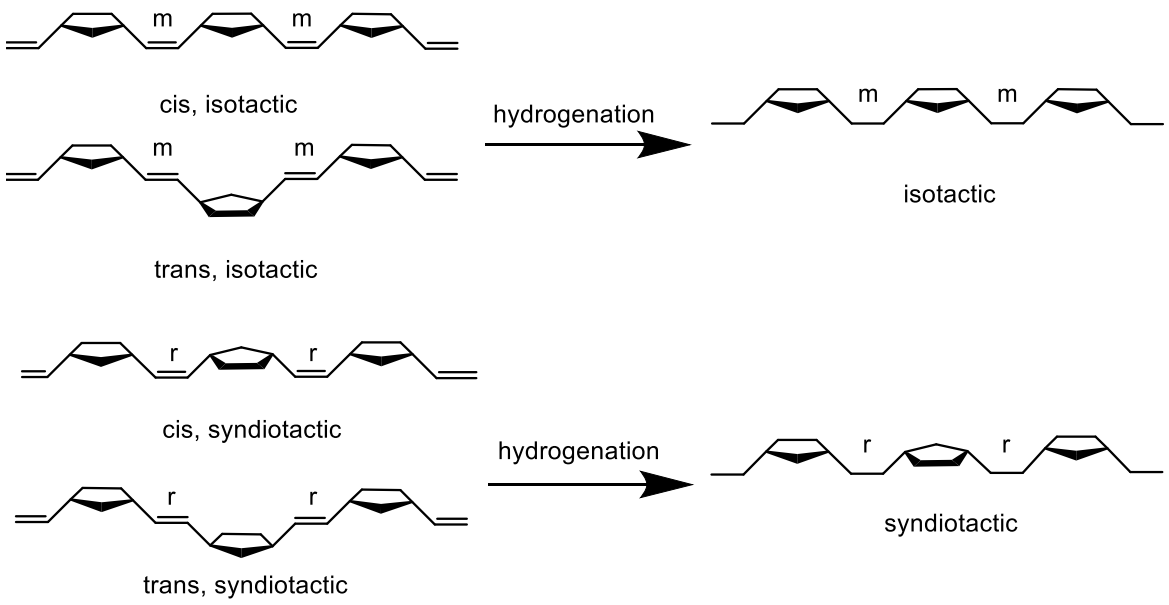


**Figure 4.1**. Polynorbornene structures and their hydrogenated forms.

Another aspect of structural control from metal-mediated ROMP that has garnered many accolades is the broad ability to produce block copolymer architectures.[6] Although it is thus far evident that metal-free ROMP does not enjoy the same breadth of functional group tolerance that has been achieved with metal-based initiators, living characteristics have manifested during investigations of the organocatalyzed photoredox method. A summary of key observations includes: the ability to reinitiate polymer growth upon cycled exposure to light, linear increase in polymer molecular weight with increasing monomer conversion, and narrow molecular weight dispersity for some monomers. Herein, we evaluate the ability of metal-free ROMP to produce diblock copolymers, and the fidelity with which chain extension occurs between pNB and pDCPD-$H_2$.

**Section 2: Results and Discussion**

*4.2.a MF-ROMP Stereochemistry: Olefin Geometry and Tacticity*

To investigate the polymer microstructure obtained from metal-free ROMP, we prepared pNB, pDCPD, and pDCPD-$H_2$ using ethyl propenyl ether initiator and trimethoxyphenyl pyrylium tetrafluoroborate photocatalyst as previously described.[5] Additionally, we prepared each polymer's saturated derivative using previously described conditions for diimide reduction.[4c,d] For pNB and pDCPD-$H_2$, which impart no heterogeneity with regard to head-to-head versus head-to-tail coupling, analysis of the olefin geometry by $^1$H NMR spectroscopy is straightforward (Figure 4.2A). We found pNB to be 23% cis olefin content, similar to that observed for pDCPD-$H_2$ (24% cis) (Table 1). For pDCPD, quantitative $^{13}$C NMR analysis was used to determine a cis olefin content of 28% (Figure 4.2B). The preference for trans olefin geometry is not surprising, however the kinetic outcome appears to have greater cis content than non-stereoselective variants of metal-mediated ROMP. Importantly, the cis/trans ratio was found to remain consistent during the polymerization of norbornene, indicating that secondary metathesis (e.g., chain transfer) or other isomerization pathways were not operative.

**Table 4.1.** Summary of Metal-Free ROMP Polymer Properties.

| polymer | $M_w$ (kDa) | *Đ* | % *cis* olefin | % syndiotactic |
|---|---|---|---|---|
| pNB | 11.2 | 1.2 | 23% | n.d. |
| pDCPD-$H_2$ | 18.5 | 1.3 | 24% | n.d. |
| pDCPD | 4.3 | 1.2 | 28% | n.d. |
| pNB-$H_2$ | n.d. | n.d. | N.A. | 33% |
| pDCPD-$H_2$ → pDCPD-$H_4$ | n.d. | n.d. | N.A. | 58% |
| pDCPD → pDCPD-$H_4$ | n.d. | n.d. | N.A. | 55% |

[a)]Weight-average molecular weight determined by SEC using multiangle laser light scattering (MALS) of polymer samples purified by precipitation; [b)]Molecular weight dispersity using the calculated number-average molecular weight determined by SEC using refractive index detection (values are for polymer samples purified by precipitation); [c)]Determined by $^1$H NMR analysis; [d)]Estimated from quantitative $^{13}$C analysis.

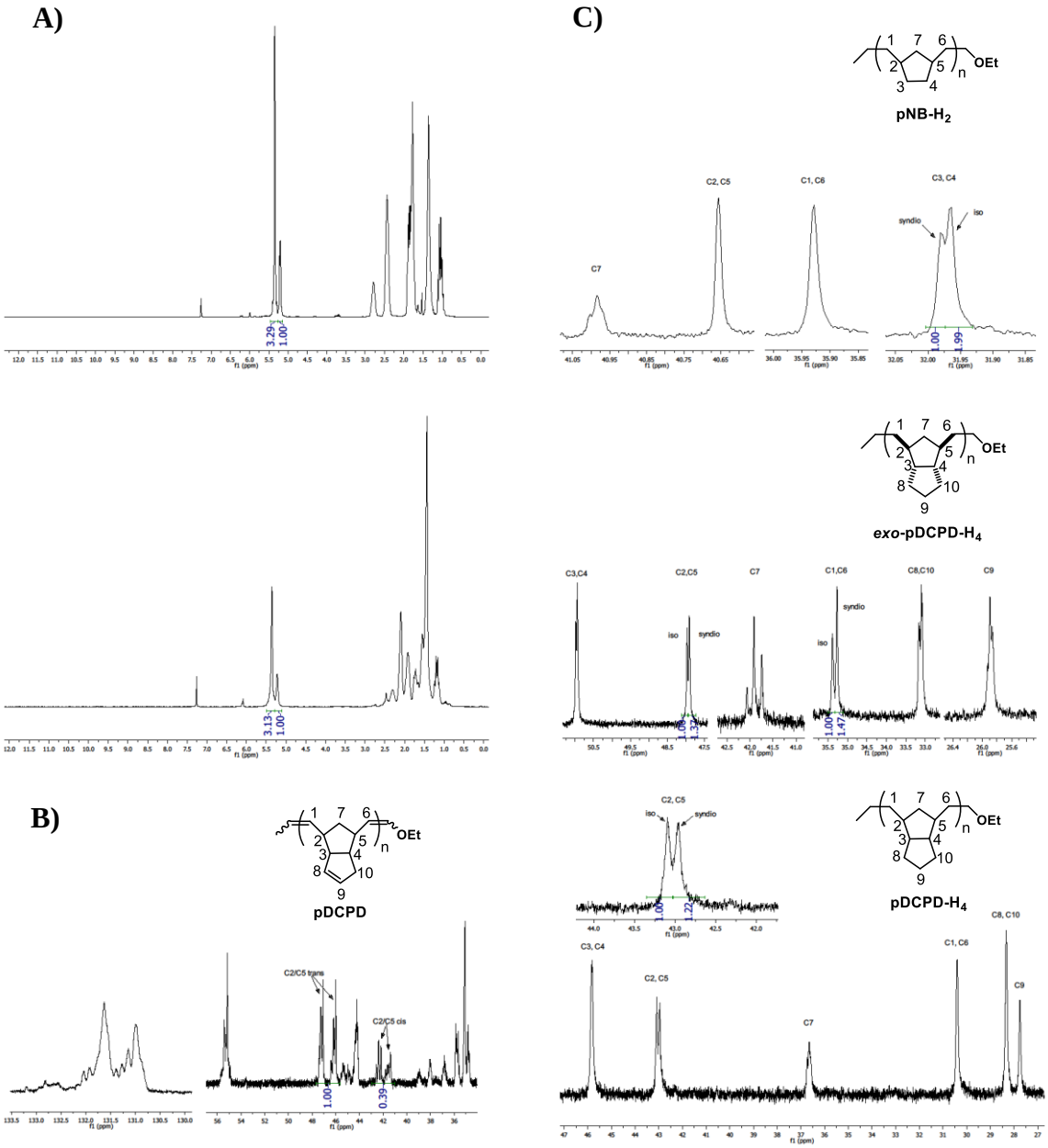


**Figure 4.2**. A) $^{1}H$ NMR spectra of pNB (top) and pDCPD-$H_2$ (bottom). B) $^{13}C$ NMR spectrum of pDCPD. C) $^{13}C$ NMR spectra of pNB-$H_2$ (top), *exo*-pDCPD-$H_4$ (middle), and *endo*-pDCPD-$H_4$ (bottom).

The hydrogenated polymers were used to assess the tacticity obtained from each polymerization. In general, diimide reductions were unremarkable and full conversion of olefin was observed as previously reported. In each case, tacticities were determined by integrating diagnostic $^{13}C$ NMR signals previously identified in the literature.[3,4] These tacticities are only approximate, as key $^{13}C$ NMR signals could not be fully resolved. For hydrogenated pNB (pNB-$H_2$), $^{13}C$ resonances at ≈32 ppm, which correspond to C3/C4, are diagnostic for the C2/C5 stereochemistry (Figure 4.2C).[3c] Using peak integration to estimate the relative amount of syndiotactic and isotactic relationships, we found pNB to be 33% syndiotactic. This indicates that pNB synthesized via metalfree ROMP yields atactic polymer with an isotactic bias.

The dicyclopentadiene-based congeners, pDCPD and pDCPD-$H_2$, each provide pDCPD-$H_4$ upon hydrogenation. Notably, endo-dicyclopentadiene was used to produce pDCPD, whereas *exo*-DCPD-$H_2$ was used to produce pDCPD-$H_2$. Analysis of the quantitative $^{13}C$ NMR spectra of the pDCPD-$H_4$ produced from each polymer source revealed similar tacticity (Figure 4.2C). Specifically, pDCPD and pDCPD-$H_2$ were found to be 55% and 58% syndiotactic, respectively, by correlation with their saturated derivatives. Therefore, both pDCPD and pDCPD-$H_2$ synthesized via metal-free ROMP are atactic, with a slight syndiotactic bias.

*4.2.b Block Copolymer Synthesis*

In addition to microstructural analyses, we also investigated the feasibility of preparing block copolymer structures via metal-free ROMP. As stated previously, block copolymer synthesis is a well-established capability of metal-mediated ROMP. To our knowledge, block copolymers have yet to be reported for metal-free ROMP variations. Chain end stability is critical for the living characteristics that enable successful chain extension from one block to

another in a tandem copolymerization. For metal-free ROMP, we viewed the reactivity of the envisioned vinyl ether radical cation intermediate to be suspect, and therefore sought to determine the parameters within which successful block copolymerization could be achieved.

In previous studies, we reported characteristics typical of living polymerizations, which we speculate arise in metal-free ROMP from reversible deactivation of the active chain end.[5a] Also evident in our previous investigations was an emergence of high molecular weight shoulders observed by size-exclusion chromatography (SEC) as polymerizations reached high conversion. This indicated to us that chain–chain coupling may be occurring as monomer is depleted. We considered the possibility of non-metathetical reactions of the radical cation and olefins within the polymer backbone (or neutral vinyl ether chain ends). Importantly, such reactivity would consume active chains and inhibit successful block copolymer formation.

To explore this further, we attempted block copolymerizations of norbornene and *exo*-dihydrodicyclopentadiene, as each of these monomers was found to undergo metal-free homopolymerization with relatively high conversion and efficiency. With either monomer, high conversion using a 35:1 initial ratio of monomer to initiator is usually observed within 60 min. We evaluated chain end stability and relative success of chain extension to the second po+lymer block by varying the reaction time for the first block formation.

Norbornene was first polymerized in parallel with reaction times of 1, 2, and 3 h. Interestingly, SEC analysis revealed increasing $M_n$ values with increasing reaction time despite the fact that each polymerization achieved essentially the same conversion (97%–99%). Specifically, the $M_n$ values for polymerizations conducted for 1, 2, and 3 h were found to be 5.8, 7.5, and 10.1 kDa, respectively (see Experimental section). Since the increase in $M_n$ cannot be ascribed to differences in conversion and are likely not due to varying initiator efficiencies, we

hypothesize that chain–chain coupling is occurring upon prolonged exposure to blue light. When the second monomer, *exo*-dihydrodicyclopentadiene, was introduced we observed varied extents of successful chain extension depending upon the length of the initial reaction time. As can be seen in the SEC traces in Figure 4.3 (left), increased reaction time for the initial block resulted in qualitatively greater number of dead chains. Importantly, successful block copolymer synthesis was achieved when the reaction times did not exceed 60 min. The moderately broad molecular weight dispersity ($Đ$) in each case appeared to be a manifestation of the pNB synthesis rather than pDCPD-$H_2$ block formation. Additionally, chain transfer did not appear to be significant during polymerization.

When the monomer sequence was reversed, we observed narrower $Đ$ and more consistent $M_n$ values during preparation of the first block (pDCPD-$H_2$). As shown in Figure 4.3 (right), the $Đ$ values were consistently below 1.2 for the pDCPD-$H_2$ block and only slight increase in $M_n$ was observed with increasing reaction time (see the Experimental section). Upon introduction of norbornene to extend to the diblock structure, we again observed increasing number of dead chains from increased block-A reaction time, but to lesser extents than when norbornene was used as the first monomer. Inspection of the SEC traces also revealed high molecular weight shoulders protruding during formation of the second (pNB) block. Collectively, these results indicated to us that increased reaction times may lead to chain–chain coupling between vinyl ether chain ends and polymer backbone, with more sterically hindered repeat units being less susceptible.

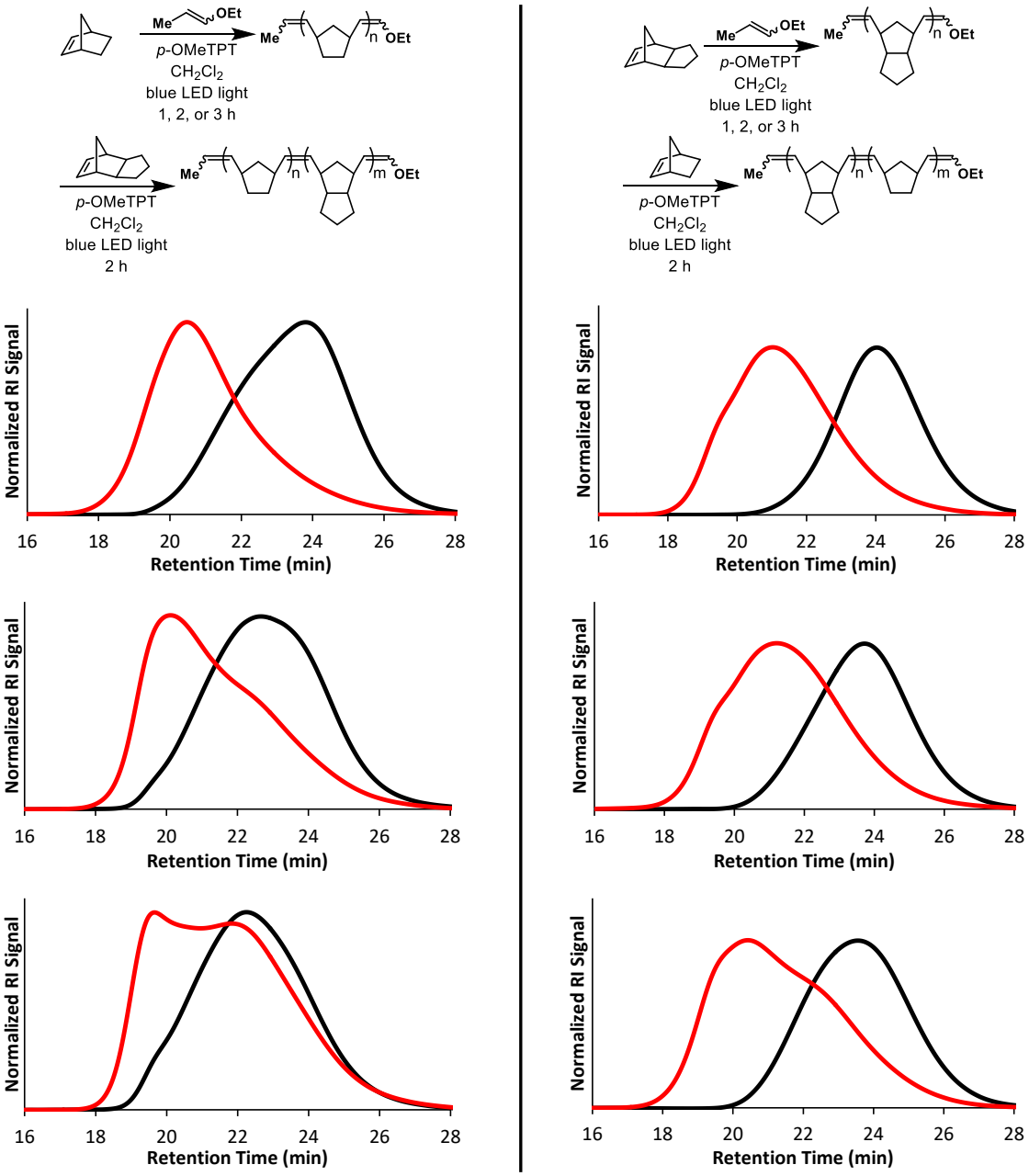


**Figure 4.3**. SEC traces for block copolymer synthesis. Solid = SEC trace after first block formation, dashed = SEC trace after diblock formation. (Left) norbornene used for first block, reaction times top-to-bottom = 1, 2, and 3 h. *exo*-DCPD-$H_2$ then used for second block with reaction time = 2 h. (Right) *exo*-DCPD-$H_2$ used for first block, reaction times top-to-bottom = 1, 2, and 3 h. Norbornene then used for second block with reaction time = 2 h.

## Section 3: Conclusions

In conclusion, we have successfully demonstrated block copolymerization via metal-free ROMP using NB and *exo*-DCPD-$H_2$. In polymerizations where pNB was the first block, chain extension was substantially more successful with shorter reaction times, consistent with irreversible termination of the end groups. By contrast, *exo*-DCPD-$H_2$ exhibited more complete chain extension, presumably due to increased steric shielding of the polymer backbone that inhibited untoward reaction with chain ends. Additionally, we demonstrated that metal-free ROMP polymers are largely atactic. These analyses are the first steps toward achieving broader structural versatility and tactoselectivity in metal-free ROMP.

## Section 4: Experimental

*4.4.a General Considerations*

For reactions set up inside the glovebox, dichloromethane ($CH_2Cl_2$) was obtained from a solvent purification system and stored in the glovebox. For reactions set up outside the glovebox, $CH_2Cl_2$ (Fisher Chemical, HPLC grade) was dried over 3 Å molecular sieves. Norbornene (NB, Acros Organics, 99%) was sublimed prior to use. Dicyclopentadiene (DCPD, Aldrich), p-toluenesulfonyl hydrazide (p-Tos-NHNH2, Alfa Aesar), and chloroform ($CHCl_3$, Fisher Chemical) were used as-received. $^1$H NMR spectra were recorded with a 300 MHz Bruker AVance NMR spectrometer. Quantitative $^{13}$C NMR spectra were recorded with a 700 MHz Bruker AVance NMR spectrometer. Chemical shifts are reported in delta (δ) units, expressed in parts per million (ppm) downfield from tetramethylsilane using the residual protio-solvent as an internal standard ($CDCl_3$, $^1$H: 7.26 ppm and $^{13}$C 77.16 ppm). Size-exclusion chromatography

(SEC) was performed using a SEC setup consisting of: a Shimadzu pump, 3 in-line columns (MZ Gel), and Wyatt Technology Corporation light scattering and refractive index detectors with tetrahydrofuran (THF) as the mobile phase. Number average molecular weights ($M_n$) and weight-average molecular weights ($M_w$) were calculated from light scattering and refractive index data. Irradiation of photochemical reactions was done using a 2 W Miracle blue LED indoor gardening bulb. The pyrylium tetrafluoroborate salt was prepared according to literature procedure.[7,8] *exo*-Dihydrodicyclopentadiene (*exo*-DCPD-$H_2$) was prepared according to literature procedure (89% *exo* isomer, 11% *endo* isomer).[5b] Polymer hydrogenations were carried out according to literature procedure using a Parr reactor.[9,10]

*Abbreviations*

pNB = polynorbornene, pDCPD = polydicyclopentadiene, pDCPD-$H_2$ = poly(dihydrodicyclopentadiene), p-OMeTPT = 2,4,6-tris(4-methoxyphenyl)pyrylium tetrafluoroborate.

*4.4.b Tacticity Studies*

*General Procedure for Photoredox-Mediated ROMP*

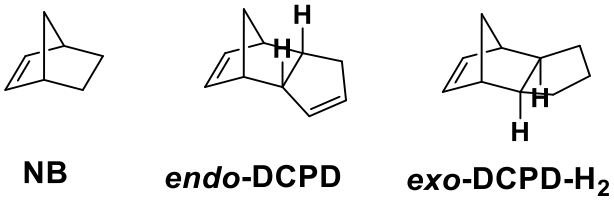


**Figure 4.4**. Monomers used in this study.

In a 2 dram screw-cap vial, 1.0 equivalent ethyl propenyl ether, 100 equivalents monomer, and 0.05-0.07 equivalents p-OMeTPT were dissolved in $CH_2Cl_2$ (2.25 M initial monomer concentration). The solution was stirred in the sealed vial under ambient atmosphere and irradiated with a 450 nm 2 W blue LED light source for 75 min. The distance between the light source and vial was 1 cm. Polymers were then hydrogenated according to literature procedure.[9,10]

**Table 4.2.** Results of polymerizations and molecular weight data for polymers after purification by precipitation.

| **Polymer** | **conversion (yield)** | $M_n$ **(kDa)** | $M_w$ **(kDa)** | $Đ$ |
|---|---|---|---|---|
| pNB | 71% (52%) | 9.5 | 11.2 | 1.2 |
| pDCPD-$H_2$ | 81% (68%) | 13.8 | 18.5 | 1.3 |
| pDCPD | 19% (7%) | 3.5 | 4.3 | 1.2 |

*Quantitative $^{13}C$ NMR Experiments*

Quantitative $^{13}C$ NMR spectra were obtained using a concentration of 25 - 50 mg/mL of hydrogenated polymer, or 100 mg/mL of pDCPD, each in $CDCl_3$. For pDCPD and *endo*-pDCPD-$H_4$, $^{13}C$ NMR data was collected at 298 K. For all other polymers, $^{13}C$ NMR data was collected at 328 K. The following acquisition and processing parameters were used:

- Number of data points (TD) = size of data processed (SI) = 64k (65,536)
- Delay time (d1) = 90 seconds
- Lorentzian broadening factor (LB) = 0.30 Hz
- Scan width of 220 ppm, centered at 110 ppm
- Number of Scans (NS) = 64, Number of Experiments (TD0) = 8 (512 scans)

o For pDCPD, NS = 64, TD0 = 16, or 1,024 scans total

*4.4.c Block Copolymerization and Chain End Stability Studies*

In a 2 dram screw-cap vial equipped with a stirbar and, 5 μL (0.045 mmol, 1 eq) ethyl propenyl ether, 35 eq of the first monomer (NB or *exo*-DCPD-$H_2$), and 1.6 mg (0.003 mmol, 0.07 eq) p-OMeTPT were dissolved in 2.0 mL $CH_2Cl_2$ and sealed under nitrogen atmosphere in a glovebox. The vial was then removed from the glovebox and irradiated with 4 W blue LEDS for 1, 2, or 3 hrs. Under a stream of $N_2$ (g), the 65 eq of the second monomer (*exo*-DCPD-$H_2$ or NB) was added. The vial was sealed and the reaction was irradiated an additional 2 hrs. Both reaction steps were monitored using $^1$H NMR spectroscopy and SEC (crude reaction aliquots). Upon completion of the experiment, each reaction mixture was then filtered through a plug of neutral alumina, eluted with $CH_2Cl_2$, concentrated to 5 - 7 mL $CH_2Cl_2$, and precipitated into 75 mL MeOH. The polymer was the collected by filtration, and washed with MeOH and acetone. The isolated polymer was then characterized by $^1$H NMR spectroscopy and SEC.

**Table 4.3.** Block copolymerization using NB as first monomer and *exo*-DCPD-$H_2$ as second monomer. Time listed refers to block-A synthesis.

| | Conversion | | | Block A | | | AB Diblock | | | |
|---|---|---|---|---|---|---|---|---|---|---|
| Time (h) | NB | DCPD-$H_2$ | Yield | $M_n$ (kDa) | $M_w$ (kDa) | $Đ$ | $M_n$ (kDa) | $M_w$ (kDa) | $Đ$ | NB:DCPD-$H_2$ in copolymer |
| 1 | 97% | 80% | 51% | 5.8 | 9.1 | 1.6 | 18.5 | 31.1 | 1.7 | 0.71:1.0 |
| 2 | 98% | 47% | 37% | 7.5 | 12.0 | 1.6 | 13.4 | 27.7 | 2.1 | 1.14:1.0 |
| 3 | 99% | 30% | 29% | 10.1 | 14.7 | 1.5 | 12.7 | 24.6 | 2.0 | 2.11:1.0 |

**Table 4.4.** Block copolymerization using *exo*-DCPD-$H_2$ as first monomer and NB as second monomer. Time listed refers to block-A synthesis.

| | Conversion | | | Block A | | | AB Diblock | | | |
|---|---|---|---|---|---|---|---|---|---|---|
| Time (h) | NB | DCPD-$H_2$ | Yield | $M_n$ (kDa) | $M_w$ (kDa) | $Đ$ | $M_n$ (kDa) | $M_w$ (kDa) | $Đ$ | NB:DCPD-$H_2$ in copolymer |
| 1 | 98% | 94% | 60% | 6.2 | 7.0 | 1.1 | 15.2 | 23.2 | 1.5 | 1.39:1.0 |
| 2 | 99% | 82% | 55% | 7.6 | 9.1 | 1.2 | 14.5 | 22.2 | 1.6 | 1.20:1.0 |
| 3 | 99% | 83% | 52% | 8.6 | 10.0 | 1.2 | 15.8 | 27.2 | 1.7 | 1.31:1.0 |

*4.4.d NMR Spectra*

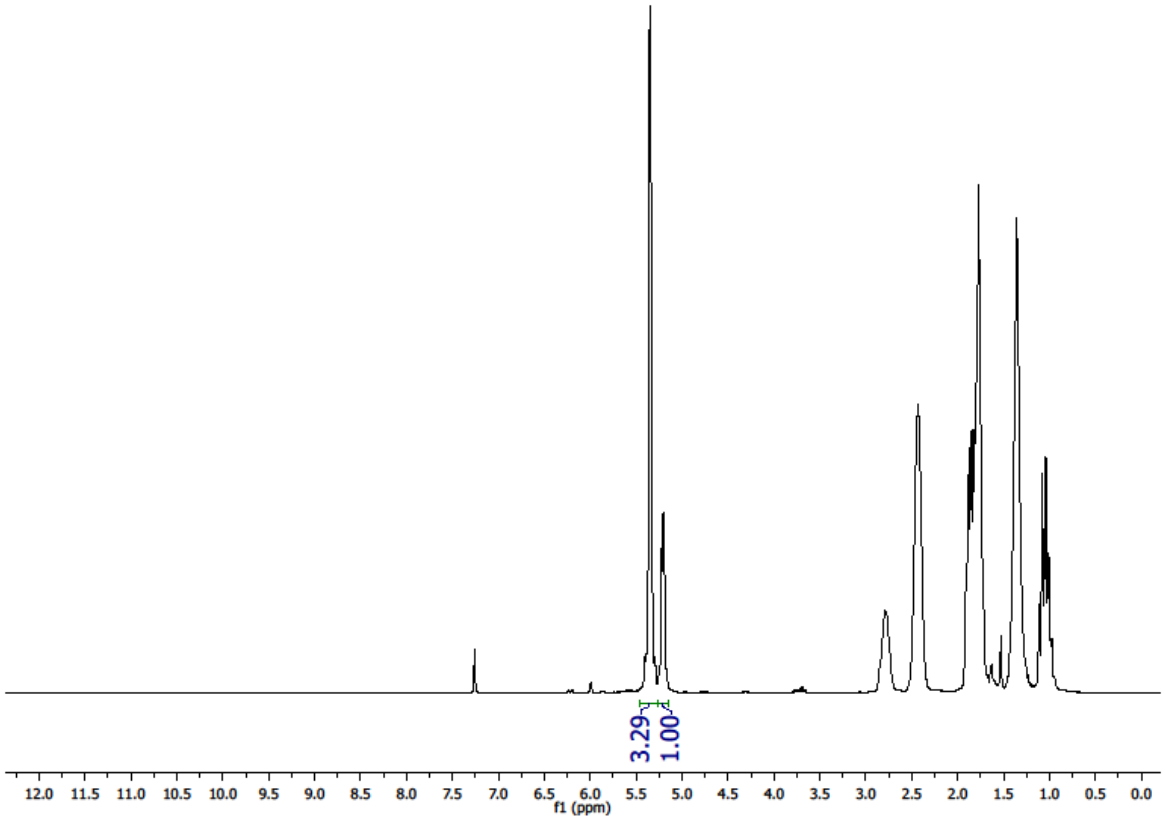


**Figure 4.5**. $^{1}$H NMR spectrum of pNB (23% cis, 77% trans).

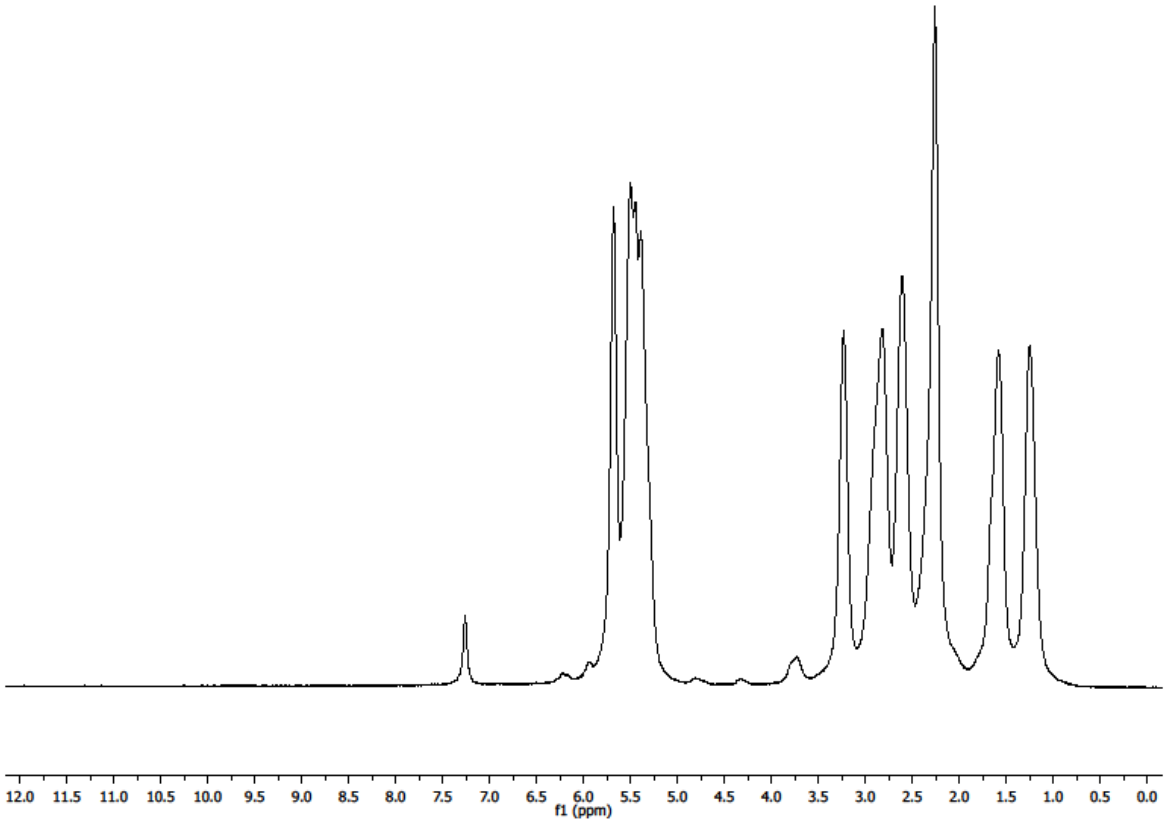


**Figure 4.6**. $^{1}H$ NMR spectrum of *endo*-pDCPD.

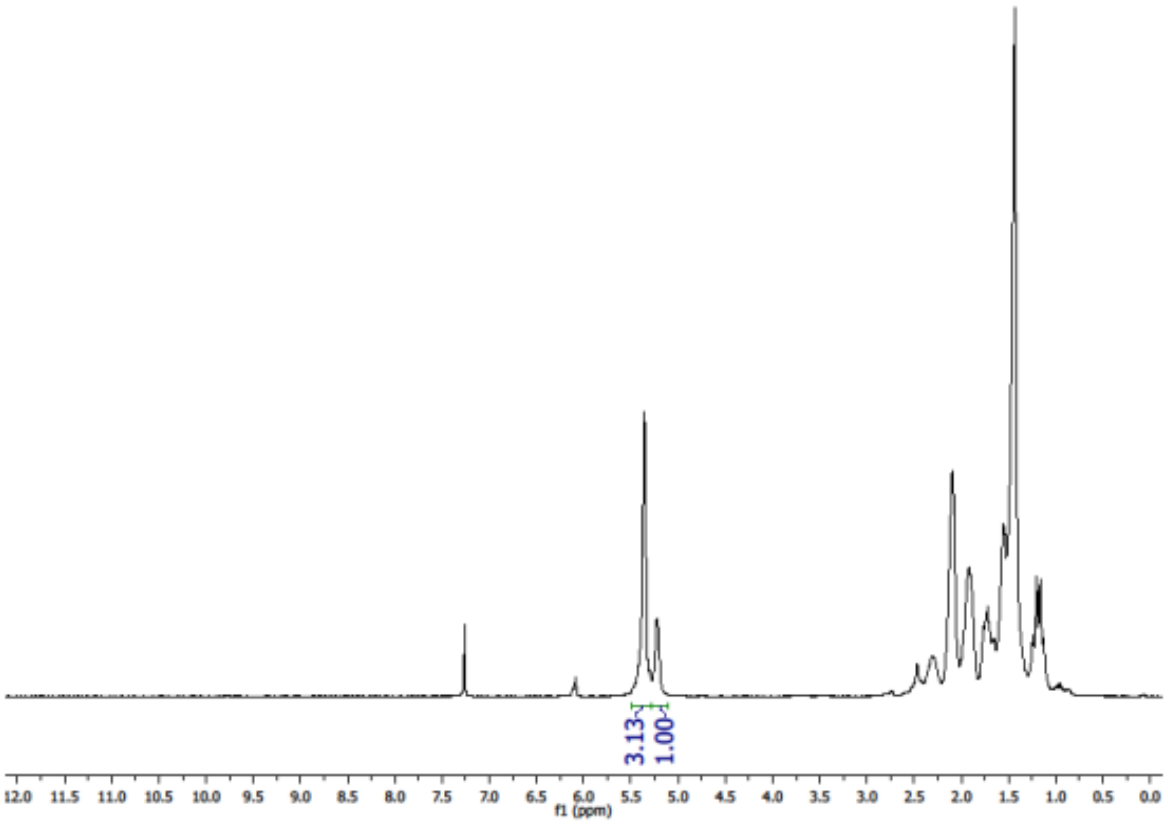


**Figure 4.7**. $^{1}H$ NMR spectrum of *exo*-pDCPD-$H_2$ (24% cis, 76% trans).

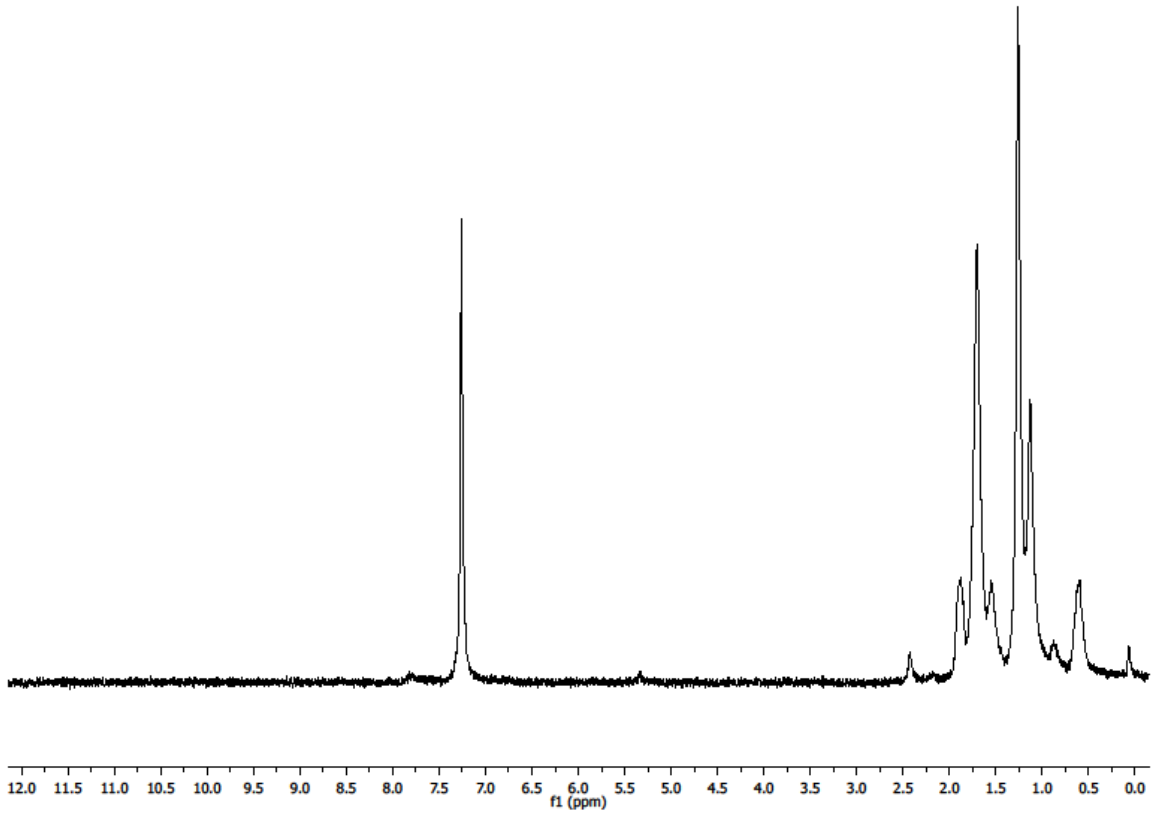


**Figure 4.8**. $^{1}H$ NMR spectrum of pNB-$H_2$.

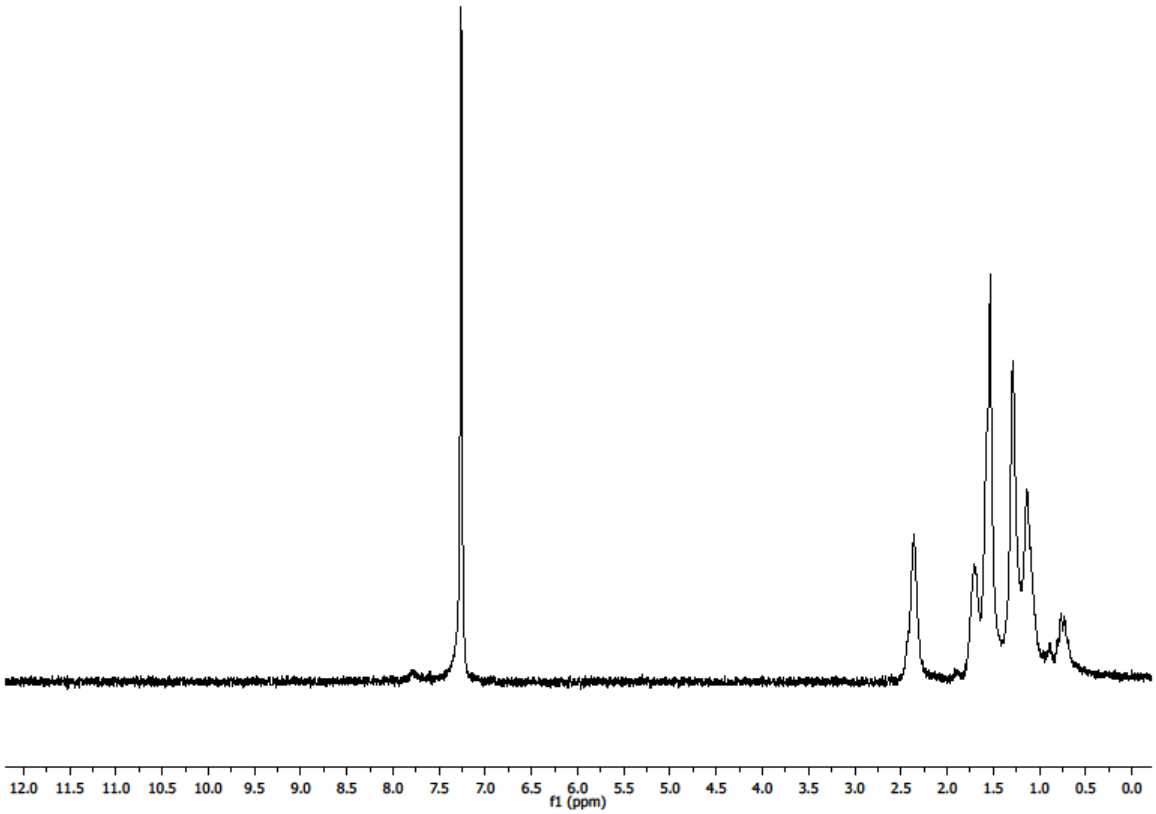


**Figure 4.9**. $^{1}H$ NMR spectrum of *endo*-pDCPD-$H_4$ (produced from *endo*-pDCPD).

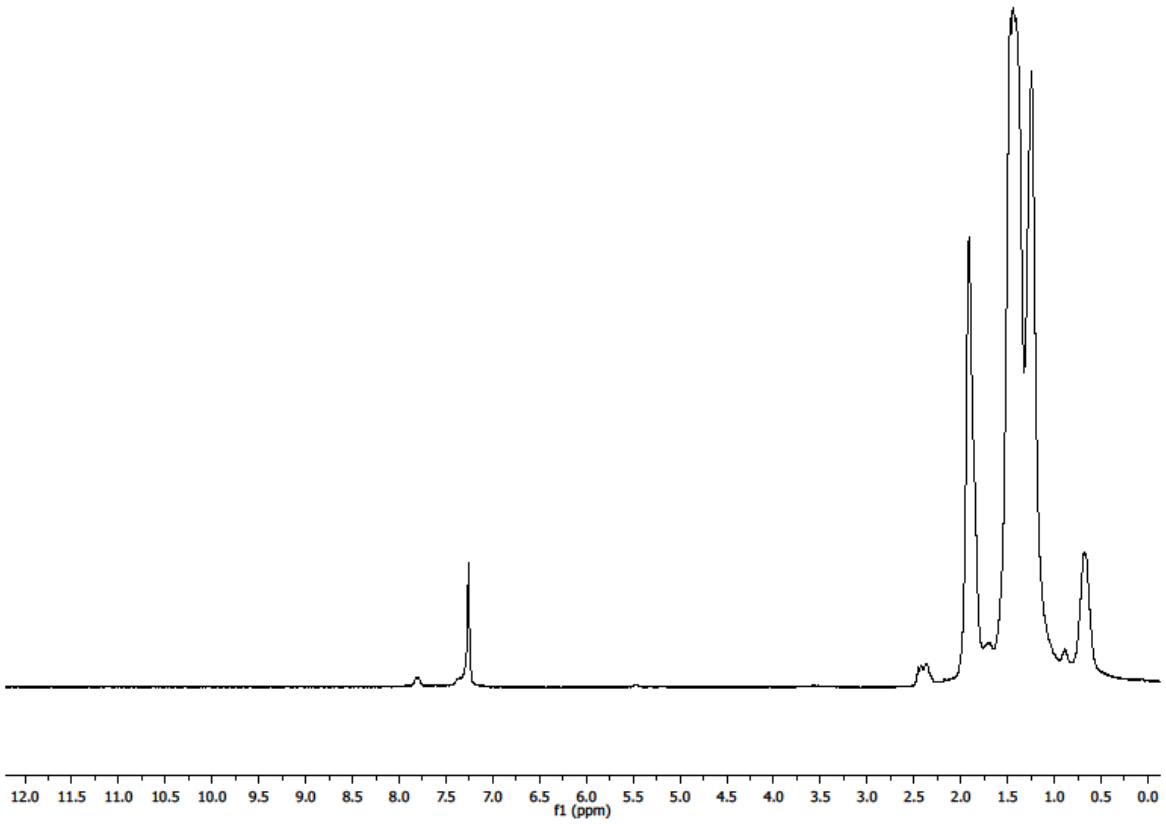


**Figure 4.10**. $^{1}H$ NMR spectrum of *exo*-pDCPD-$H_4$ (produced from *exo*-pDCPD-$H_2$).

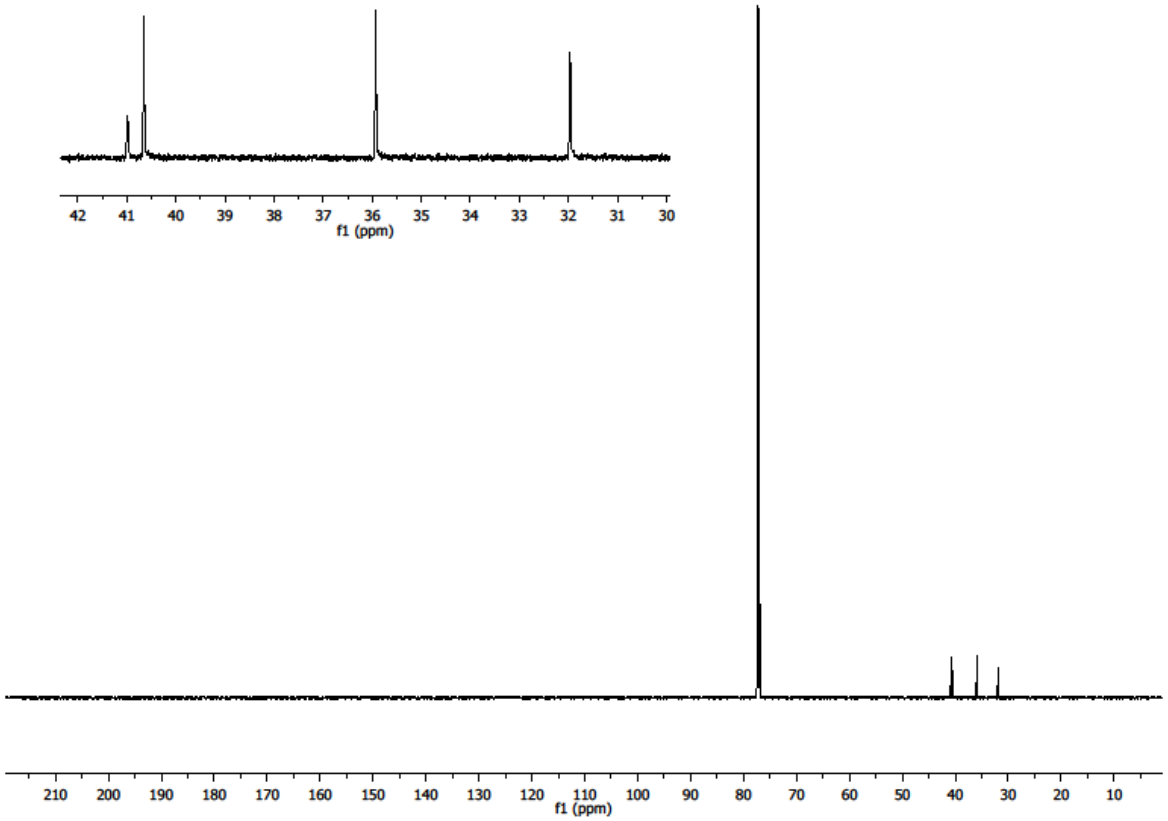


**Figure 4.11**. Quantitative $^{13}C$ NMR spectrum of pNB-$H_2$.

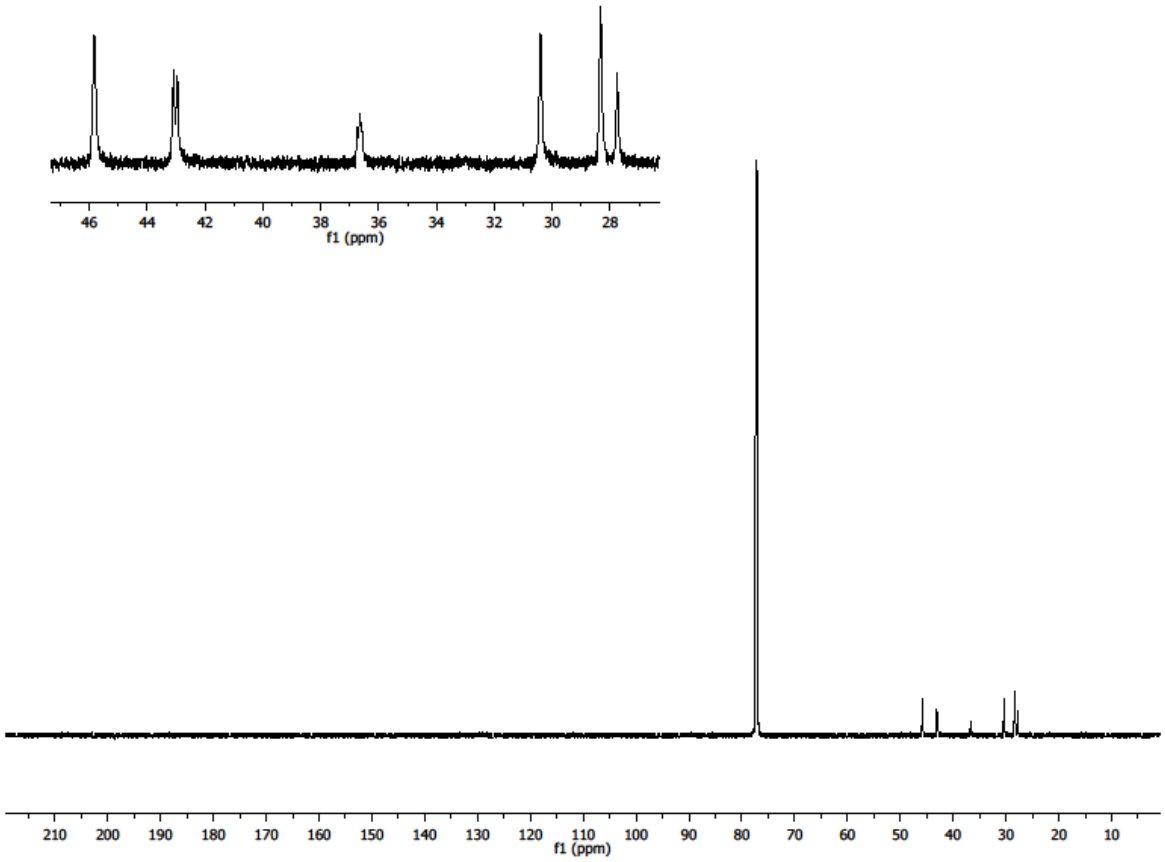


**Figure 4.12**. Quantitative $^{13}C$ NMR spectrum of *endo*-pDCPD-$H_4$ (produced from *endo*-pDCPD).

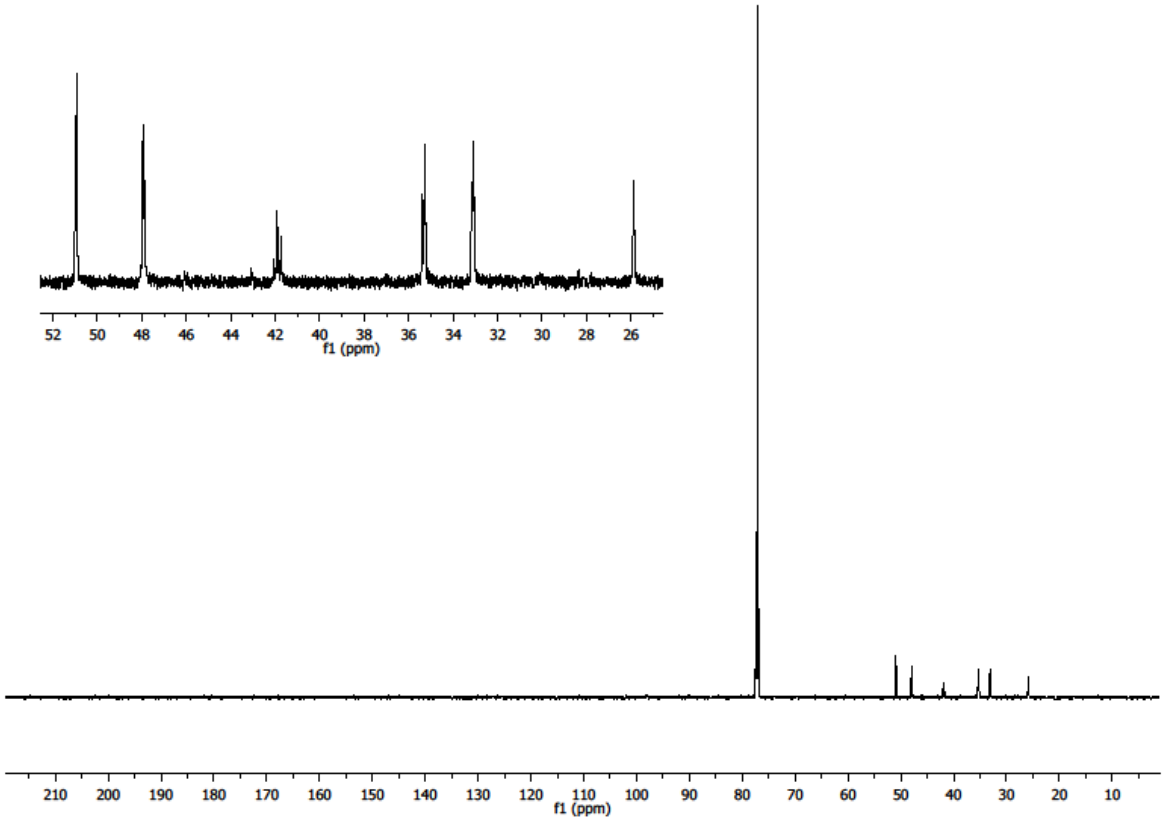


**Figure 4.13**. Quantitative $^{13}C$ NMR spectrum of *exo*-pDCPD-$H_4$ (produced from *exo*-pDCPD-$H_2$).

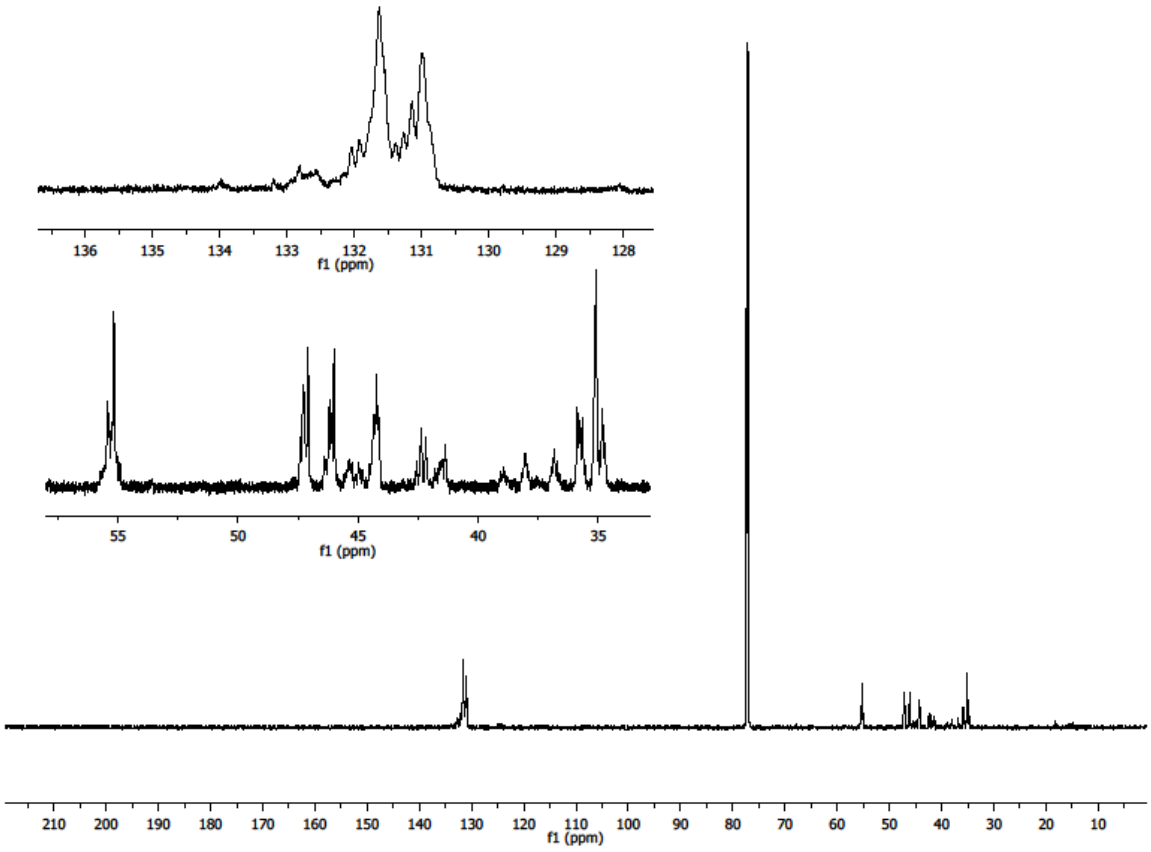


**Figure 4.14**. Quantitative $^{13}C$ NMR spectrum of *endo*-pDCPD.

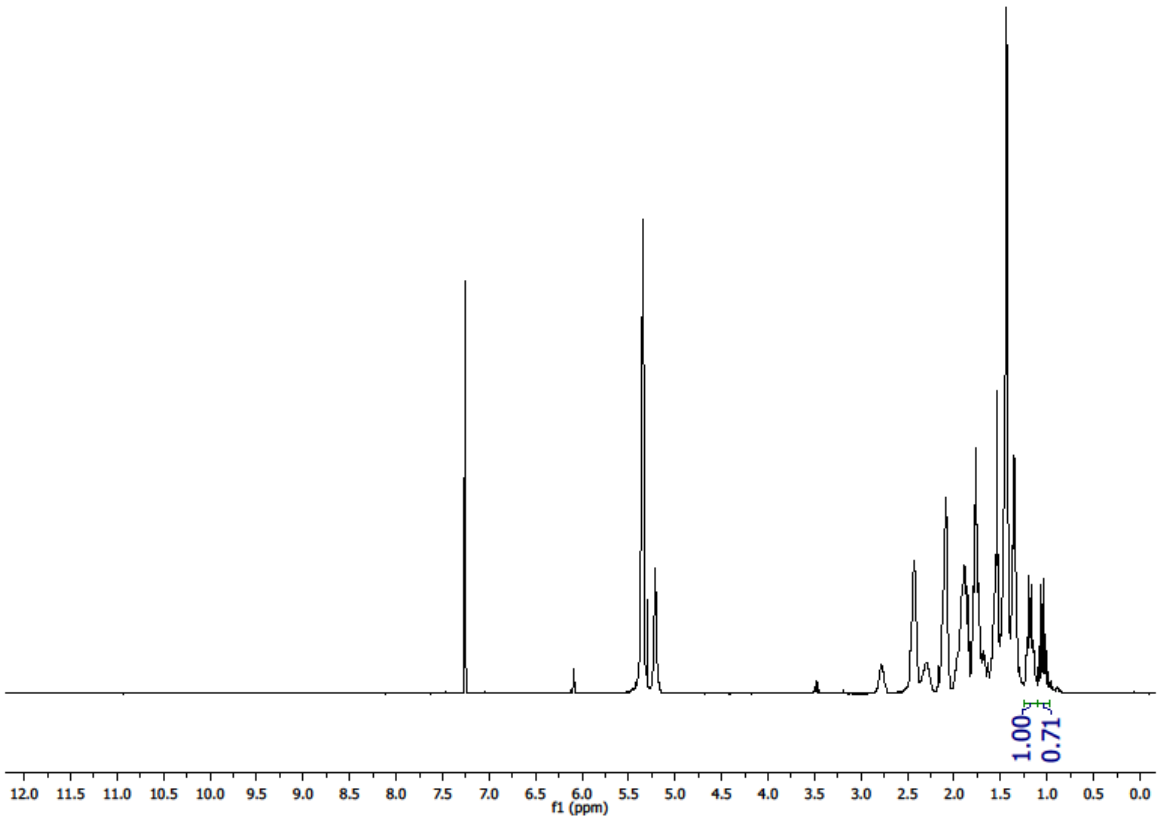


**Figure 4.15**. Diblock copolymer (NB first, 1 h, Table 4.3 row 1) having 42% NB, 58% exo-pDCPD-$H_2$.

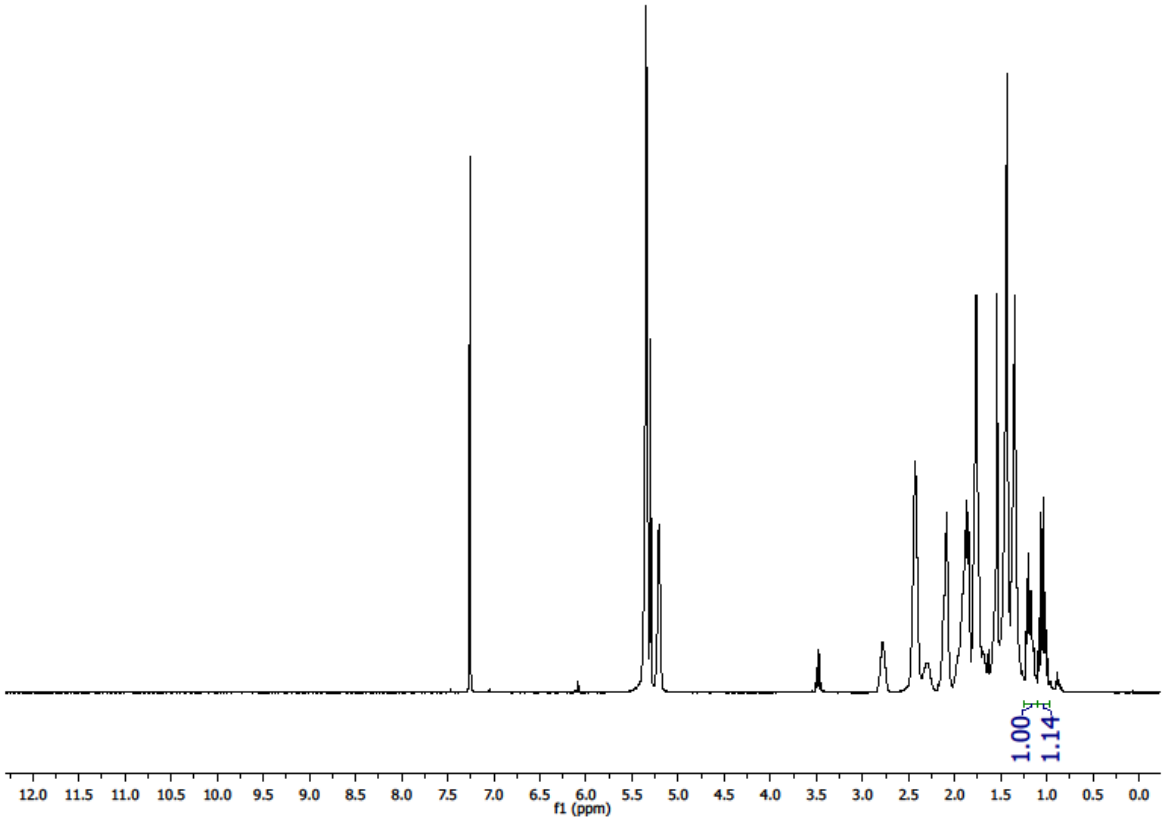


**Figure 4.16**. Diblock copolymer (NB first, 2 h, Table 4.3 row 2) having 53% NB, 47% exo-pDCPD-$H_2$.

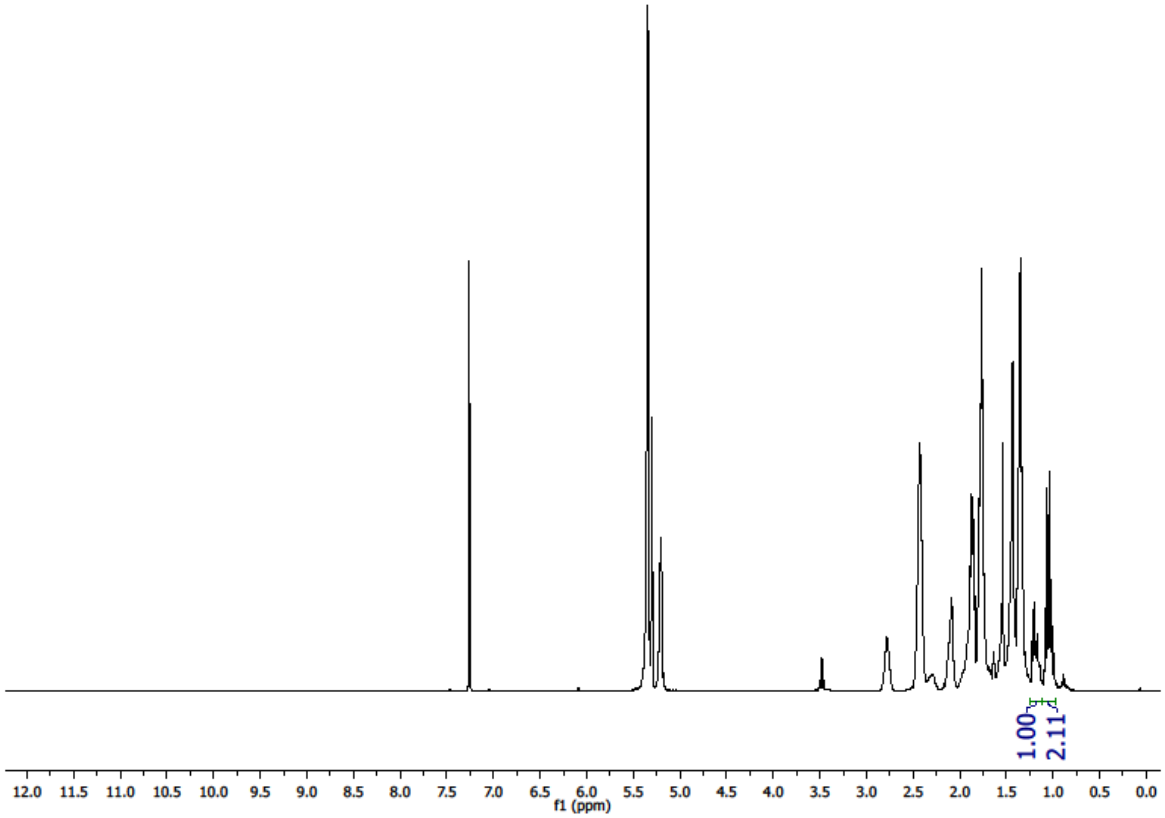


**Figure 4.17**. Diblock copolymer (NB first, 3 h, Table 4.3 row 3) having 68% NB, 32% exo-pDCPD-$H_2$.

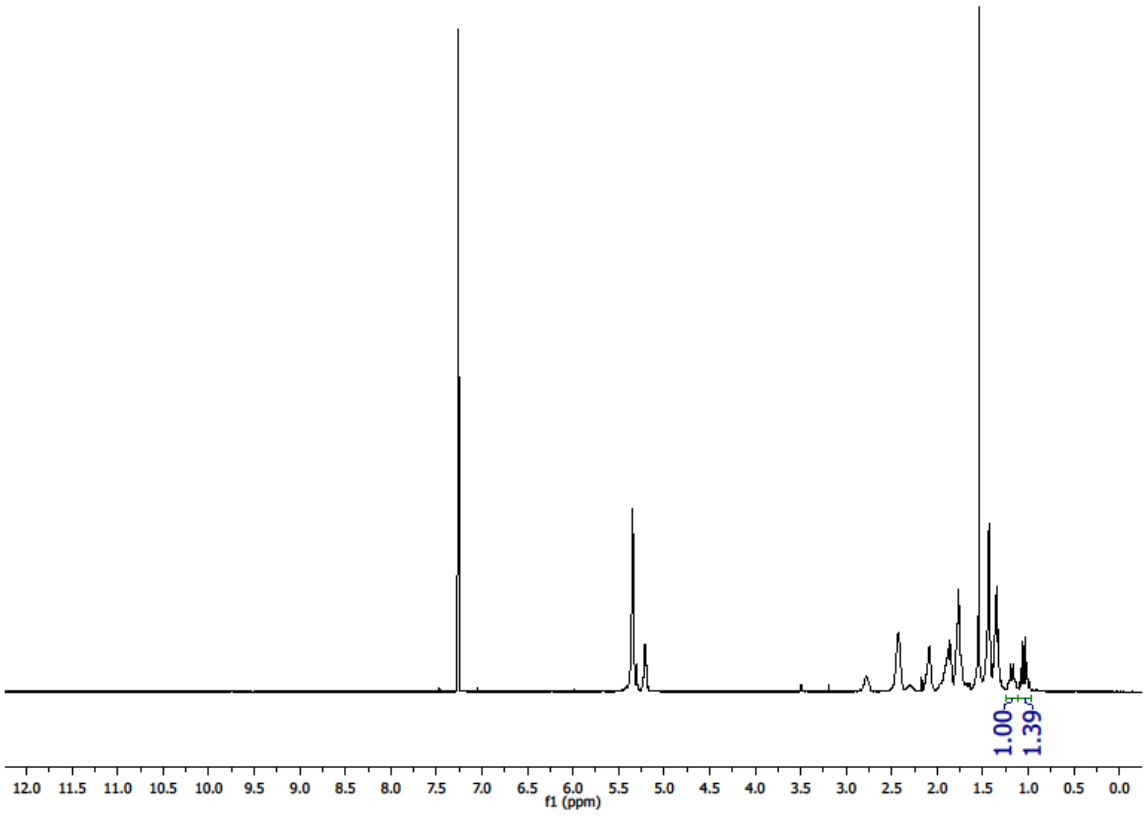


**Figure 4.18**. Diblock copolymer (*exo*-PDCPD-$H_2$ first, 1 h, Table 4.4 row 1) having 58% NB, 42% exo-pDCPD-$H_2$.

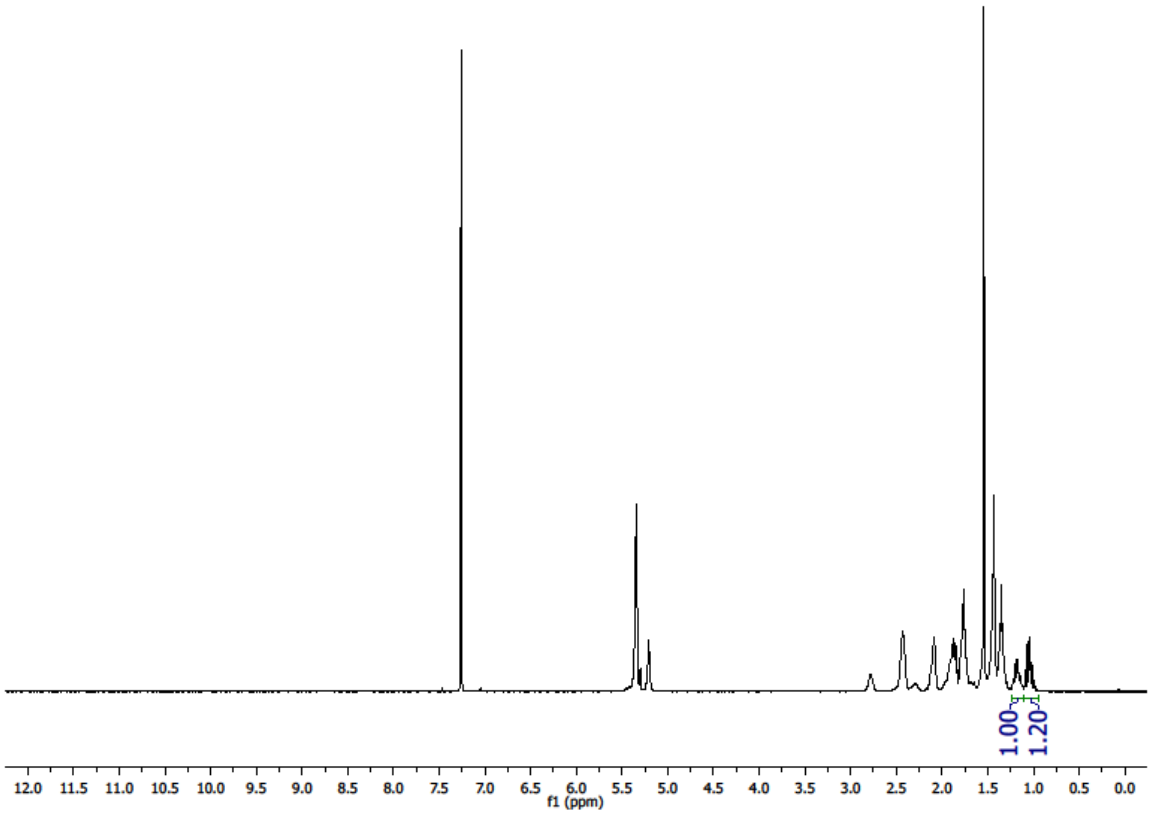


**Figure 4.19**. Diblock copolymer (*exo*-PDCPD-$H_2$ first, 2 h, Table 4.4 row 2) having 55% NB, 45% exo-pDCPD-$H_2$.

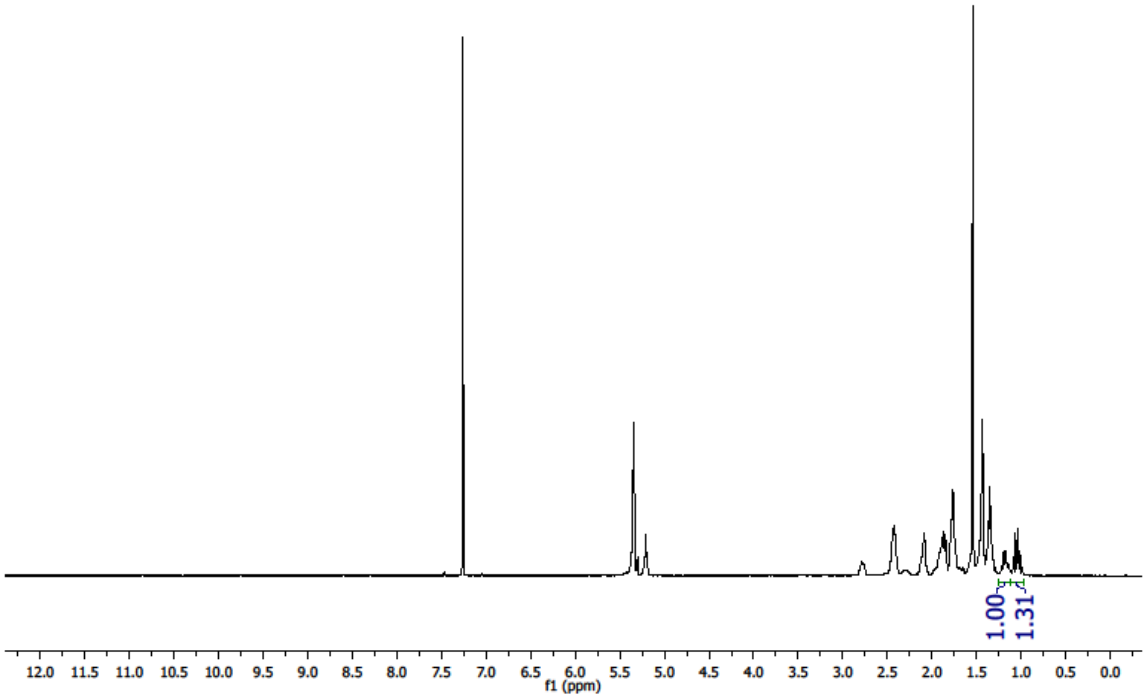


**Figure 4.20**. Diblock copolymer (*exo*-PDCPD-$H_2$ first, 3 h, Table 4.4 row 3) having 57% NB, 43% exo-pDCPD-$H_2$.

**Notes and References for Chapter 4**


[1] a) A. M. Rosales, R. A. Segalman, R. N. Zuckermann, *Soft Matter* **2013**, *9*, 8400; b) E. M. Woo, C. Ling, *Tacticity in Vinyl Polymers: The Encyclopedia of Polymer Science and Technology*, 4th ed., Wiley, Hoboken, NJ **2014**, Vol. *13*, pp. 650–671.
[2] a) R. M. Weiss, A. L. Short, T. Y. Meyer, *ACS Macro Lett*. **2015**, *4*, 1039; b) T. Soejima, K. Satoh, M. Kamigaito, *ACS Macro Lett*. **2015**, *4*, 745; c) B. N. Norris, S. Zhang, C. M. Campbell, J. T. Auletta, P. Calvo-Marzal, G. R. Hutchinson, T. Y. Meyer, *Macromolecules* **2013**, *46*, 1384; d) L. Ren, G. L. Li, J. Shen, D. Jia, *Polym. Int*. **2005**, *54*, 1097; e) J. Li, S. N. Rothstein, S. R. Little, H. M. Edenborn, T. Y. Meyer, *J. Am. Chem. Soc*. **2012**, *134*, 16352; f) J. P. Bishop, R. A. Register, *J. Polym. Sci. Pol. Phys*. **2011**, *49*, 68; g) T. Steinhäusler, W. J. Koros, *J. Polym. Sci. Pol. Phys*. **1997**, *35*, 91; h) E. Rojo, M. E. Muñoz, A. Santamaría, B. Peña, *Macromol. Rapid Commun*. **2004**, *25*, 1314; i) C. Agatemor, M. P. Shaver, *Biomacromolecules* **2013**, *14*, 699; j) T. D. Jones, K. A. Chaffin, F. S. Bates, *Macromolecules* **2002**, *35*, 5061.
[3] a) S. Hayano, Y. Nakama, *Macromolecules* **2014**, *47*, 7797; b) J. G. Hamilton, K. J. Ivin, J. J. Rooney, *J. Mol. Catal*. **1986**, *36*, 115; c) B. Al-Samak, V. Amir-Ebrahimi, A. G. Carvill, J. G. Hamilton, J. J. Rooney, *Polym. Int*. **1996**, *41*, 85; d) V. Amir-Ebrahimi, D. A. K. Corry, J. G. Hamilton, J. J. Rooney, *J. Mol. Catal. A: Chem*. **1998**, *133*, 115.
[4] a) R. Schrock, *Dalton Trans*. **2011**, *40*, 7484; b) R. R. Schrock, *Acc. Chem. Res*. **2014**, *47*, 2457; c) B. Autenrieth, H. Jeong, W. P. Forrest, J. C. Axtell, A. Ota, T. Lehr, M. R. Buchmeiser, R. R. Schrock, *Macromolecules* **2015**, *48*, 2480; d) B. Autenrieth, R. R. Schrock, *Macromolecules* **2015**, *48*, 2493; e) W. P. Forrest, J. G. Weis, J. M Johan, J. C. Axtell, J. H. Simpson, T. M. Swager, R. R. Schrock, *J. Am. Chem. Soc*. **2014**, *136*, 10910; f) L. E. Rosebrugh, V. M. Marx, B. K. Keitz, R. H. Grubbs, *J. Am. Chem. Soc*. **2013**, *135*, 10032; g) R. K. M. Khan, S. Torker, A. H. Hoveyda, *J. Am. Chem. Soc*. **2013**, *135*, 10258; h) S. Hayano, Y. Takeyama, Y. Tsunogae, I. Igarashi, *Macromolecules*, **2006**, *39*, 4663; i) S. Hayano, T. Sugawara, Y. Tsunogae, *J Polym. Sci., Part A: Polym Chem*, **2006**, *44*, 3153; j) S. Hayano, Y. Tsunogae, *Macromolecules*, **2006**, *39*, 30; k) S. Hayano, Y. Tsunogae, *Chem. Lett.* **2005**, *34*, 1520; l) S. Hayano, H. Kurakata, Y. Tsunogae, Y. Nakayama, Y. Sato, J. Yasuda, *Macromolecules*, **2003**, *36*, 7422; m) S. Hayano, H. Kurakata, D. Uchida, M. Sakamoto, N. Kishi, H. Matsumoto, Y. Tsunogae, I. Igarashi, *Chem. Lett.* **2003**, *32*, 670.
[5] a) K. A. Ogawa, A. E. Goetz, A. J. Boydston, *J. Am. Chem. Soc*. **2015**, *137*, 1400; b) A. E. Goetz, A. J. Boydston, *J. Am. Chem. Soc*. **2015**, *137*, 7572; c) L. M. M. Pascual, D. G. Dunford, A. E. Goetz, K. A. Ogawa, A. J. Boydston, *Synlett* **2016**, *27*, 759; e) A. E. Goetz, L. M. M. Pascual, D. G. Dunford, K. A. Ogawa, D. B. Knorr Jr., A. J. Boydston, *ACS Macro. Lett*. **2016**, *5*, 579.
[6] a) C. Slugovc, *Macromol. Rapid Commun*. **2004**, *25*, 1283; b) A. Leitgeb, J. Wappel, C. Slugovc, *Polymer* **2010**, *51*, 2927; c) S. Riegler, C. Slugovc, G. Trimmel, F. Stelzer, *Macromol. Symp*. **2004**, *217*, 231; d) K. Nomura, M. M. Abdellatif, *Polymer* **2010**, *51*, 1861; e) W. J. Feast, E. Khosravi, *J. Fluorine Chem*. **1999**, 100, 117; f) S. Sutthasupa, M. Shiotsuki, F. Sanda, *Polym. J*. **2010**, *42*, 905; g) C. W. Bielawski, R. H. Grubbs, *Prog. Polym. Sci*. **2007**, *32*, 1.
[7] Martiny, M; Steckhan, E; Esch, T. *Chem. Ber*. **1993**, *126*, 1671.
[8] Heyes, D; Menon, R. S; Watt, I. F; Wiseman, J; Kubinski, P. *J. Phys. Org. Chem*. **2002**, *15*, 689.
[9] Autenrieth, B.; Schrock, R. R. *Macromolecules*. **2015**, *48*, 2493.

[10] Autenrieth, B.; Jeong, H.; Forrest, W. P.; Axtell, J. C.; Ota, A.; Lehr, T.; Buchmeiser, M. R.; Schrock, R. R. *Macromolecules*. **2015**, *48*, 2480.

# Chapter 5: Molecular Weight Control and Chain End Modification via Chain Transfer in Metal-Free Ring-Opening Metathesis Polymerization

## Section 1: Introduction

While the ability to install a vinyl ether chain end is unique to MF-ROMP and may offer synthetic advantages, the vinyl ether initiator remains a substantial recurring cost. Low initiation efficiencies at lower initial ratios of moles of monomer to initiator (such as 53% at NB:EPE of 97:1) increase the cost of targeting a specific molecular weight.[1] Furthermore, for many post-polymerization modifications, such as secondary metathesis with ruthenium-based catalysts, it is necessary to have a method for removing the vinyl ether.

Furthermore, the synthesis of oligomers is attractive for applications requiring low $T_g$ or $T_m$, such as molding. In the synthesis of oligomers via MF-ROMP, vinyl ether polymerization begins to occur as a substantial side-reaction. These oligomers can be difficult to separate. This further increases the demand for a means of removing the vinyl ether chain end.

Addition of an acyclic olefin chain transfer agent (CTA) to ROMP polymerizations has successfully been used to control molecular weight, regenerate initiator, and synthesize end-functionalized ROMP polymers for various subsequent reactions, such as block copolymerizations.[2] Remarkably low dispersities have been achieved in ROMP with chain transfer using pulsed-addition ROMP (PA-ROMP).[2b,e,m] In this approach, continual addition of CTA results in CTA reacting only with the active chain end, regenerating initiator and yielding polymer of narrow dispersity.

## Section 2: Results and Discussion

*5.2.a Molecular Weight Control*

We envisioned a mechanism by which an internal olefin could undergo cross metathesis with a vinyl ether chain end to cleave the vinyl ether and achieve molecular weight control. Initial trials with internal olefins, which have enjoyed success as CTAs in metal-mediated ROMP, did not cause chain transfer in MF-ROMP. However, we observed successful chain transfer with α-olefins such as 1-hexene, which is particularly appealing as it is a low-cost product of the Shell Higher Olefin Process.[3]

In the envisioned mechanism, ethyl propenyl ether initiates the MF-ROMP polymerization of a ROMP monomer such as dicyclopentadiene (**1**). Propagation followed by chain transfer can produce either polydicyclpentadiene **2** and ethyl hexenyl ether (EHE) or **3** ethyl vinyl ether (EVE), depending on relative olefin orientations. The vinyl ethers byproducts could then initiate MF-ROMP, with EHE followed by chain transfer with 1-hexene producing **4** and **5**, while initiation by EVE followed by chain transfer with 1-hexene yields **6** and **7**. The cycle of MF-ROMP and chain transfer would repeat until monomer was consumed, the reaction reached equilibrium, or the reaction was otherwise terminated. In theory, free vinyl ethers could also undergo metathesis with the propenyl chain ends of **2** and **3**.

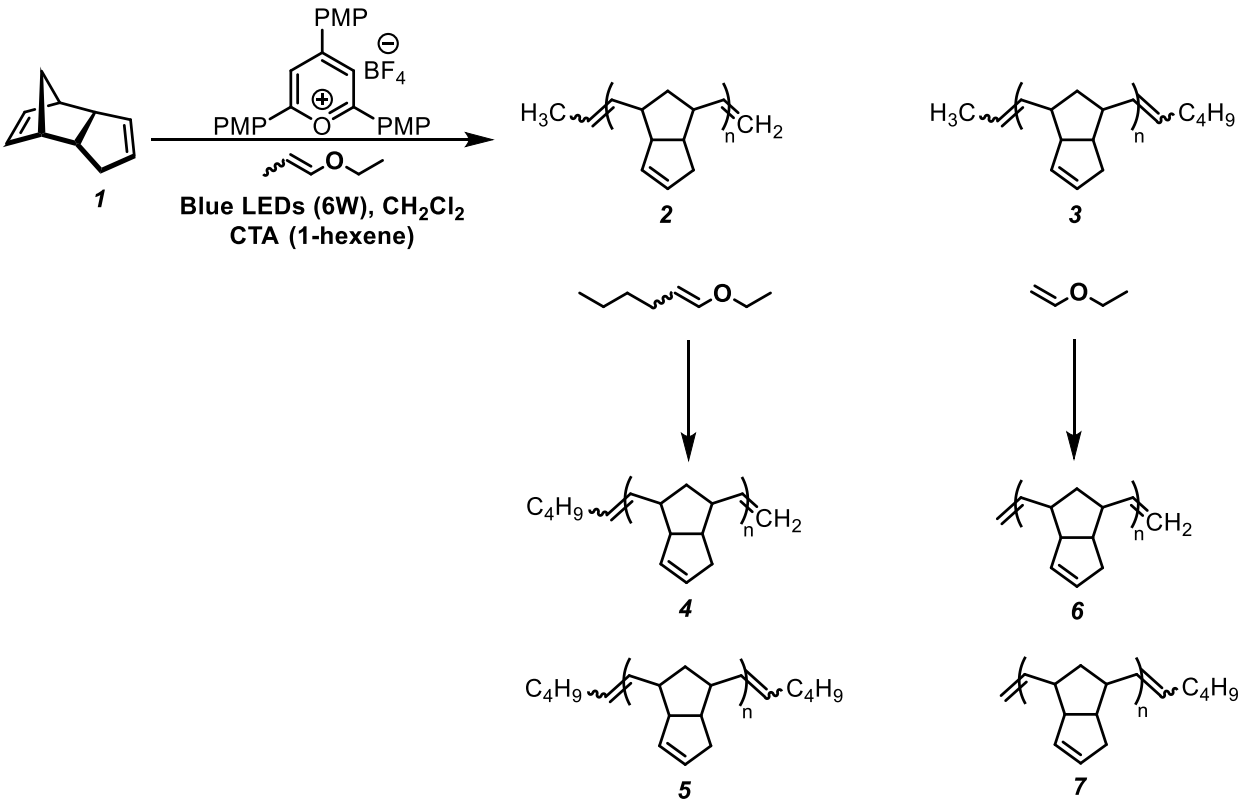


**Figure 5.1.** Possible products of chain transfer with α-olefins in MF-ROMP.

In homopolymerizations of norbornene (NB) via MF-ROMP using an initial NB:EPE:*p*-OMeTPT 200:1:0.2, 1-hexene was evaluated as a CTA at loadings ranging from 0 to 400 eq relative to EPE. Lower molecular weight polynorbornene (PNB) was observed at higher CTA loadings, as observed by GPC with refractive index detection, with PNB synthesized with higher loadings of CTA eluting at longer retention times (Figure 5.2).

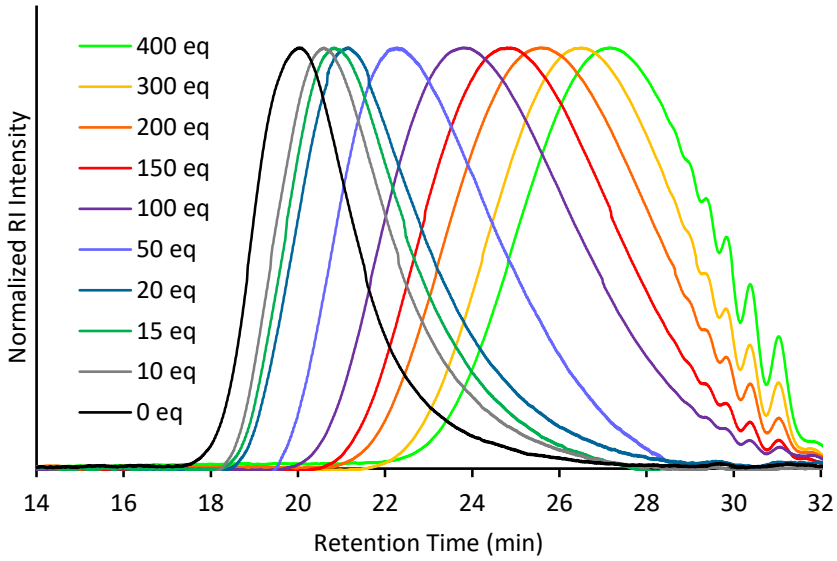


**Figure 5.2**. Normalized GPC refractive index traces of PNB synthesized via MF-ROMP in the presence of 1-hexene CTA (0 to 400 eq relative to EPE initiator).

The number-average molecular weight ($M_n$) for each polymer was calculated from weight-average molecular weight ($M_w$) determined by GPC with multi-angle laser light scattering (MALLS) from the peak of the refractive index trace (peak +/- 30 seconds) to exclude small molecules co-eluting at longer retention times. The calculated molecular weights are plotted as $M_n$ vs equivalents CTA (Figure 5.3) and $1/M_n$ (Figure 5.4). The non-linearity of the plot of $M_n$ vs equivalents of CTA is consistent with non-living polymerization characteristics.[4] While the plot of $M_n$ vs equivalents CTA is non-linear, the plot of $1/M_n$ vs equivalents CTA is linear and can be used to predict and modulate molecular weights by varying CTA loading.

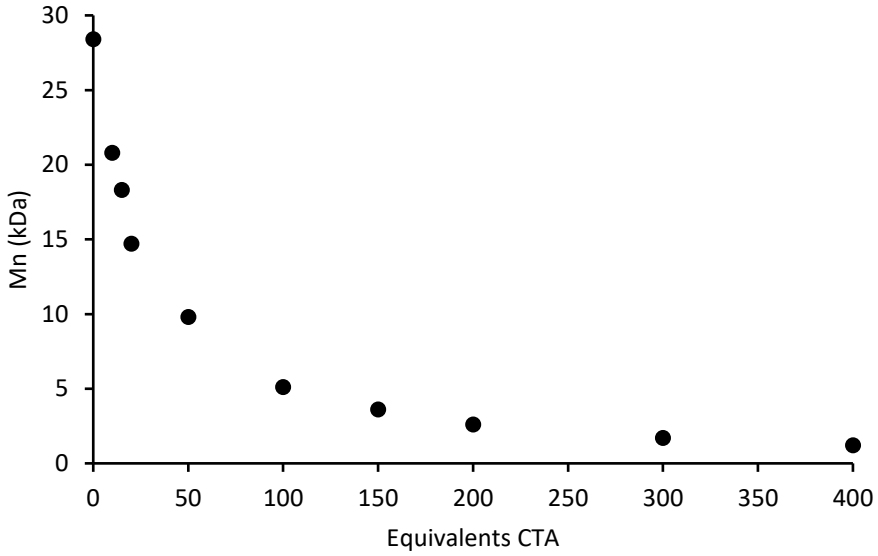


**Figure 5.3**. Plot of number-average molecular weight $M_n$ (kDa) as a function of equivalents of CTA relative to EPE initiator in a polymerization of NB, using a typical polymerization ratio of 200:1:0.2 NB:EPE:*p*-OMeTPT. $M_n$ was calculated form weight-average molecular weight $M_w$, determined by GPC with multi-angle laser light scattering (MALLS), calculated from the peak (peak +/- 30 sec.) of the RI trace.

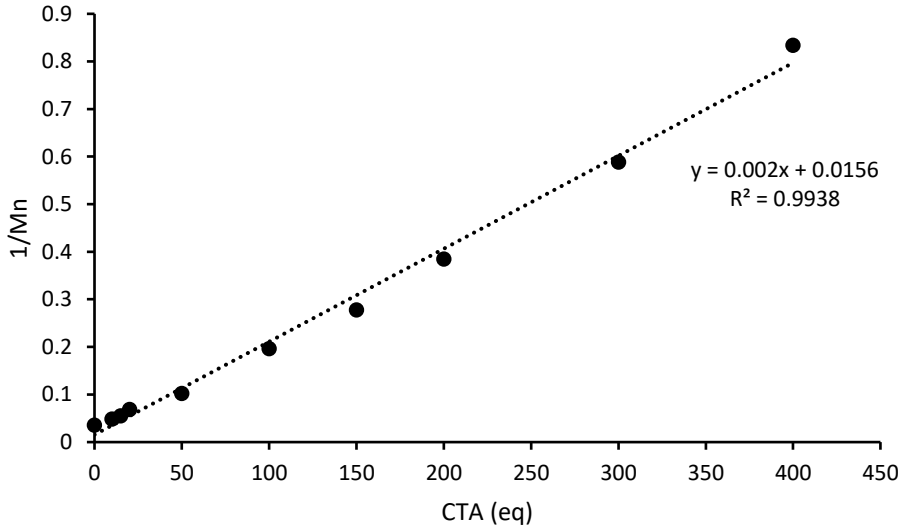


**Figure 5.4**. Plot of $1/M_n$ vs equivalents of CTA for the same polymerization. $M_n$ was calculated form weight-average molecular weight $M_w$, determined by GPC with multi-angle laser light scattering (MALLS), calculated from the peak (peak +/- 30 sec.) of the RI trace.

Due to the high oxidation potential of the backbone olefins relative to the vinyl ether chain end, we hypothesized that chain transfer was occurring predominantly as metathesis at the vinyl ether chain end to cleave the vinyl ether. Adding 1-hexene as CTA at the end of the polymerization did not significantly reduce molecular weight, which is consistent with chain transfer occurring at the vinyl ether chain end and not along the polyolefin backbone. The ability to undergo chain transfer strictly at the chain end could be an advantage of MF-ROMP, as many ROMP catalyst systems will also undergo chain transfer along the backbone, broadening dispersities. Given this evidence that chain transfer occurs selectively at the vinyl ether chain ends, we sought to further understand the mechanism of chain transfer in MF-ROMP via end group analysis with mass spectrometry.

Metathesis between the α-olefin CTA and the vinyl ether chain end could, depending on orientation, produce EVE or EHE as a byproduct (Figure 5.1), each of which could theoretically subsequently act as MF-ROMP initiators. To evaluate the activity of these vinyl ethers and determine which was the initiating species following the first chain transfer event, EVE was screened as an initiator in MF-ROMP. Polymerization of norbornene initiated with ethyl vinyl ether (EVE) achieved low initiation efficiency (2.8%) and went to low conversion (12%). The low initiation efficiency and conversion indicate that EVE is likely not responsible for initiating a significant number of new chains following the first chain transfer event. The other vinyl ether byproduct, ethyl hexenyl ether (EHE), then is likely the active initiator following chain transfer. Additionally, no high MW peaks were observed by GPC, an observation consistent with the conclusion that EVE is not initiating following chain transfer.

To evaluate the impact of chain transfer on the rate of monomer consumption, conversions of NB to PNB MF-ROMP polymerizations with 100:1:0.2 NB:EPE:*p*-OMeTPT

were monitored using $^{1}$H NMR. Conversion vs. time are shown in Figure 5.5 for NB polymerization with (white circles) and without (black circles) 1-hexene CTA. In the absence of CTA, the polymerization achieved more rapid and more complete conversion of NB, reaching 90% conversion at 5.5 min, whereas the polymerization with CTA had only reached 69% conversion by the same timepoint. This demonstrates that the consumption of monomer via MF-ROMP is slower in the presence of a competing metathetical event with CTA.

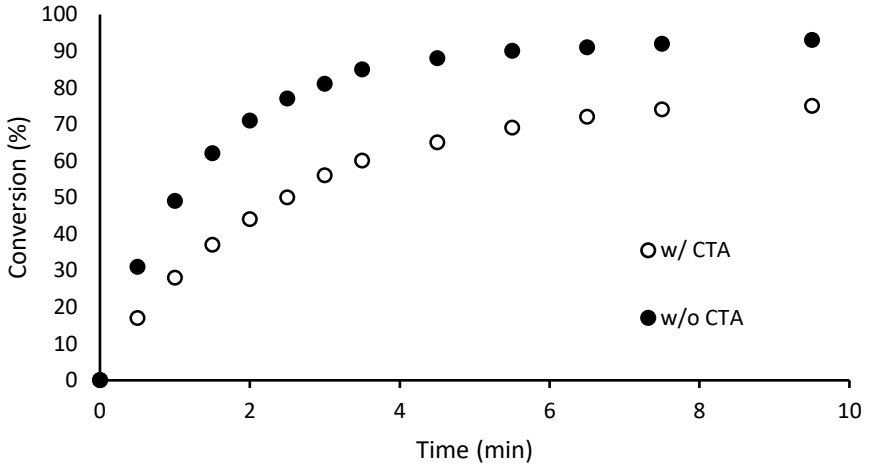


**Figure 5.5**. Conversion of norbornene to polynorbornene with (white circles) and without (black circles) 1-hexene as chain transfer agent. Conversion calculated using *$^{1}$H* NMR analysis.

*5.2.b Chain End Identification by MALDI-TOF*

Mass spectrometry was an analytical tool employed to explore the mechanism of chain transfer in MF-ROMP by determining polymer end group through accurately measuring the isotopic molecular weight of n-mers. Shown in Figure X, the polymerization of **1** was carried out using 1-hexene (Figure 5.6 A) and 1-octene as CTAs (Figure 5.6 B). Based on a polymerization scheme with EPE as the initiator and 1-hexene as the CTA (Figure 5.6 A), n-

mers of PDCPD are observed with a spacing of 132.05 m/z (Theo: 132.09 m/z), which is the expected repeat unit isotopic mass of PDCPD.

In the polymerization of **1** with 1-hexene as a CTA (Figure 5.6 A), a signal appears at 1161.68 m/z which is thought to be PDCPD with an α-olefin produced by the EPE initiation of the polymerization of **1**, followed by metathesis of the vinyl ether chain end with 1-hexene, producing **2** with EHE as a byproduct. This product ought to be produced independently of the CTA present in the reaction, which is likely why the same signal is observed when the CTA is changed to 1-octene (Figure 5.6 B).

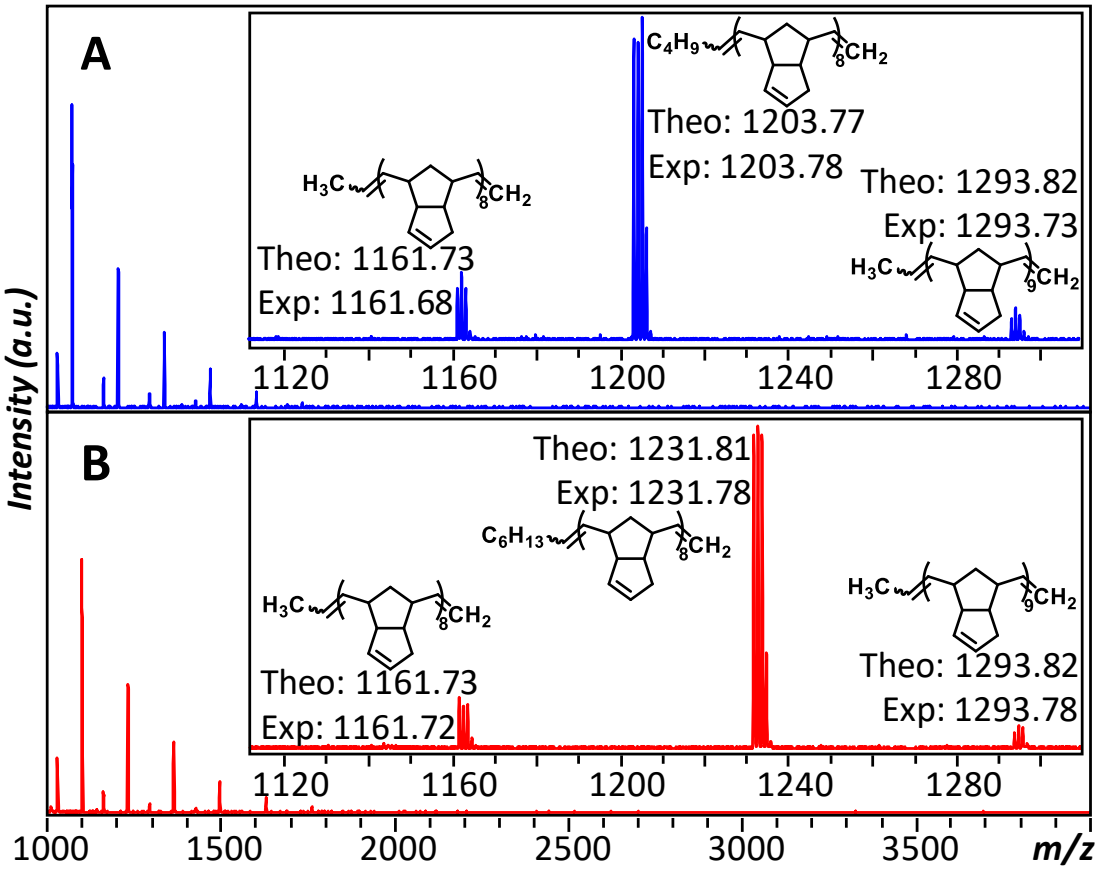


**Figure 5.6**. MALDI-TOF mass spectra of **1** initiated with A) 1-hexene and B) 1-octene, with expanded spectra from *m/z* = 1110 to 1310. The spectra were taken in positive reflector mode, and all labeled signals represent adducts via $Cu^+$ ionization.

Based on signal intensities, however, the major product in MF-ROMP of **1** with 1-hexene CTA appears to be **4**, resulting from initiation by ethyl hexenyl ether (EHE) followed by metathesis to give an α-olefin chain end, as indicated by the signal at 1203.78 m/z (Figure 5.X A). Similarly, the major distribution in Figure 5.X B is **1** initiated with the analogous ethyl octenyl ether (EOE), which provides additional evidence of correct end group identification. The aforementioned signal is -28.00 m/z (Theo 28.03 m/z) from the EHE initiated polymer, which is to be expected for the additional $-CH_2-CH_2-$ group in the 1-octene CTA. It must be noted that signal intensity in MALDI-TOF MS only functions as a quantitative technique to determine relative product ratios, if all structures have the same ionization efficiency; end groups are known to effect changes in the mode of ionization.

Finally, to confirm the mode of ionization, a cation study was performed (see Experimental section) on the same polymers, comparing the ionization with silver to copper. The MS data demonstrates that the polymers were ionizing with the added cation, rather than self-ionization or ionization with residual cations (e.g. catalyst).

**Scheme 5.1.** Products of chain transfer in MF-ROMP as confirmed by MALDI-TOF.

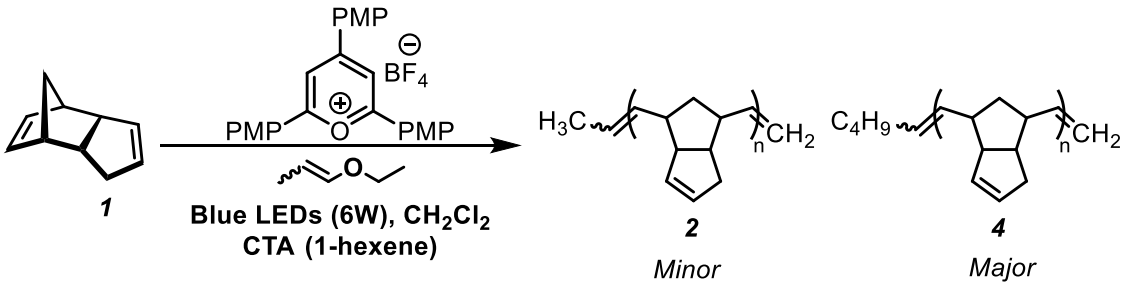

The products observed by MALDI-TOF are shown in Scheme 5.1. Based on this data, chain transfer produces exclusively polymers **2** and **4** with α-olefin chain ends. This is likely the kinetically favored chain transfer product due to steric hinderance in the between the CTA and the polyolefin precluding formation of the cyclobutene radical cation intermediate to PDCPD with an internal olefin chain end (Figure 5.X).

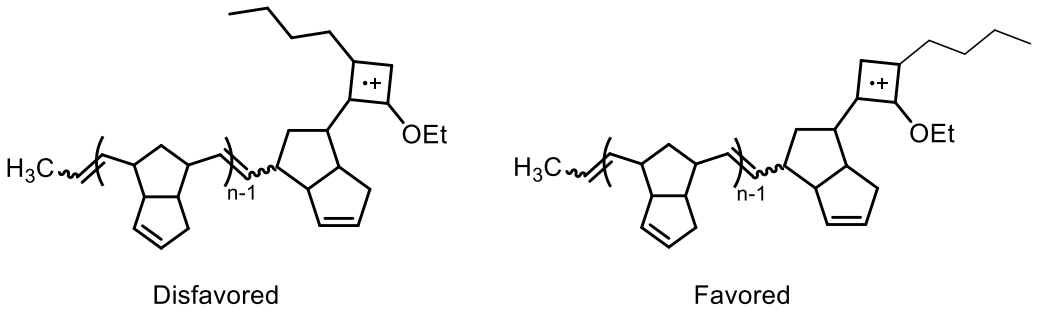


**Figure 5.7**. Disfavored (left) and favored (right) cyclobutane radical cation intermediates for chain transfer in MF-ROMP.

## Section 3: Conclusions

Chain transfer in photoredox-mediated MF-ROMP can be accomplished using α-olefin CTAs. Chain transfer occurs via metathesis at the vinyl ether chain end. This method can be used to modulate molecular weight in MF-ROMP, but does decrease the rate of monomer consumption and final conversion. Chain transfer results in an α-olefin polymer chain end and produces a vinyl ether with internal olefin, such as EHE, which can initiate MF-ROMP following the first metathesis event. Since chain transfer via MF-ROMP has been successful only with α-olefin CTAs and produces a mixture of products, using CTAs to functionalize chain ends in MF-ROMP remains a challenge. Ongoing work includes evaluating the kinetics of chain transfer in MF-ROMP.

## Section 4: Experimental

*5.4.a General Considerations*

For all reactions, $CH_2Cl_2$ was dried over 3 Å molecular sieves before use. All polymerizations were carried out in standard borosilicate glass vials purchased from Fisher Scientific with magnetic stirring unless otherwise noted. Irradiation of photochemical reactions was done using a 6 W Miracle blue LED indoor gardening bulb purchased from Amazon. Norbornene was sublimed prior to use. Dicyclopentadiene was obtained from Aldrich and used as-received. Chain transfer agents (CTAs) were obtained from commercial sources and dried over 3 Å molecular sieves prior to use. The pyrylium tetrafluoroborate salt (p-OMeTPT) was prepared according to literature procedure.[1] $^1$H and NMR spectra were recorded on Bruker AVance 300 MHz or 500 MHz spectrometers. Chemical shifts are reported in delta (δ) units, expressed in parts per million (ppm) downfield from tetramethylsilane using the residual protio-solvent as an internal standard ($CDCl_3$, $^1$H: 7.26 ppm). Data are reported as follows: chemical shift, multiplicity (s = singlet, d = doublet, dd= doublet of doublets, br = broad, m = multiplet), coupling constants (Hz) and integration. Gel permeation chromatography (GPC) was performed using a GPC setup consisting of: an Agilent pump, 3 in-line columns, and Wyatt light scattering and refractive index detectors with tetrahydrofuran (THF) as the mobile phase. Number-average molecular weights ($M_n$) and weight-average molecular weights ($M_w$) were calculated from light scattering.

*5.4.b Polymerization Procedures*

*General Procedure for Chain Transfer Trials*

To a 2 dram vial containing a magnetic stirbar was added norbornene monomer (2.3 mmol, 200 equiv, unless otherwise specified), followed by *p*-OMeTPT (2.00 mL 0.55 mg/mL stock solution in $CH_2Cl_2$, for 1.1 mg, 0.002 mmol, 0.2 equivs), 1.50 mL $CH_2Cl_2$, 0.50 mL of 2.5 μL/mL ethyl propenyl ether (EPE) in $CH_2Cl_2$ stock solution (1.25 μL EPE, 0.0113 mmol, 1 equivs), and 0 to 400 equivs 1-hexene CTA. Total volumes of 4.56 mL were achieved for each trial by adding $CH_2Cl_2$ to offset CTA volumes. The vial was capped and irradiated with blue LEDs (6 W) 1 cm from bulb for 80 minutes. A small scoop of hydroquinone was added to the vial and an aliquot taken for analysis.

*Procedure for Conversion vs Time Analysis*

To a 2 dram vial with Teflon cap was added *p*-OMeTPT (1.1 mg, 0.002 mmol, 0.2 equivs) followed by norbornene (0.106 g, 1.13 mmol, 100 equivs), $CH_2Cl_2$ (2 mL) and EPE (1.25 uL, 0.0113 mmol, 1 equiv), followed by either $CH_2Cl_2$ (280 μL, control) or 1-hexene (280 μL, 2.25 mmol, 200 equivs). The vial was capped and shaken to mix, and 1.0 mL was transferred to a capped NMR tube, which was irradiated with blue LEDs (6 W) 1 cm from bulb, pausing to take $^1H$ NMRs at time intervals indicated in the main text. Reaction mixtures were shaken vigorously before and after each NMR.

*General Procedure for Preparation of Polymers for End Group Analysis by MALDI-TOF*

To a 30 mL scintillation vial with Teflon cap containing a magnetic stirbar was added *p*-OMeTPT (10.9 mg, 0.022 mmol, 0.2 equivs) followed by monomer (norbornene or dicyclopentadiene) (11.3 mmol, 100 equivs). Dichloromethane (20 mL) was added, followed by CTA (1-hexene, 1-octene, 4-phenyl-1-butene, 22.5 mmol, 200 eq) and ethyl propenyl ether (12.5 µL, 0.113 mmol, 1 equiv). The vial was capped and irradiated with blue LEDs (6 W) 1 cm from bulb for 80 minutes. A small scoop of hydroquinone was added to the vial and an aliquot taken for analysis. The remaining reaction mixture was filtered through a plug of neutral alumina, eluting with $CH_2Cl_2$. The eluent was concentrated, redissolved in 20 mL $CH_2Cl_2$ and precipitated into 200 mL of cold, stirring MeOH in a dry ice/acetone bath and the precipitate was collected via filtration and washed with cold MeOH. The precipitation was repeated.

*Ethyl Vinyl Ether Screening*

In a 2 dram vial with Teflon cap containing magnetic stir bar, p-OMeTPT (1.1 mg, 2.3 µmol, 0.05 eq), NB (0.4231 g, 4.5 mmol, 100 eq), 2.0 mL $CH_2Cl_2$, EVE (4.3 µL, 0.045 mmol, 1 eq) were combined. The reaction was stirred and irradiated with a 6 W blue LED bulb for 80 min. A small scoop of hydroquinone was added to the vial and an aliquot taken for analysis by $^1$H NMR. The NMR sample was subsequently filtered through a cotton plug and concentrated for GPC analysis.

*5.4.c MALDI-TOF Methods*

Mass spectral data were collected using a Bruker-Daltonics Matrix Assisted Laser Desorption Ionization Time-of-Flight (MALDI-TOF) Autoflex III mass spectrometer in reflector

mode with positive ion detection. Typical sample preparation for MALDI-TOF MS data was performed by making stock solutions in THF of matrix (50 mg/ml), polymer analyte (2 mg/ml), and an appropriate cation source (2 mg/ml). The data herein were acquired using trans-2-[3-(4-tert-Butylphenyl)-2-methyl-2-propenylidene]malononitrile (DCTB) as a matrix, and CuBr and AgTFA were used as cation sources. With the $Ag^+$ cation, the stock solutions were mixed in a 4/2/1 ratio (matrix/analyte/cation). With the $Cu^+$ cation, the stock solutions were mixed in a 4/2/3 ratio for the 1-octene initiated pDCPD and 1-hexene initiated pNB; a ratio of 2/1/4 was used for the 1-hexene initiated pDCPD. The prepared solutions were vortexed and deposited onto the MALDI target plate and allowed to evaporate via the dried droplet method. MALDI-TOF MS data were calibrated against Poly(ethylene glycol) methyl ether ($M_n$ = 550) from Sigma Aldrich and SpheriCal dendritic calibrants from Polymer Factory (Stockholm, Sweden). $M_n$ and Đ of the resultant spectra were calculated using Polytools software.

For AgTFA:

8/4/2 was always used

For CuBr:

8/4/16 143 hexene

8/4/6 147 octene

8/4/6 159

*5.4.d Polymerization Data*

**Table 5.1.** Results of chain transfer screenings with 1-hexene.

| | | | From GPC | | | GPC Peak (+/- 30 sec) |
|---|---|---|---|---|---|---|
| NB:EPE: *p*-OMeTPT | 1-hexene (equivs) | Conversion (%)[a] | $M_n$[b] | $M_w$[c] | $Đ$[d] | $M_n$[e] |
| 100:1:0.2 | 0 | 95 | 13.1 | 19.6 | 1.5 | 17.0 |
| 100:1:0.2 | 200 | 91 | 1.0 | 1.4 | 1.4 | 1.1 |
| 200:1:0.2 | 0 | 86 | 19.3 | 35.6 | 1.9 | 39.2 |
| 200:1:0.2 | 400 | 82 | 0.7 | 1.0 | 1.5 | 1.0 |

[a] % conversion of norbornene, determined by $^1$H NMR spectroscopy. [b] Determined from crude, unprecipitated reaction aliquots: Experimental number-average molecular weight $M_n$ calculated from [b] experimental weight-average molecular weight ($M_w$) determined by GCP using multi-angle laser light scattering (MALLS). [d] Dispersitites ($Đ$) determined by GPC analysis. [e] Number-average molecular weight ($M_n$) calculated from weight-average molecular weight determined by GPC analysis with MALLS, using central minute of refractive index peak. These values were plotted in Figure 2 of main text.

**Table 5.2.** Results of molecular weight modulation with 1-hexene CTA with initial NB:EPE:*p*-OMeTPT of 200:1:0.2.

| | | | From GPC | | | GPC Peak (+/- 30 sec) |
|---|---|---|---|---|---|---|
| Sample | 1-hexene (equivs) | Conversion (%)[a] | $M_n$[b] | $M_w$[c] | $Đ$[d] | $M_n$[e] |
| A | 400 | 76 | 1 | 1.5 | 1.5 | 1.2 |
| B | 300 | 76 | 1.6 | 2.4 | 1.5 | 1.7 |
| C | 200 | 84 | 1.6 | 2.7 | 1.6 | 2.6 |
| D | 150 | 81 | 2.7 | 4 | 1.5 | 3.6 |
| E | 100 | 84 | 3 | 5.1 | 1.7 | 5.1 |
| F | 50 | 86 | 5.8 | 8.8 | 1.5 | 9.8 |
| G | 20 | 84 | 9.8 | 14.7 | 1.5 | 14.7 |
| H | 15 | 85 | 14 | 18.4 | 1.3 | 18.3 |
| I | 10 | 83 | 13.6 | 20.6 | 1.5 | 20.8 |
| J | 0 | 78 | 19.2 | 30 | 1.6 | 28.4 |

[a] % conversion of norbornene, determined by $^1$H NMR spectroscopy. [b] Determined from crude, unprecipitated reaction aliquots: Experimental number-average molecular weight $M_n$ calculated from [b] experimental weight-average molecular weight ($M_w$) determined by GCP using multi-angle laser light scattering (MALLS). [d] Dispersitites ($Đ$) determined by GPC analysis. [e] Number-average molecular weight ($M_n$) calculated from weight-average molecular weight determined by GPC analysis with MALLS, using central minute of refractive index peak. These values were plotted in Figure 2 of main text.

*Samples for MALDI-TOF*

**Table 5.3.** Molecular weight data for MALDI-TOF polymer samples.

| | | | | From GPC | | | GPC Peak (+/- 30 sec) |
|---|---|---|---|---|---|---|---|
| Monomer | CTA | NB:EPE: *p*-OMeTPT:CTA | Conversion (%)[a] | $M_n$[b] | $M_w$[c] | $Đ$[d] | $M_n$[e] |
| NB | 1-hexene | 100:1:0.2:200 | 84 | 1.1 | 1.4 | 1.3 | 1.1 |
| DCPD | 1-hexene | 100:1:0.2:200 | 16 | 1.6 | 1.9 | 1.2 | 1.6 |
| DCPD | 1-octene | 100:1:0.2:200 | 17 | 1.1 | 1.4 | 1.2 | 1.1 |

[a] % conversion of norbornene, determined by $^1$H NMR spectroscopy. [b] Determined from crude, unprecipitated reaction aliquots: Experimental number-average molecular weight $M_n$ calculated from [b] experimental weight-average molecular weight ($M_w$) determined by GCP using multi-angle laser light scattering (MALLS). [d] Dispersitites ($Đ$) determined by GPC analysis. [e] Number-average molecular weight ($M_n$) calculated from weight-average molecular weight determined by GPC analysis with MALLS, using central minute of refractive index peak. These values were plotted in Figure 2 of main text.

*5.4.e MALDI-TOF Cation Studies*

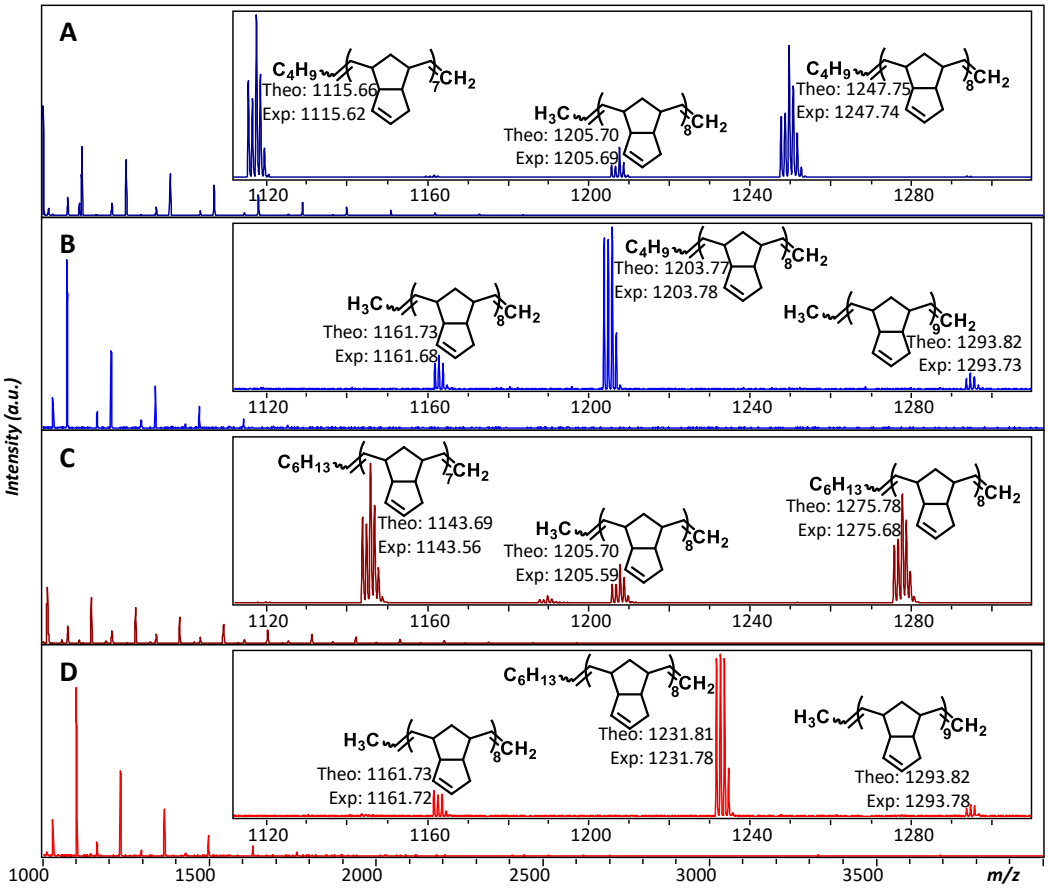


**Figure 5.8**. MALDI-TOF mass spectra of dicylopentadiene initiated with A) 1-hexene ionized with $Ag^+$, B) 1-hexene ionized with $Cu^+$, C) 1-octene ionized with $Ag^+$, and D) 1-octene ionized with $Cu^+$, with expanded spectra from m/z = 1110 to 1310. The spectra were taken in positive reflector mode.

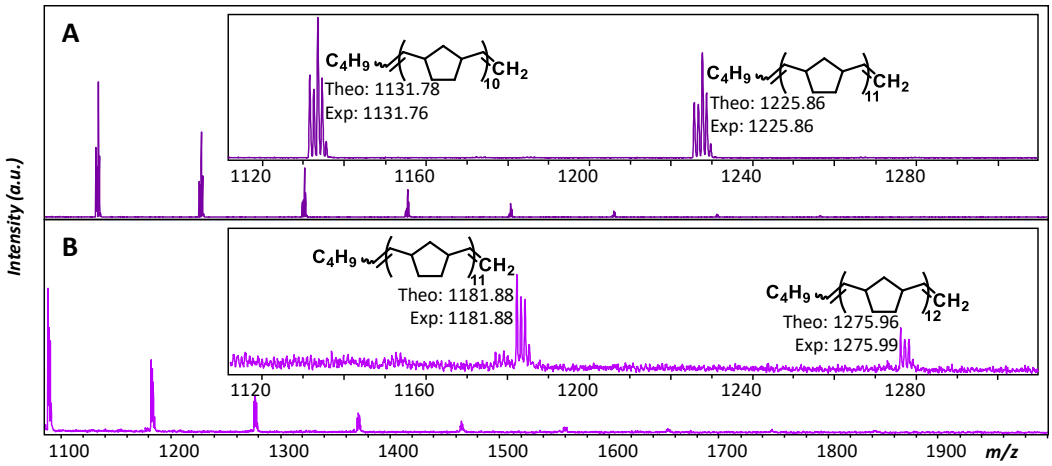


**Figure 5.9**. MALDI-TOF mass spectra of 1-hexene initiated norbornene ionized with A) $Ag^+$ and B) $Cu^+$, with expanded spectra from *m/z* = 1110 to 1310. The spectra were taken in positive reflector mode.

*5.4.f $^1$H NMR and GPC Data*

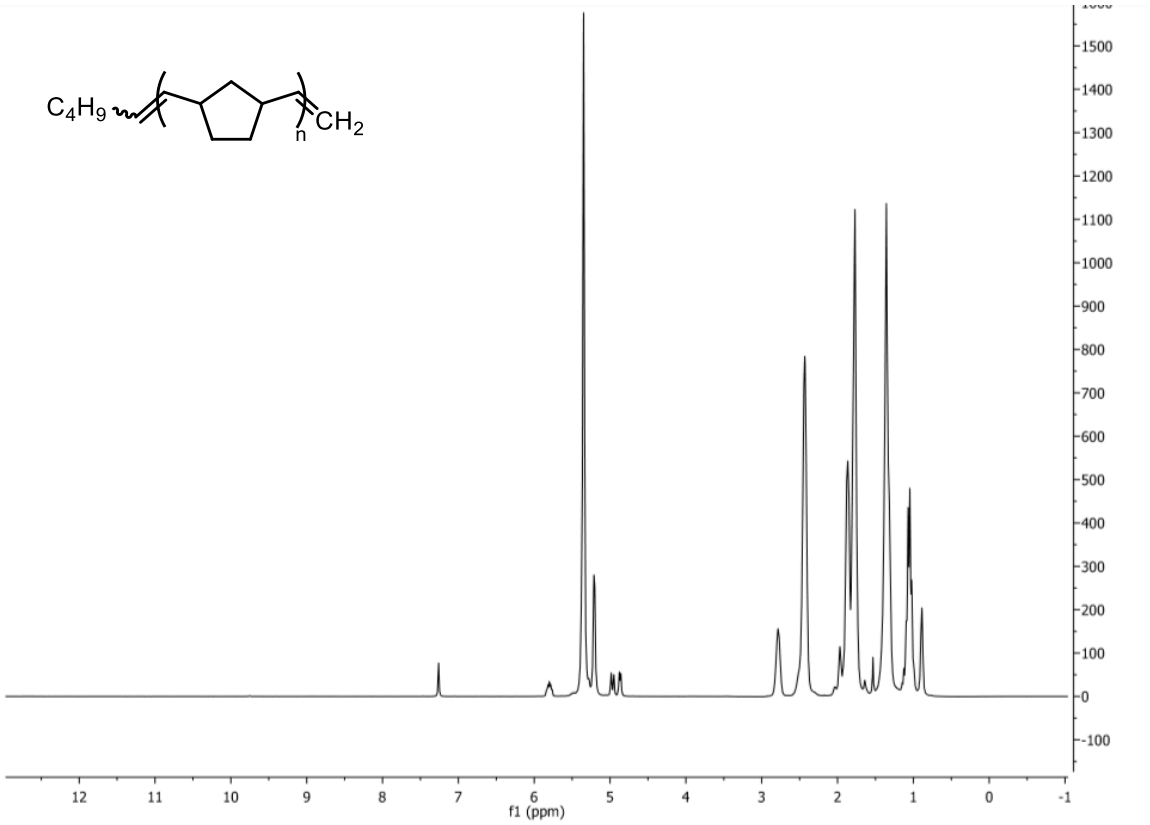


**Figure 5.10**. $^1$H NMR spectrum of PNB synthesized via MF-ROMP in the presence of 1-hexene CTA (corresponds to Table 5.3, row 1). Product determined by MALDI-TOF overlaid.

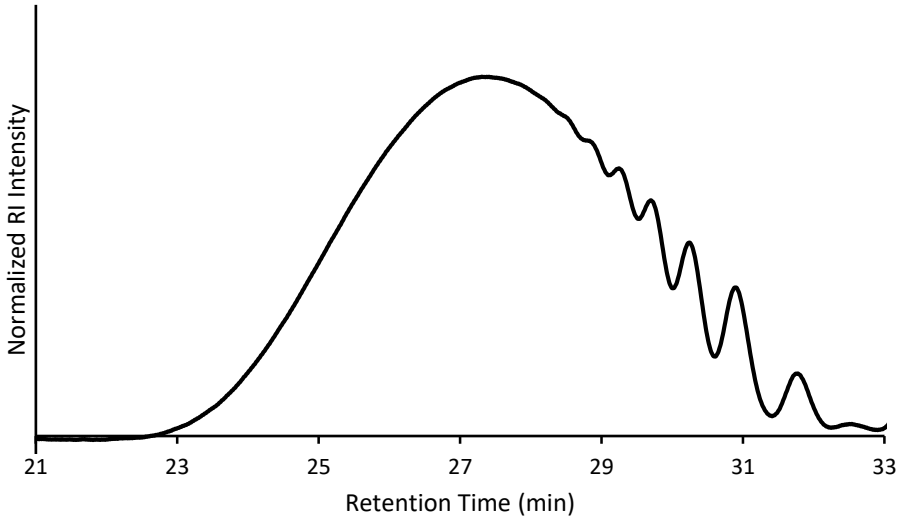


**Figure 5.11**. GPC refractive index of PNB synthesized via MF-ROMP in the presence of 1-hexene CTA (corresponds to Table 5.3, row 1).

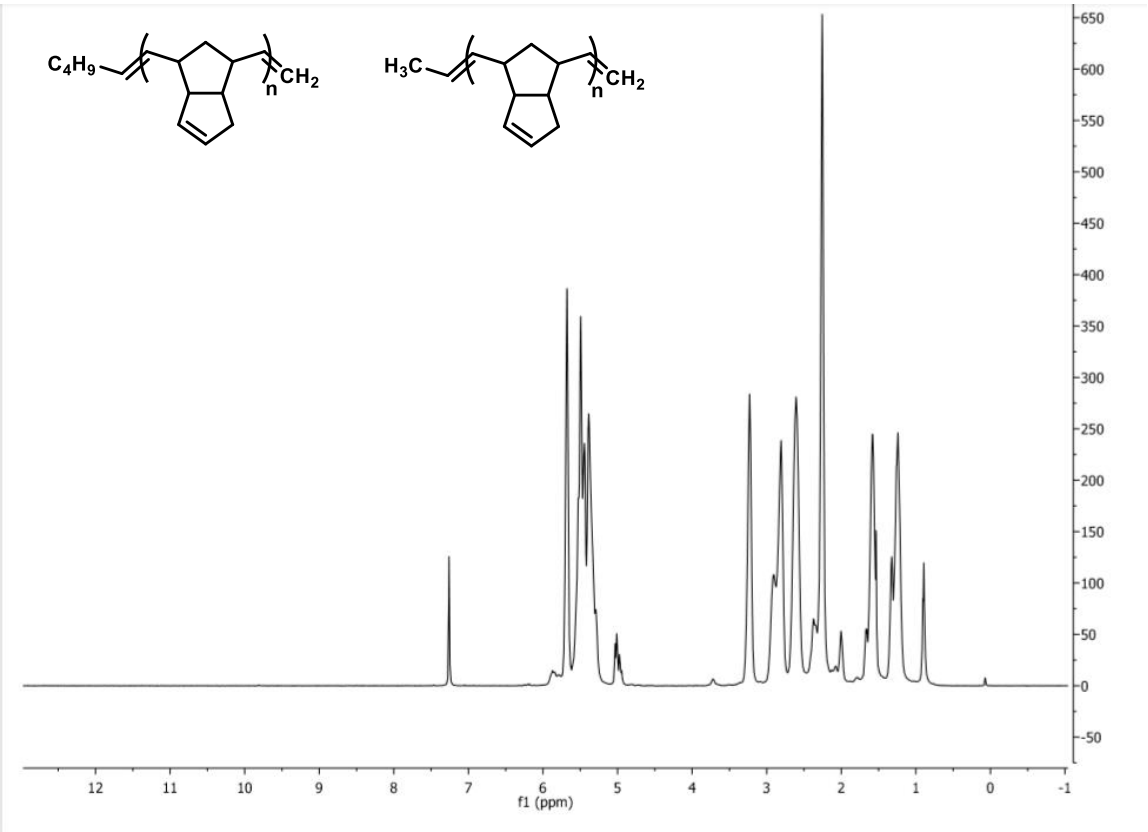


**Figure 5.12**. $^{1}$H NMR spectrum of PDCPD synthesized via MF-ROMP in the presence of 1-hexene CTA (corresponds to Table 5.3, row 2). Products determined by MALDI-TOF overlaid, major product on the left.

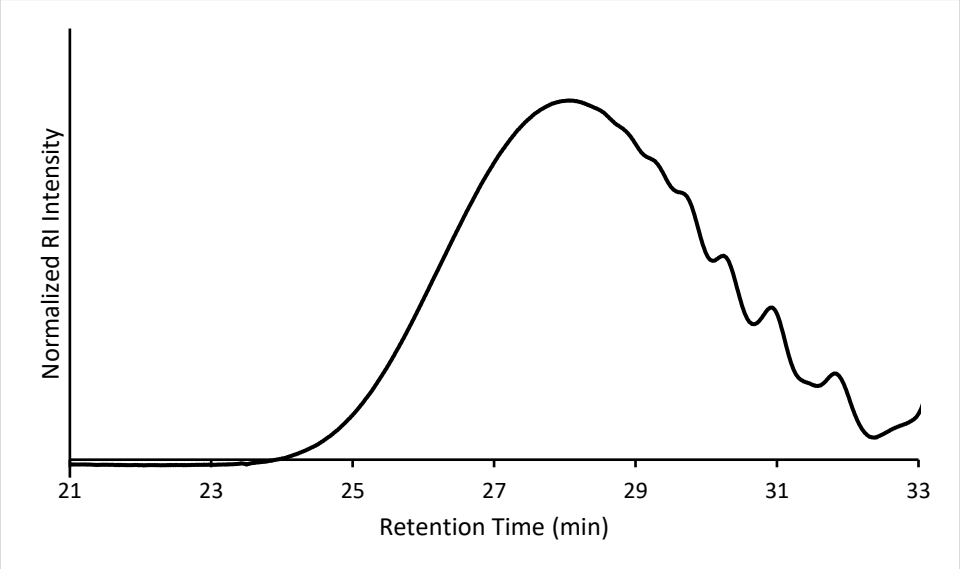


**Figure 5.13**. GPC refractive index of PDCPD synthesized via MF-ROMP in the presence of 1-hexene CTA (corresponds to Table 5.3, row 2).

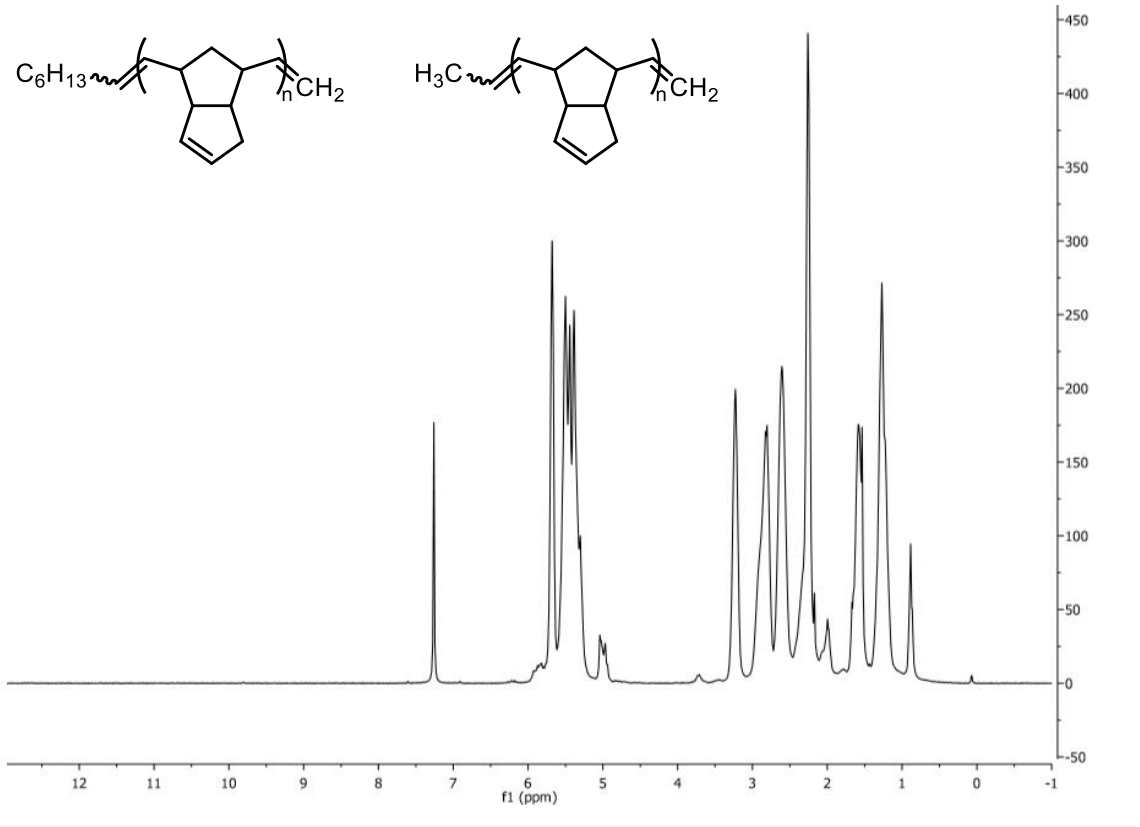


**Figure 5.14**. $^{1}$H NMR spectrum of PDCPD synthesized via MF-ROMP in the presence of 1-octene CTA (corresponds to Table 5.3, row 2). Products determined by MALDI-TOF overlaid, major product on the left.

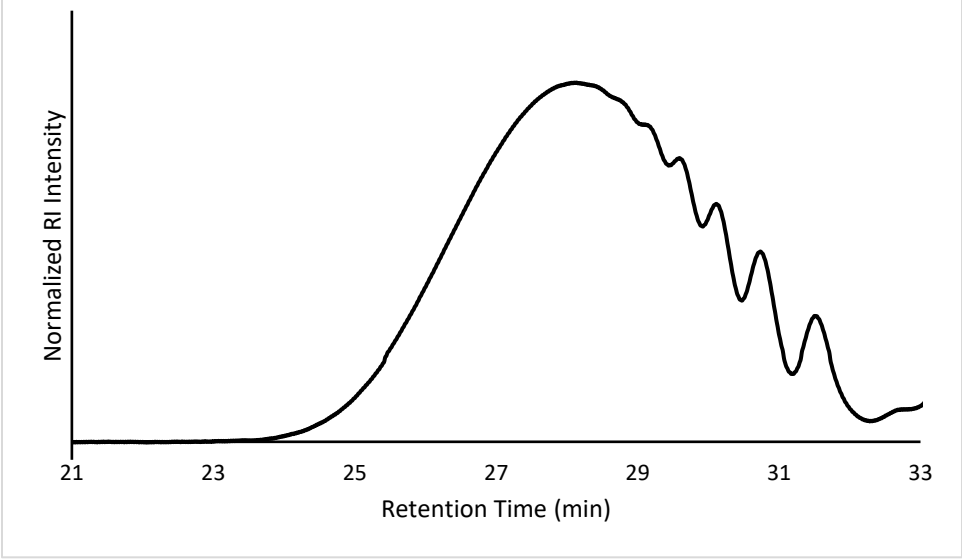


**Figure 5.15**. GPC refractive index of PDCPD synthesized via MF-ROMP in the presence of 1-octene CTA (corresponds to Table 5.3, row 3).

**Notes and References for Chapter 4**

[1] Ogawa, K. A.; Goetz, A. E.; Boydston, A. J. *J. Am. Chem. Soc.* **2015**, *137*, 1400–1403.
[2] a) Matson, J. B.; Grubbs, R. H. *Macromolecules*. **2010**, *43*, 213-221. b) Matson, J. B.; Grubbs, R. H. *J. Am. Chem. Soc.* **2009**, *131*, 3355-3362. c) Matson, J. B.; Grubbs, R. H. *Macromolecules*. **2008**, *41*, 5626-5631. d) Bielawski, C. W.; Benitez, D.; Morita, T.; Grubbs, R. H. *Macromolecules*. **2001**, *34*, 8610-8618. e) Gibson, V. C.; Okada, T. *Macromolecules*. **2000**, *33*, 655-656. f) Hilf, S.; Kiblinger, A. F. M. *Nature Chem.* **2009**, *1*, 537-546. f) Ji, S.; Hoye, T. R.; Macosko, C. W. *Macromolecules*. **2004**, *37*, 5485-5489. g) Maughon, B. R.; Morita, T.; Bielawski, C. W.; Grubbs, R. H. *Macromolecules*. **2000**, *33*, 1929-1935. g) Scherman, O. A.; Rutenberg, I. M.; Grubbs, R. H. *J. Am. Chem. Soc.* **2003**, *125*, 8515-8522. h) Xia, Y.; Verduzco, R.; Grubbs, R. H.; Kornfield, J. A. *J. Am. Chem. Soc.* **2008**, *130*, 1735-1740. i) Morita, T.; Maughon, B. R.; Bielawski, C. W.; Grubbs, R. H. *Macromolecules*, **2000**, *33*, 6621-6623. j) Hillmyer, M. A.; Grubbs, R. H. *Macromolecules*. **1995**, *28*, 8662-8667. k) Schrock, R. R.; Yap, K. B; Yang, D. C.; Sitzmann, H.; Sita, L. R.; Bazan, G. C. *Macromolecules*. **1989**, *22*, 3191-3200. l) Cramail, H.; Fontanille, M.; Soum, A. *J. Mol. Catal.* **1991**, *65*, 193-203. m) Crowe, W.E.; Mitchell, J. P.; Gibson, V. C.; Schrock, R. R. *Macromolecules*. **1990**, *23*, 3434-3536. n) Reyx, D.; Hamza, M.; Capistron, I. *J. Mol. Catal.* **1987**, *42*, 289-299. o) Otton, J.; Colleuille, Y.; Varagnat, J. *J. Mol. Catal.* **1980**, *8*, 313-324.
[3] a) Keim, W. *Angew. Chem. Int. Ed.* **2013**, *52*, 12492-12496. b) Keim, W. *Angew. Chem. Int. Ed.* **1990**, *29*, 239-244. c) Lutz, E. F. *J. Chem. Ed.* **1986**, *63*, 202.
[4] a) Benedicto, A. D.; Claverie, J. P.; Grubbs, R. H. *Macromolecules*. **1995**, *28*, 500-511. (b) Gregg, R. A,; Mayo, F. R. J. Am. Chem. Soc. 1948, 70, 2373. (c) Mayo, F. R. J. Am. Chem. Soc. 1943, 65, 2324.